U.PORTO
FACULDADE DE CIÊNCIAS
UNIVERSIDADE DO PORTO

PhD

PhD

PhD

PhD

PhD

3.º CICLO

FCUP
UA
UM
2015

U.PORTO

Improving Variable Selection and Mammography-based Machine Learning Classifiers for Breast Cancer CADx

Noel Pérez Pérez

FC

U.PORTO
FACULDADE DE CIÊNCIAS
UNIVERSIDADE DO PORTO

universidade de aveiro

Universidade do Minho

Improving Variable Selection and Mammography-based Machine Learning Classifiers for Breast Cancer CADx

Noel Pérez Pérez

Thesis submitted to the Faculty of Sciences of the University of Porto, University of Aveiro and University of Minho in partial fulfillment of the requirements for the degree of Doctor of Philosophy in Computer Science

March 2015

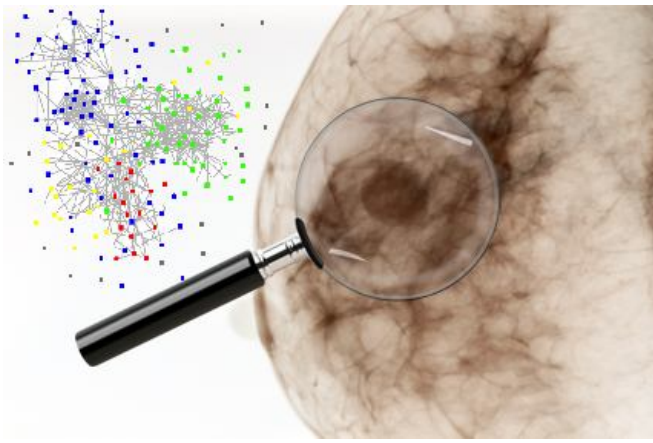

Improving Variable Selection and Mammography-based Machine Learning Classifiers for Breast Cancer CADx

Noel Pérez Pérez

Doctoral Program in Computer Science of the Universities of Minho, Aveiro and Porto

Department of Computer Science

March 2015

Supervisor

Miguel Angel Guevara López, Senior Researcher, Institute of Electronics and Telematics Engineering of Aveiro, University of Aveiro

Co-Supervisor

Augusto Marques Ferreira da Silva, Assistant Professor, Department of Electronics, Telecommunications and Informatics, University of Aveiro

To My Parents Magalys and Noel Pérez

Acknowledgement

Many people have played important roles during the course of my doctoral studies. It is time to reflect on those whose support and encouragement were essential components for a successful completion of this thesis.

I am grateful to my supervisor Prof. Miguel Angel Guevara López for introducing me to the field of medical image analysis and for his supervision during this thesis.

Special thanks to Prof. Augusto Silva, my co-supervisor (IEETA) for his helpful remarks during our scientific discussion.

I am also fortunate for the time I spent at the Laboratory of Optics and Experimental Mechanics (LOME) - Institute of Mechanical Engineering and Industrial Management (INEGI), University of Porto. All the members deserve special recognition for the friendly atmosphere, supportive environment, and logistic assistance they provided.

I also wish to acknowledge the FCT (Fundação para a Ciência e a Tecnologia) for the financial support (grant SFRH/BD/48896/2008).

I am also grateful to Prof. Fernando Silva, Alexandra Ferreira (DCC) and Sofia Santos (FCUP) for their valuable help and guidance during this time.

I am greatly indebted to Dr. Alexis Oliva and his family for their help, support and fraternal love during this hardest time.

Thanks to my friends in Portugal and Cuba for their friendship and support. All their comments were always well received.

Finally, I would like to show my deepest appreciation to my parents; Magalys and Noel, my sisters and nieces, my brother in law Danilo, and my girlfriend Lizbeth Oliva for their unparalleled love and support.

Abstract

Breast Cancer is a major concern and the second-most common and leading cause of cancer deaths among women. According to public statistics in Portugal estimates point to 4500 new diagnosed cases of breast cancer and 1600 women death from this disease. At present, there are no effective ways to prevent breast cancer, because its cause remains unknown. However, efficient diagnosis of breast cancer in its early stages can give a woman a better chance of full recovery. Breast imaging, which is fundamental to cancer risk assessment, detection, diagnosis and treatment, is undergoing a paradigm shift: the tendency is to move from a primarily qualitative interpretation to a more quantitative-based interpretation model. In term of diagnosis, the mammography and the double reading of mammograms are two useful and suggested techniques for reducing the proportion of missed cancers. But the workload and cost associated are high.

Breast Cancer CADx systems is a more recent technique, which has improved the AUC-based performance of radiologists and the classification of breast cancer in its early stages. But the performance of current commercial CADx systems still needs to be improved so that they can meet the requirements of clinics and screening centers.

Feature selection techniques constitute one of the most important steps in the lifecycle of Breast Cancer CADx systems. It presents many potential benefits such as: facilitating data visualization and data understanding, reducing the measurement and storage requirements, reducing training and utilization times and, defining the curse of dimensionality to improve the predictions performance. It is therefore convenient that feature selection methods are fast, scalable, accurate and possibly with low algorithmic complexity.

This thesis was motivated by the need of developing new feature selection methods to provide more accurate and compact subsets of features to feed machine learning classifiers supporting breast cancer diagnosis. In our study, we realized that most of the developed approaches were focused on the wrapper or hybrid paradigm and, in fewer degrees on filter paradigm. We considered exploring the filter paradigm because filter methods provide lower algorithmic

complexity, faster performance and are independent of classifiers. However, feature selection methods based on this paradigm present two main limitations: (1) ignore the dependencies among features and (2) assume a given distribution (Gaussian in most cases) from which the samples (observations) have been collected. In addition, assuming a Gaussian distribution includes the difficulties to validate distributional assumptions because of small sample sizes.

The first contribution of this thesis is an ensemble feature selection method (named *RMean*) based on the mean criteria (assigned by the mean of the feature) for indexing relevant features. When applied to the breast cancer datasets under study, the subsets of ranked features produced by using the *RMean* method improved the AUC performance in almost all the explored machine learning classifiers. Despite the good performance of the *RMean* method, it still preserves the limitations of filter methods and this may lead the Breast Cancer CADx methods to classification performances bellow of its potential.

To overcome these limitations, the second contribution proposes a new feature selection method (named *uFilter*) based on the Mann Whitney U-test for ranking relevant features, which asses the relevance of features by computing the separability between class-data distribution of each feature. The *uFilter* method solves some difficulties remaining on previous developed methods, such as: it is effective in ranking relevant features independently of the samples sizes (tolerant to unbalanced training data); it does not need any type of data normalization; and the most important, it presents a low risk of data overfitting. When applied to the breast cancer datasets under study, the *uFilter* method statistically outperformed the U-Test (baseline method), *RMean* (contribution 1) and four classical feature selection methods. This method revealed competitive and appealing cost-effectiveness results on selecting relevant features, as a support tool for breast cancer CADx methods. Finally, the redundancy analysis as a complementary step to the *uFilter* method provided us an effective way for finding optimal subsets of features.

Resumo

O Cancro da Mama é segunda causa de morte mais comum entre as mulheres, sendo a mais comum dentro das mortes por cancro. De acordo com as estatísticas nacionais, estima-se que em Portugal sejam diagnosticados 4500 novos casos por ano que acabam por vitimar 1600 mulheres. Atualmente não há formas eficazes de prevenir o cancro da mama uma vez que a sua causa permanece desconhecida. Contudo, o diagnóstico precoce do cancro da mama aumenta a possibilidade de uma recuperação completa. A imagiologia da mama, que é fundamental para a avaliação de risco, detecção, diagnóstico e terapia está sob um processo de mudança de paradigma: a tendência é passar de uma interpretação maioritariamente qualitativa para modelos de interpretação mais quantitativos. Em termos de diagnóstico, a mamografia e a avaliação dos mamogramas por dois profissionais são técnicas úteis que são sugeridas para a redução da proporção de cancros não diagnosticados. No entanto, a carga de trabalho e os custos envolvidos são elevados.

Os sistemas de Diagnóstico Assistido por Computador (CADx) são uma técnica recente que tem melhorado o desempenho dos radiologistas e a classificação dos casos de cancro em estágios iniciais. Contudo, o desempenho dos sistemas comerciais de CADx necessita de ser melhorado para que cumpram os requisitos estabelecidos para a sua utilização na prática clínica.

As técnicas de seleção de caraterísticas são um dos passos mais importantes no ciclo de vida de um sistema de CADx. Estas técnicas apresentam vários benefícios potenciais, tais como: facilitam a visualização e compreensão dos dados, reduzem os requisitos de medição e armazenamento, reduzem os tempo de treino e de resposta dos sistemas, evitando os problemas da alta dimensionalidade e permitindo aumentar o poder preditivo dos sistemas. Por isso, é desejável que os métodos de seleção de caraterísticas sejam rápidos, escaláveis, exatos e com baixa complexidade algorítmica.

Esta tese foi motivada pela necessidade de novos métodos de seleção de caraterísticas que permitam obter subconjuntos de caraterísticas mais compactos e discriminativos para o treino de classificadores de suporte ao diagnostico do cancro da mama. Neste estudo, constatou-se que a maior parte das abordagens focam-se nos paradigmas wrapper, híbrido e em menor grau

no paradigma filtro. Esta tese assenta na exploração do paradigma filtro porque envolve uma complexidade algorítmica mais baixa, desempenho mais rápido e porque é independente de classificadores. No entanto, os métodos de seleção de caraterísticas baseados neste paradigma tem duas limitações principais: (1) ignoram dependências entre caraterísticas e (2) assumem uma dada distribuição (Gaussiana na maior parte dos casos) a partir da qual as amostras (observações) são recolhidas. A assunção de distribuição Gaussiana pode trazer problemas adicionais relacionados com dificuldades em validar as assunções desta distribuição, principalmente quando o número de amostras é baixo.

A primeira contribuição desta tese é um método *ensemble* de seleção de caraterísticas (denominado *RMean*) baseado no critério da média (atribuida pelo promedio da característica) para indexação de caraterísticas relevantes. Quando aplicado a conjuntos de dados de cancro da mama, o *RMean* permite aumentar o desempenho ao nível do AUC (área debaixo da curva da caraterística de operação do receptor) em quase todos os algoritmos de classificação explorados. Apesar da boa performance do método *RMean,* este método sofre das limitações dos métodos de filtro o que pode levar a desempenhos do sistema CADx abaixo do seu potencial.

Tendo em vista ultrapassar estas limitações, a segunda contribuição propõe um novo método de seleção de caraterísticas (denominado *uFitler*) baseado no teste U de Mann Whitney para ordenar as características por relevância. A avaliação da relevância é feita através do cálculo da separabilidade entre as distribuições de cada classe para cada caraterística. O método *uFilter* resolve alguns dos problemas dos métodos anteriores, tais como: é eficaz a ordenar as caraterísticas por relevância independentemente do tamanho da amostra (sendo tolerante a desequilíbrios nos dados de treino); não necessita de normalização dos dados; e, o mais importante, apresenta um risco baixo de sobreajuste aos dados. Quando aplicado aos conjuntos de dados de cancro da mama em estudo, o *uFilter* obteve melhores resultados com significado estatístico que o teste de U, *RMean* (contribuição 1) e que quatro métodos clássicos de seleção de caraterísticas. Este método mostrou-se competitivo e apelativo em termos de custo-eficiência na seleção de caraterísticas relevantes para sistemas de CADx de Cancro da Mama. Finalmente, um passo complementar, a análise de redundância mostrou ser uma forma eficaz de encontrar subconjuntos ótimos de caraterísticas.

Contents

List of Figures

List of Tables

Acronyms

ACR: American College of Radiology.

ANN: Artificial Neural Networks.

AUC: Area Under the receiver operating characteristic Curve.

BCDR: Breast Cancer Digital Repository.

BI-RADS: Breast Imaging Reporting and Data System.

CAD: Computer Aided Detection/Diagnosis.

CADe: Computer Aided Detection.

CADx: Computer Aided Diagnosis.

CC: Craniocaudal.

CHI2: Chi-Square.

DDSM: Digital Database for Screening Mammography.

DT: Decision Tree.

FFBP: Feed Forward Back-Propagation.

FFDM: Full-Field Digital Mammography.

GLCM: Gray-Level Co-occurrence Matrices.

IG: Information Gain.

kNN: k-Nearest Neighbors.

LDA: Linear Discriminants Analysis.

MCs: Microcalficiations.

MIAS: Mammographic Image Analysis Society.

MLC: Machine Learning Classifier.

MLO: Mediolateral-Oblique.

NB: Naive Bayes.

ROI: Region of Interest.

SFM: Screen-Film Mammography.

SVM: Support Vector Machine.

CHAPTER 1

Introduction

Breast Cancer is a major concern and the second-most common and leading cause of cancer deaths among women [1]. According to published statistics, breast cancer has become a major health problem in both developed and developing countries over the past 50 years. Its incidence has increased recently with an estimated of 1,152,161 new cases in which 411,093 women die each year [2]. In Portugal estimates point to 4500 new diagnosed cases of breast cancer and 1600 women death from this disease [3]. At present, there are no effective ways to prevent breast cancer, because its cause remains unknown. However, efficient diagnosis of breast cancer in its early stages can give a woman a better chance of full recovery. Therefore, early detection of breast cancer can play an important role in reducing the associated morbidity and mortality rates [4].

For research scientists, there are several interesting research topics in cancer detection and diagnosis systems, such as high-efficiency, high-accuracy lesion detection/classification algorithms, including the detection of Calcifications, Masses, etc. Radiologists, on the other hand, are paying attention to the effectiveness of clinical applications of Breast Cancer CAD systems [5].

1.1. Background

1.1.1. Breast Cancer

Cancer occurs as a result of mutations, or abnormal changes, in the genes responsible for regulating the growth of cells and keeping them healthy. The genes are in each cell's nucleus, which acts as the "control room" of each cell. Normally, the cells in our bodies replace themselves through an orderly process of cell growth: healthy new cells take over as old ones die out. But over time, mutations can "turn on" certain genes and "turn off" others in a cell. That changed cell gains the ability to keep dividing without control or order, producing more cells just like it and forming a tumor [6].

A tumor can be benign (not dangerous to health) or malignant (has the potential to be dangerous). Benign tumors are not considered cancerous: their cells are close to normal in appearance, they grow slowly, and they do not invade nearby tissues or spread to other parts of the body. Malignant tumors are cancerous. Left unchecked, malignant cells eventually can spread beyond the original tumor to other parts of the body [6].

Usually breast cancer either begins in the cells of the lobules, which are the milk-producing glands, or the ducts, the passages that drain milk from the lobules to the nipple (see Figure 1 A and B). Less commonly, breast cancer can begin in the stromal tissues, which include the fatty and fibrous connective tissues of the breast (see Figure 1 E). Over time, cancer cells can invade nearby healthy breast tissue and make their way into the underarm lymph nodes, small organs that filter out foreign substances in the body. If cancer cells get into the lymph nodes, they then have a pathway into other parts of the body [6].

Breast cancer is always caused by a genetic abnormality (a "mistake" in the genetic material). However, only 5-10% of cancers are due to an abnormality inherited from your mother or father. About 90% of breast cancers are due to genetic abnormalities that happen as a result of the aging process and the "wear and tear" of life in general [6]. Figure 1 shows an overview of the breast anatomy.

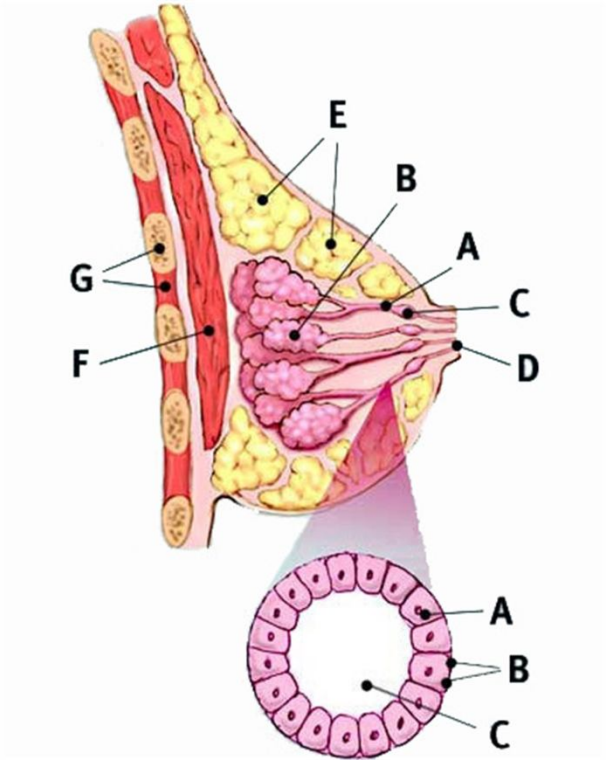

Figure 1 The breast anatomy; A- Ducts, B- Lobules, C- Dilated section of duct to hold milk, D- Nipple, E- Fat, F- Pectoral major muscle and G- Chest wall/rib cage. Cortical section of a duct (enlargement), A- Normal duct cells, B- Basement membrane, C- Lumen (center of duct).

1.1.2. BI-RADS

The Breast Imaging-Reporting and Data System (BI-RADS) Atlas is designed to serve as a comprehensive guide providing standardized breast imaging terminology, a report organization, assessment structure and a classification system for mammography, ultrasound and magnetic resonance image of the breast [7]. It also provides a complete follow up and outcome monitoring system that allows a screening or clinical practice to determine performance outcomes such as the positive predictive value and the percentage of small and node negative cancers. These quality assurance data are meant to improve the quality of patient care [7]. Several studies have shown that the use of BI-RADS in a clinical setting can be useful in predicting the presence of malignancy and improving the choice and efficiency of further necessary examinations [8-10]. It has been widely adopted in clinical practice throughout the world. BI-RADS is also implemented in screening programmes in the United States [11] and Europe [12, 13].

The American College of Radiology (ACR), who is the owner of the BI-RADS atlas, has developed a standard way of describing mammogram findings. In this system, the results are

sorted into BI-RADS categories numbered 0 through 6 [7, 14]. A brief description of what the categories mean is presented:

- Category 0: Additional imaging evaluation and/or comparison to prior mammograms is needed. This means a possible abnormality may not be clearly seen or defined and more tests are needed, such as the use of spot compression (applying compression to a smaller area when doing the mammogram), magnified views, special mammogram views, or ultrasound. This also suggests that the mammogram should be compared with older ones to see if there have been changes in the area over time.
- Category 1: Negative. There's no significant abnormality to report. The breasts look the same (they are symmetrical) with no masses (lumps), distorted structures, or suspicious calcifications. In this case, negative means nothing bad was found.
- Category 2: Benign (non-cancerous) finding. This is also a negative mammogram result (there's no sign of cancer), but the reporting doctor chooses to describe a finding known to be benign, such as benign calcifications, lymph nodes in the breast, or calcified fibroadenomas. This ensures that others who look at the mammogram will not misinterpret the benign finding as suspicious. This finding is recorded in the mammogram report to help when comparing to future mammograms.
- Category 3: Probably benign finding – Follow-up in a short time frame is suggested. The findings in this category have a very good chance (greater than 98%) of being benign (not cancer). The findings are not expected to change over time. But since it's not proven benign, it's helpful to see if an area of concern does change over time.
- Category 4: Suspicious abnormality – Biopsy should be considered. Findings do not definitely look like cancer but could be cancer. The radiologist is concerned enough to recommend a biopsy.
- Category 5: Highly suggestive of malignancy – Appropriate action should be taken. The findings look like cancer and have a high chance (at least 95%) of being cancer. Biopsy is very strongly recommended.
- Category 6: Known biopsy-proven malignancy – Appropriate action should be taken. This category is only used for findings on a mammogram that have already been shown to be cancer by a previous biopsy. Mammograms may be used in this way to see how well the cancer is responding to treatment.

The ACR guidelines [7] also define the BI-RADS reporting for breast density. This report includes an assessment of breast density into 4 groups:

- BI-RADS 1: The breast is almost entirely fat. This means that fibrous and glandular tissue makes up less than 25% of the breast.
- BI-RADS 2: There are scattered fibroglandular densities (low-density). Fibrous and glandular tissue makes up from 25 to 50% of the breast.
- BI-RADS 3: The breast tissue is heterogeneously dense (Isodense). The breast has more areas of fibrous and glandular tissue (from 51 to 75%) that are found throughout the breast. This can make it hard to see small masses (cysts or tumors).
- BI-RADS 4: The breast tissue is extremely dense (High-density). The breast is made up of more than 75% fibrous and glandular tissue. This can lead to missing some cancers.

1.1.3. Mammography

Mammography is a specific type of imaging that uses a low-dose X-ray system to examine the breast, and is currently the most effective method for detection of breast cancer before it becomes clinically palpable. It can reduce breast cancer mortality by 20 to 30% in women over 50 years old in high-income countries when the screening coverage is over 70% [15]. Mammography offers high-quality images from a low radiation dose, and is currently the only widely accepted imaging method used for routine breast cancer screening [16].

There are two types of mammography images capturing systems [17-20]: Screen-Film Mammography (SFM) and Full-Field Digital Mammography (FFDM). In the first one, the image is created directly on film, while the second one takes an electronic image of the breast and stores it directly on a computer [17]. Although both types of mammography present advantages and disadvantages, FFDM has some potential advantages over SFM, due to some limitation such as: limited range of X-ray exposure; image contrast cannot be altered after the image is obtained; the film acts as the detector, display, and archival medium; and film processing is slow and introduces artifacts [21]. All of these limitations have motivated many researchers to develop advanced techniques and algorithms for digital mammography analysis. Therefore, FFDM is overcoming and will continue to overcome the limitations of SFM described before. Some advantages of FFDM are: wider dynamic range and lower noise;

improved image contrast; enhanced image quality; and lower X-ray dose [21]. Despite FFDM have many potential advantages over traditional SFM, examples of clinical trials show that, the overall diagnostic accuracy levels of SFM and FFDM are similar when used in breast cancer screening [20].

According to the breast imaging lexicon described in the BI-RADS atlas, the most common abnormalities seen on a mammography image which lead to recall are: Masses, Calcifications and Microcalcifications and, Architectural distortion [7, 22]; being the first two lesions, the most prominent targets for a wide range of developed CAD systems [23-28].

1.1.4. Masses

A mass is defined as a space occupying lesion seen in at least two different projections [7]. If a potential mass is seen in only a single projection it should be called "Asymmetry" or "Asymmetric Density" until its three-dimensionality is confirmed.

Masses have different density (see BI-RADS section), different margins (circumscribed, microlobular, obscured, indistinct, spiculated) and different shape (round, oval, lobular, irregular). Fat-containing radiolucent and mixed-density circumscribed lesions are benign, whereas isodense to high-density masses may be of benign or malignant origin [29]. Benign lesions tend to be isodense or of low density, with very well defined margins and surrounded by a fatty halo, but this is certainly not diagnostic of benignancy. The halo sign is a fine radiolucent line that surrounds circumscribed masses and is highly predictive that the mass is benign.

Circumscribed (well-defined or sharply-defined) margins are sharply demarcated with an abrupt transition between the lesion and the surrounding tissue [7]. Without additional modifiers there is nothing to suggest infiltration. Two examples of benign mass with oval shape and circumscribed margin are shown in Figure 2. Lesions with microlobular margins have wavy contours. Obscured (erased) margins of the mass are erased because of the superimposition with surrounding tissue. This term is used when the physician is convinced that the mass is sharply-defined but has hidden margins. The poor definition of indistinct (ill-defined) margins raises concern that there may be infiltration by the lesion and this is not likely due to superimposed normal breast tissue.

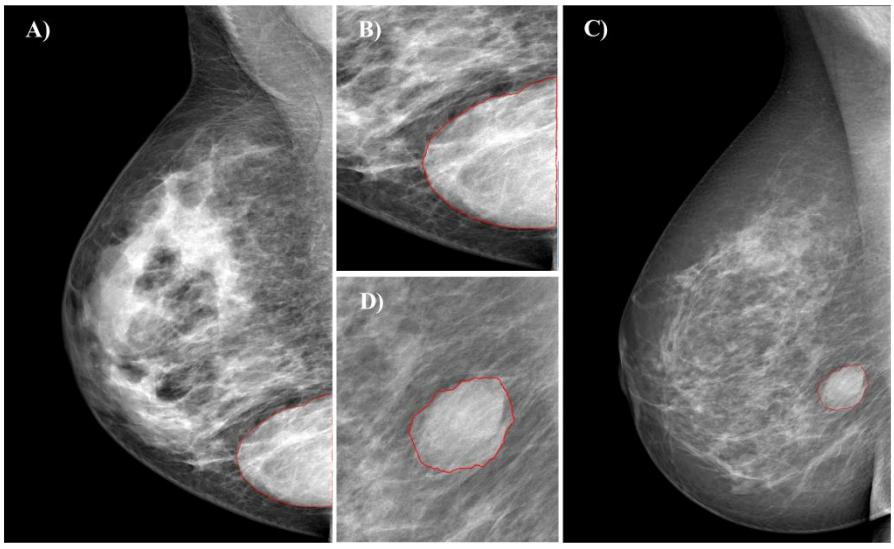

Figure 2 Mediolateral oblique mammograms with oval, well-circumscribed and extremely density mass (diagnosis: benign) in right breast extracted from the public BCDR [30]; A) patient #134 with 23 years old, (B) magnification of the lesion in patient #134; C) patient #429 with 35 years old, D) magnification of the lesion in patient #429.

The lesions with spiculated margins are characterized by lines radiating from the margins of a mass. A lesion that is ill-defined or spiculated and in which there is no clear history of trauma to suggest hematoma or fat necrosis suggests a malignant process [29]. Masses with irregular shape usually indicate malignancy as it is depicted in Figure 3. Regularly shaped masses such as round and oval very often indicate a benign change (see Figure 2).

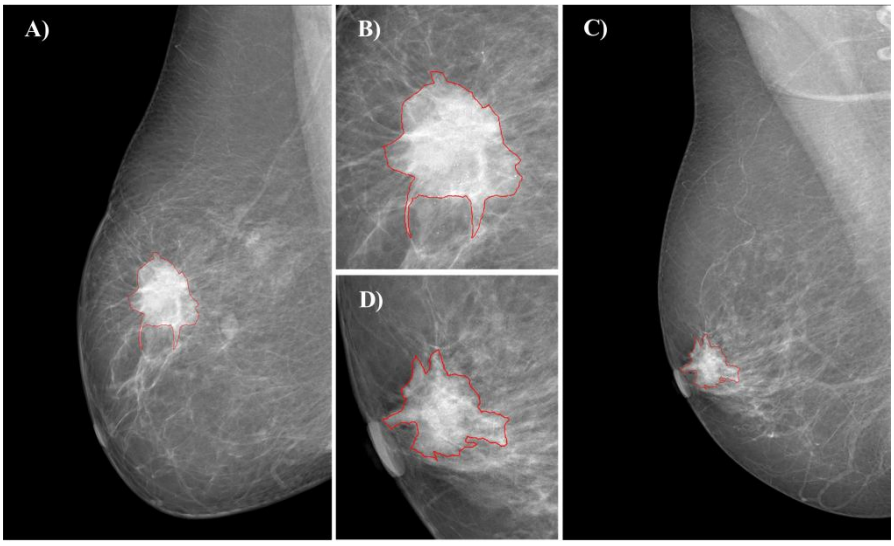

Figure 3 Mediolateral oblique mammograms with irregular, spiculated and entirely-fat density mass (diagnosis: invasive carcinoma) in right breast extracted from the public BCDR [30]; A) patient #105 with 51 years old, (B) magnification of the lesion in patient #105; C) patient #143 with 67 years old.

1.1.5. Microcalcifications

The Microcalficiations (MCs) are tiny granule like deposits of calcium and are relatively bright (dense) in comparison with the surrounding normal tissue [31]. MCs detected on mammogram are important indicator for malignant breast disease. Unfortunately, MCs are also present in many benign variant. Malignant MCs tend to be numerous, clustered, small, varying in size and shape, angular, irregularly shaped and branching in orientation [31]. Benign MCs are usually larger than MCs associated with malignancy. They are usually coarser, often round with smooth margins, smaller in number, more diffusely distributed, more homogeneous in size and shape, and are much more easily seen on a mammogram [7]. One of the key differences between benign and malignant MCs is the roughness of their shape. Typically benign MCs are skin MCs, vascular MCs, coarse popcorn-like MCs, large rod-like MCs, round MCs, lucent-centered MCs, eggshell or rim MCs, milk of calcium MCs, suture MCs and dystrophic MCs [7] (see Figure 4).

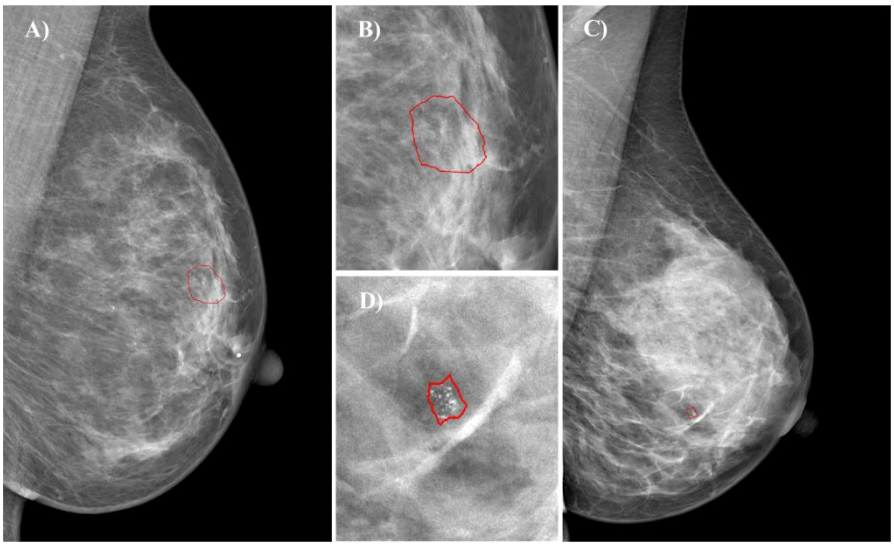

Figure 4 Mediolateral oblique mammograms with cluster of heterogeneous MCs (diagnosis: benign) in left breast extracted from the public BCDR [30]; A) patient #32 with 49 years old, (B) magnification of the lesion in patient #32; C) patient #293 with 48 years old, (D) magnification of the lesion in patient #293.

Malignancy suspicious MCs are amorphous and coarse heterogeneous MCs. Malignancy highly suspicious MCs are fine pleomorphic, fine-linear and fine linear-branching MCs (see Figure 5). While observing MCs it is important to consider their distribution (diffuse, regional, cluster, linear, segmental). In diffuse distribution MCs are diffusely dispersed in the breast. MCs in regional distribution are distributed in larger breast tissue volume (> 2 cm^3) and are very often part of the benign changes. Cluster of MCs is indicated if five or more MCs

are present in small breast tissue volume (< 1 cm^3) and it is shown in Figure 4. Linear distribution of MCs indicates malignant disease. Segmental distribution of MCs also indicates malignant disease, but if the MCs in segmental distribution are larger, smooth and rod-like they indicate benign changes [7].

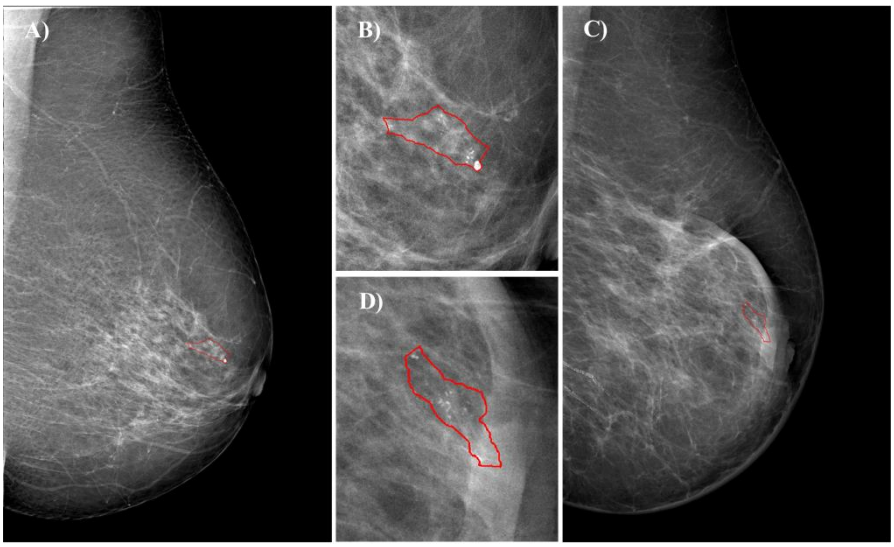

Figure 5 Mediolateral oblique mammograms with fine, pleomorphic MCs in left breast extracted from the public BCDR [30]; A) patient #457 with 58 years old and diagnosed with carcinoma in situs, (B) magnification of the lesion in patient #457; C) patient #488 with 73 years old and diagnosed with invasive carcinoma, (D) magnification of the lesion in patient #488.

An analysis of the MCs as to their distribution, size, shape or morphology, variability, number and the presence of associated findings, such as ductal dilatation or a mass, will assist one in deciding which are benign, which should be followed carefully and which should be biopsied [29]. The size of individual MCs is less important than their morphology for deciding their classification and potential etiology. Variability in size, shape and density of MCs is a worrisome feature, but variability must be assessed in conjunction with morphology [7]. Those MCs with sharp, jagged margins that are variable in appearance are much more likely to be malignant than are variably sized and shaped but smoothly marginated MCs.

1.1.6. Early Detection

Although some risk reduction might be achieved with prevention, these strategies cannot eliminate the majority of breast cancers that develop in low- and middle-income countries. Therefore, early detection in order to improve breast cancer outcome and survival remains the cornerstone of breast cancer control [32].

There are two early detection methods:

- Early diagnosis or awareness of early signs and symptoms in symptomatic populations in order to facilitate diagnosis and early treatment. This strategy remains an important early detection strategy, particularly in low- and middle-income countries where the diseases is diagnosed in late stages and resources are very limited. There is some evidence that this strategy can produce "down staging" (increasing in proportion of breast cancers detected at an early stage) of the disease to stages that are more amenable to curative treatment [16, 32].
- Screening, defined as the systematic application of a screening test in a presumably asymptomatic population. It aims to identify individuals with an abnormality suggestive of cancer [32, 33].

1.1.7. Breast Cancer CAD

Breast Cancer CAD is a supervised pattern recognition task employed with some ambiguity; the literature uses the CAD term to refer both to CADe:Computer Aided Detection (CADe) and the Computer Aided Diagnosis (CADx). While CADe is concerned with locating suspicious regions within a certain medical image (such a mammogram), CADx is concerned with offering a diagnosis to a previously located region. A general architecture of a Breast Cancer CAD system is presented through the following stages [34, 35]:

1. Region of Interest (ROI) selection: the specific image region where the lesion or abnormality is located. The selection can be manual, semiautomatic or fully automatic).

2. Image Preprocessing: the ROI subimage is enhanced so that, in general, noise is reduced and image details are enhanced.

3. Segmentation: the suspected lesion or abnormality is marked out and separated from the rest of the ROI by identifying its contour or a pixels region. Segmentation can be fully automatic (the CAD system determines the region to be segmented), manual or semi-automatic, where the user segments the region assisted by the computer through some interactive technique such as deformable models or intelligent scissors (livewire).

4. Features Extraction and Selection: quantitative measures (features) of different nature are extracted out from the segmented region to produce a features vector. These might include representative image-based features such as: statistics (skewness, kurtosis, perimeter, area, etc.), shape (elongation, roughness, etc.) and texture (contrast, entropy, etc.). Then, the most relevant features are identified for dimensionality reduction of the feature space and, therefore, for reducing also the time consume by the classifiers in the training phase. This occurs according to a single strategy: filter or wrapper methods, or any combination of them: hybrid methods.

5. Automatic Classification: this last step that is crucial for CADx attempts to offer a diagnostic that can be used as a first or second opinion, by assigning the vector of extracted features to a certain class, corresponding to a lesion type and/or a benignancy/malignancy status.

There is good evidence in the literature that Breast Cancer CADx systems can improve the Area Under the receiver operating characteristic Curve (AUC) performance of radiologists (see Table 1). Other studies report that Breast Cancer CADe systems detect around 50 to 77% of clinically missed cancers [36] or find cancers earlier than radiologists [37], but did increase the number of women who needed to come back for more tests and/or to have breast biopsies [38].

Table 1 Overview of some Breast Cancer CADx studies where it is improved the AUC performance of radiologists.

Author	Year	Number of lesions	Setup	AUC without CADx	AUC with CADx
Leichter et al. [39]	2000	40	Singleview	0.66	0.81
Huo et al. [40]	2002	110	Multiview	0.93	0.96
Hadjiiski et al. [41]	2004	97	Multiview, temporal	0.79	0.84
Hadjiiski et al. [42]	2006	90	Multiview, temporal	0.83	0.87
Horsch et al. [43]	2006	97	Multimodal	0.87	0.92
Meinel et al. [44]	2007	80	Multiview	0.85	0.96
Eadie et al. [37]	2012	20071	Multimodal	0.86	0.85

1.1.8. Features Selection Methods

Feature selection methods broadly fall into two main categories, depending on how they combine the feature selection search with the construction of the classification model: the filter (univariate and multivariate) [45-47] and wrapper [48-50] models, and more recently, the hybrid methods, which combine filter and wrapper paradigms as an unique model [51-55]. Wrapper methods utilize a Machine Learning Classifier (MLC) as a black box to score subsets of features according to their predictive power. Meanwhile, filters methods are considered the earliest approaches to features selection within machine learning and they use heuristics based on general characteristics of the data rather than a MLC to evaluate the merit of features [56, 57]. As consequences, filter methods generally present lower algorithm complexity and are much faster than wrapper or hybrid methods.

In Breast Cancer classification problems, the discriminative power of features employed in CADx systems varies: while some are highly significant for the discrimination of mammographic lesions, others are redundant or even irrelevant, which increase complexity and degrade classification accuracy. Hence, some features have to be removed from the original feature set in order to mitigate these negative effects before a machine learning classifier is utilized. The task of redundant/irrelevant feature removal is termed feature selection [58] in machine learning [59].

The feature selection constitutes one of the most important steps in the lifecycle of Breast Cancer CADx systems. It presents many potential benefits such as: facilitating data visualization and data understanding, reducing the measurement and storage requirements, reducing training and utilization times, defining the curse of dimensionality to improve the predictions performance [56, 60]. The objectives are related: to avoid overfitting and improve model performance and; to provide faster and more cost-effective models [61, 62]. Although these benefits, the problem of selecting the optimal subset of features is still a challenging task. Because, it is requires an exhaustive search of all possible subsets of features of the chosen cardinality, which is not practical in most situations as the number of possible subsets given N features is 2^N-1 (the empty set is excluded), which means *NP*-hard algorithms [56]. Hence, in practical machine learning applications, usually a satisfactory instead of the optimal feature subset is searched.

1.1.9. Machine Learning Classifiers

Machine learning classifiers rise at the center of CADx systems as one of the most prominent techniques with a special advantage: the comparable performance to humans. In many radiology applications (see Table 1), CADx systems have shown comparable, or even higher, performance compared with well-trained and experienced radiologists and technologists [37, 40-44, 63-66]. This advantage is supported by the hypothesis that a good machine learning predictor usually will give predictions with low bias and variance at any time. Meanwhile, radiologists' performance may be affected by various factors such as: fatigue, emotion, reading time and environment, etc. In principle, machine learning-based computer systems will perform more consistently than human beings.

A wide variety of MLCs that have been applied to solve the problem of Breast Cancer detection/classification. The Artificial Neural Networks (ANN) [67-75] seem to be the most employed classifier in CADx systems; the Support Vector Machine (SVM) [75-78] appear as the most used classifier in CADe systems and, the Linear Discriminants Analysis (LDA) [23, 28, 79-83] and k-Nearest Neighbors (kNN) [84-88] are also popular in both for CADe and CADx community. Others less frequently classifiers applied in CADx systems include the Naive Bayes (NB) classifier [70, 88-90] and binary Decision Tree (DT) [75, 90-92].

1.2. Motivation and Objectives

With the advances in modern medical technologies and the evolution of different diseases, the amount of imaging data is rapidly increasing as well as the need to improve diseases treatment.

Mammography is currently the only recommended imaging method for breast cancer screening. Mammography is especially valuable as an early detection tool because it can identify breast cancer before physical symptoms appears. However, the high sensitivity of mammography is accomplished at a cost of low specificity. As a result, only 15–30% of patients referred to biopsy are found to have malignancy [93]. Unnecessary biopsies not only cause patient anxiety and morbidity but also increase health care costs.

Another useful and suggested approach is the double reading of mammograms (two radiologists read the same mammograms) [33], which has been advocated to reduce the

proportion of missed cancers, but the workload and cost associated are high. Therefore, it is important to improve the accuracy of interpreting mammographic lesions, thereby increasing the positive predictive value of mammography.

Breast Cancer CAD systems are recent valuable auxiliary means, which have been proven that can improve the detection/classification rate of cancer in its early stages (see "CADe and CADx Systems in Breast Cancer" section in Chapter 2). Despite these prominent results, current research suggests that a CAD system is not a substitute for an experienced radiologist in the procedure for reading mammograms. Thus, the performance of current and future CADe and CADx systems still needs to be improved [20, 94].

The core of any Breast Cancer CADx system is the set of image processing and pattern recognition methods [95], and the good performance will depend in a high grade upon the quality of the implementation (e.g. segmentation, feature extraction/selection and classification). It is therefore convenient that feature selection methods are fast, scalable, accurate and possibly with low algorithmic complexity.

This work aims to improve the process of feature selection specifically to support the development of best performed Breast Cancer CADx systems.

As it was mentioned before, the feature selection methods are mainly divided in two paradigms: filter and wrapper. We considered exploring the filter paradigm (univariate and multivariate) over the wrappers or hybrid models; because of filter methods provide lower algorithmic complexity, faster performance and are not dependent of classifiers. It means that filter methods analyze the characteristics of data for ranking the entire features space, while the wrappers or hybrid methods are extremely dependent of classifiers for selecting a satisfactory subset of features.

The principal limitation of univariate filter methods, such as Chi-Square (CHI2) discretization [96], t-test [97], Information Gain (IG) [98] and Gain Ratio [99], are that they ignore the dependencies among features and assume a given distribution (Gaussian in most cases) from which the samples (observations) have been collected. In addition, assuming a Gaussian distribution includes the difficulties to validate distributional assumptions because of small sample sizes. On the other hand, multivariate filters methods such as: Correlation based-feature selection [97, 100], Markov blanket filter [101], Fast correlation based-feature selection [102], Relief [103, 104] overcome the problem of ignoring feature dependencies

introducing redundancy analysis (models feature dependencies) at some degree, but the improvements are not always significant: domains with large numbers of input variables suffer from the curse of dimensionality and multivariate methods may overfit the data. Also, they are slower and less scalable than univariate methods [56, 57].

In order to overcome these limitations on existing filter methods, which may lead the Breast Cancer CADx methods to classification performances bellow of its potential, we considered the following objectives:

- **Objective 1:** to explore new ensembles of established feature selection method to improve Breast Cancer classification.
- **Objective 2:** to develop a novel and highly performing feature selection method based on the filter paradigm for ranking relevant features extracted from mammographic lesions.
- **Objective 3:** to validate the usefulness of the developed feature selection methods throughout the integration in the lifecycle development of Breast Cancer CADx methods.

1.3. Thesis Statement

The above objectives and consequent work was therefore carried out to prove the following set of hypothesis:

- **Hypothesis 1:** Feature selection methods supported on the filter paradigm can be improved by the creation of new ensemble methods.
- **Hypothesis 2:** Feature selection methods of the filter paradigm can be improved throughout a new filtered function, which provides index of features with better separability between two instance distributions.
- **Hypothesis 3:** Breast Cancer CADx systems can be advanced by the inclusion of a new feature selection method that provides features with more discrimination power to yield better AUC-based classifier performance.

1.4. Summary of Contributions

The following theoretical and technical contributions were obtained as part of this thesis work.

Theoretical:

- An ensemble feature selection method (we named *RMean*), supported on the filter paradigm, which surpasses traditional methods when used for indexing relevant features extracted from mammographic pathological lesions (image-based and clinical features).
- A novel feature selection method (named *uFilter*) based on the Mann Whitney U-test for ranking relevant features, which assess the relevance of features by computing the separability between class-data distribution of each feature.
- An improvement in the performance of machine learning classifiers supporting Breast Cancer CADx methods.

Technological:

- A JAVA and MATLAB framework for Breast Cancer data analysis.
- A JAVA source code plug-in for integrating the proposed *uFilter* feature selection method within the public WEKA data mining software version 3.6.

1.5. Thesis Outline

The structure of this thesis is described as follows:

- **Chapter 1** is this introduction, that provides a general background of Breast Cancer, BI-RADS lexicon, mammography images and lesions: Masses and Microcalcifications; Breast Cancer early detection procedure, practical Breast Cancer detection techniques: Mammography screening, double reading and Breast Cancer CAD methods. There is also a brief description of the importance of feature selection techniques and machine learning classifiers as support methods of Breast Cancer CAD

systems. Finally, we describe the context that motivated the development of this thesis, its objectives and summarized its contributions.

- **Chapter 2** describes the current state of the art of the principal topics related to the proposed objectives: (1) Breast Cancer supporting repositories, (2) Clinical and image-based descriptors for Breast Cancer, (3) A comprehensive explanation of feature selection methods: the most important feature selection paradigms, the main algorithms, as well as advantages and disadvantages of them, (4) A detailed description of the most used Breast Cancer machine learning classifiers and (5) CAD methods in Breast Cancer, which surveys several successful CADe and CADx systems, involving methods and techniques used for detection/classification of microcalcifications and masses.

- **Chapter 3** details the experimental methodologies used in this thesis, such as: datasets description; the elected clinical and image-based descriptors; exploration of machine learning classifiers and features selection methods. We also present the description and experimental evaluation of the *RMean* feature selection.

- **Chapter 4** addresses the theoretical description and experimental evaluation of the proposed *uFilter* method. We introduce a formal framework for understanding the proposed algorithm, which is supported on the statistical model/theory of the non-parametric Mann Whitney U-test. In addition, a software prototype implementation of the *uFilter* method using these theoretical intuitions is presented.

- **Chapter 5** presents the conclusions of this thesis and outlines the future lines of work opened by its contributions.

1.6. Auto-Bibliography

This Thesis is based primarily on the following publications:

Chapter 3:

- *"Ensemble features selection method as tool for Breast Cancer classification"*, in Advanced Computing Services for Biomedical Image Analysis. International Journal of Image Mining, InderScience, 2015. (Accepted)

- *"Improving the performance of machine learning classifiers for Breast Cancer diagnosis based on feature selection"*, in Proceedings of the 2014 Federated Conference on Computer Science and Information Systems. M. Ganzha, L. Maciaszek, and M. Paprzycki (Eds.), IEEE, Warsaw, Poland, 2014, pp. 209-217. http://dx.doi.org/10.15439/2014F249.

- *"Improving Breast Cancer Classification with Mammography, Supported on an Appropriate Variable Selection Analysis"*, Proc. SPIE 8670, Medical Imaging 2013: Computer-Aided Diagnosis, 867022 (February 26, 2013); http://dx.doi.org/10.1117/12.2007912

- *"Evaluation of Features Selection Methods for Breast Cancer Classification"*, ICEM15: 15th International Conference on Experimental Mechanics, FEUP-EURASEM-APAET, Porto/Portugal, 22-27 July 2012. ISBN: 978-972-8826-26-0.

Chapter 4:

- *"Improving the Mann–Whitney statistical test for feature selection: An approach in breast cancer diagnosis on mammography"*, Artificial Intelligence in Medicine, 2015, vol. 63, no. 1, pp. 19-31. http://dx.doi.org/10.1016/j.artmed.2014.12.004.

Other Related Publications:

- *"Grid Computing for Breast Cancer CAD. A Pilot Experience in a Medical Environment"*, In 4rd Iberian Grid Infrastructure Conference Proceedings. 2010: p. 307-318. Netbiblo, 2010. ISBN: 978-84-9745-549-7.

- *"Grid-based architecture to host multiple repositories: A mammography image analysis use case"*, Ibergrid: 3rd Iberian Grid Infrastructure Conference Proceedings, 2009: p. 327-338. Netbiblo, 2009. ISBN: 978-84-9745-406-3.

- *"A CAD Tool for mammography image analysis. Evaluation on GRID environment"*, in 3º Congresso Nacional de Biomecânica. 2009. Bragança, Portugal: Sociedade Portuguesa de Biomecânica. pp. 583-589. ISBN 978-989-96100-0-2.

CHAPTER 2

State of the Art

Among several research areas covered by the Breast Cancer CAD systems, in this chapter it is made a revision of critical topics, such as: (1) Breast Cancer supporting repositories, which presents a brief description of a wide range of publicly accessible breast cancer repositories; (2) Clinical and image-based descriptors for Breast Cancer that outlines several important image-based features extracted from detected pathological lesions on mammography images; (3) Feature selection methods, which describes the most important feature selection paradigms, the algorithms, as well as advantages and disadvantages of them; (4) Machine learning classifiers from the radiologists point of view, thus, it is addressed the most used classifiers employed in Breast Cancer detection/classification; and (5) CAD methods in Breast Cancer, this section surveys several successful CADe and CADx systems, their methods and techniques used for detection/classification of MCs and masses.

2.1. Breast Cancer Supporting Repositories

Currently, there are numerous Breast Cancer databases available to the research community, some public and others private - restricted to particular institutions (i.e. the massive database provided by the National Digital Medical Archive Inc, USA, that holds over a million mammography images [105]). Although the increasing effort of different research groups into satisfy different aspects of the ideal Breast Cancer database (more simple and well documented), each database is unique; not only are the cases different or the proportion of subtle cases versus obvious cases are different, more importantly, often do not contain all the requirements needed for a research purpose [106-110]. Therefore, different databases have different strengths and weaknesses. Due to this, it is very difficult to compare the performance of different algorithms, methods and techniques as well as to determine which would be the most useful. The Breast Cancer Digital Repository (BCDR) [30], the Mammographic Image Analysis Society (MIAS) database [111] and the Digital Database for Screening Mammography (DDSM) [112] are easily accessed databases and thus they are considered the most commonly used databases in the scientific community.

The BCDR which is the first Portuguese breast cancer image database, with anonymous cases from medical records supplied by the Faculty of Medicine "Centro Hospitalar São João" at University of Porto, Portugal [30]. BCDR is composed of 1730 patient cases with mammography and ultrasound images, clinical history, lesion segmentation and selected pre-computed image-based descriptors, for a total of 5776 images. Patient cases are classified using the BI-RADS classification and annotated by specialized radiologists (276 biopsies proven at the time of writing).

The MIAS database [111] is formed by 322 Mediolateral-Oblique (MLO) mammography image view. In this database, the image files are available in PNG (portable network graphics) format with a resolution of 1,024 x 1,024 pixels, which are also annotated with the following information: a database reference number indicating left and right breast, character of background tissue, pathology, class of lesion present and coordinates as well as size of these lesions.

The DDSM database [112] is the largest public database. Officially contains 2479 cases including two images of each breast, acquired in Craniocaudal (CC) and MLO views that have been scanned from the film-based sources by four different scanners with a resolution

between 50 and 42 microns, for a total of 9916 images with all types of findings (normal, benign and malign cases). These images are coded according to the Lossless Joint Pictures Expert Group (LJPEG) standard format and its conversion is necessary before using it.

Besides, there are more recent public developed projects of mammographic image databases. All of them available after the web-accessible registration: The BancoWeb LAPIMO (acronym of *"Laborátorio de Análise e Processamento de Imagens Médicas e Odontológicas"*) Database [113] it is a public repository which contains 320 cases, 1473 images (MLO and CC views) divided in normal images, and images with benign and malign findings. Also background patient information along with BI-RADS annotations is available.

The INbreast database [114] contains a total of 115 patient cases representing 410 images (MLO and CC) provided by the Breast Center located at the "Centro Hospitalar de São João, Porto" and in compliance with the Portuguese National Committee of Data Protection and Hospital's Ethics Committee. The images files are FFDM with a solid contrast resolution of 14 bits acquired by a MammoNovation Siemens scanner. As a ground truth, all annotations were based on the lesions contour made by specialists.

The Image Retrieval in Medical Applications (IRMA) project [115, 116] is an integration of four mammographic databases in which standardized coding of tissue type, tumor staging, and lesion description was developed according to the ACR tissue codes and the BI-RADS. IRMA database is containing 10,509 reference images divided into three categories: normal cases (12 volumes), cancer cases (15 volumes) and benign cases (14 volumes); each case may have one or more associated Pathological Lesions (PLs) segmentations, usually in MLO and CC images of the same breast.

The Dr. Josep Trueta [117] is a non-public database, which contains 320 images files representing both the MLO and CC image view of 89 archived patient cases. All images were acquired using a Siemens Mammonat Novation scanner with a resolution of 70 microns (12-bits contrast resolution) and two different image sizes depending on the breast size are included: 2560 x 3328 or 3328 x 4096 pixels. The ground truth is based on the center and radius of the circle surrounding the selected ROI (all kind of lesions).

The Nijmegen [106, 118] database is widely used by researchers developing computerized methods for detecting clustered Microcalcifications in mammograms. It is composed by 40 images belonging to 21 patient cases acquired from the National Expert and Training Centre for Breast Cancer Screening and the Department of Radiology at the University of Nijmegen,

the Netherlands. All images were SFM (recorded using various type of equipment) with a contrast resolution of 2048 x 2048 pixels and corrected for inhomogeneity of the light source.

Other mammographic databases such us: the Mammography Image reading for Radiologists and Computers Learning (MIRaCLe) [119], the Lawrence Livermore National Laboratories (LLNL) [120] and Málaga [117] are cited in the literature. However, most of them are not available and consequently details were difficult to found. A brief description of these databases could be found in Table 2.

Table 2 Brief description of developed mammographic databases.

Database	Total of images	Views	Lesion type	Ground truth
BCDR	5776	MLO, CC and Ultrasound	All kinds	Lesion contour
MIAS	322	MLO	All kinds (with special concentration of spiculated masses)	Center and radius of a circle around the interest area
DDSM	9916	MLO and CC	All kinds	Boundary chain code of the findings
BancoWeb	1400	MLO, CC and other	All kinds	ROI is available in a few images only
INBreast	410	MLO and CC	All kinds	Lesion contour
IRMA	10509	MLO and CC	All Kinds	Boundary chain code of the findings
Trueta	320	MLO and CC	All kinds	Center and radius of a circle around the interest area
Nijmegen	40	MLO and CC	MCs	NA
MIRAcle	204	NA	NA	ROI of findings
LLNL	198	MLO and CC	MCs	Binary image of MCs clusters; Contour and area of few MCs
Málaga	NA	MLO and CC	Masses	NA

NA – Not available.

2.2. Clinical and Image-based Descriptors for Breast Cancer

2.2.1. Clinical Descriptors

According to the ACR, which is the copyright owner of the BI-RADS Atlas, clinical descriptors are related to morphological description, distribution and location of pathological lesions in mammography images [7]. These descriptors were selected on the basis of their ability to discriminate between benign and malignant findings and represent the patient associated metadata.

There are three morphological categories to describe breast lesions: focus/foci, mass and non-mass-like enhancements (calcifications in most cases). A focus/foci is a breast lesion smaller than 5 mm. A mass is a lesion characterized by the shape, which can be round, oval lobulated and irregular; the margin, which could be obscured, irregular and speculated and, the internal mass enhancement characteristics such as: homogeneous, heterogeneous, rim enhancement, dark internal septations, enhancing internal septatios, and central enhancement. The non-mas-like enhancement category is characterized by different distribution patterns: focal, linear, ductal, segmental, regional, multiple regions and diffuse. Furthermore, the distribution patterns can be defined by internal characteristics, which includes homogeneous, heterogeneous, stippled/punctate, clumped and reticular/dendritic, and whether the enhancement is symmetric or asymmetric between both breasts [7].

The location of the lesion is described using the clinical orientation extrapolated from the film location where the patient's breast is considered the face of a clock facing the observer (radiologist). The first option to describe the location is the uses of quadrants (upper outer quadrant, upper inner quadrant, lower outer quadrant and lower inner quadrant). The utilization of both the clock face (left or right or both for side) and quadrants provides an internal consistency check for possible right-left confusion. Usually, the side is given first, followed by the location and depth (anterior, middle and posterior) of the lesion. The location of the lesion under and behind the nipple are considered subareolar and central regions respectively [7].

Furthermore, the inclusion of a statement describing the general breast tissue type arose from evidence in the literature establishing that increased breast density is accompanied by

decreased sensitivity. There is good evidence that increased breast density also is related with increased risk of breast cancer [121, 122]. Thus, the inclusion of four categories describing the breast density in the standard mammography report improves the communication of predicted mammographic performance and breast cancer risk [7].

Sometimes, a finding cannot be adequately described by a single descriptor. This is often true with calcification lesions and its margin characteristics. Calcifications may include several different types (punctate and amorphous); if one type predominates, a single descriptor may be the best; if not, multiple descriptors may be preferred [7]. For example, the work of Burnside et al [123] evaluates MCs descriptors (distribution or morphology) to help stratify the risk of malignancy. The study used a population of 115 women cases and the Fisher exact test was performed to determine significant difference between each descriptors. As result, each calcification descriptor was able to help stratify the probability of malignancy as follows: coarse heterogeneous (7%), amorphous (13%), fine pleomorphic (29%), and fine linear (53%).Also, the statistical test of Fisher revealed a significant difference among these descriptor categories ($p = 0.005$).

The same flexibility should be considered when describing masses margins. Sometimes, they could be partially obscured by surrounding glandular tissue. If the margin is at least 75% circumscribed and 25% obscured, the mass can be classified according to its circumscribed margin. In opposite, if the margin is partially circumscribed and partially indistinct, the classification will be on the basis of its indistinct margins [7].

Clinical descriptors presented in the BI-RADS lexicon constitute a quality assurance tool reducing confusion in breast imaging interpretations [7, 124]. Moreover, recently researches have been using combinations of clinical and image-based descriptors for improving the breast cancer classification performance [75, 88].

2.2.2. Image-based Descriptors

Breast abnormalities present varying diagnostic information on mammograms. The diagnostic features vary in terms of shape, density, texture and distribution. Many studies therefore have focused on analyzing extracted image-based descriptors from MCs and masses on mammographic. An overview of most employed group of image-based descriptors for MCs detection/classification could be observed in Table 3.

Mammographic Microcalcifications Descriptors

According to the clinician procedure of radiologists, MCs clusters can be characterized by its morphology and location, the morphologies of the individual calcification particles, and the distribution of the particles within the cluster. Different approaches for automatic characterization of calcifications simulate the radiologists' strategy, and hence, four principal classes of features for the discrimination of MCs clusters can be defined: features based on the morphology and location of the cluster, morphology-based features of individual microcalcification particles, features based on the spatial distribution and optical density of the individual particles within the cluster, and texture-based features of the MCs surrounding background tissue [125].

Morphology and Location of Microcalcifications Clusters

Several researchers considered the representation of the cluster shape based on the calculation of the convex hull of the centroids or the contour pixels of the particles in a cluster. From this shape representation, a set of descriptors such as: area, perimeter, circularity, rectangularity, orientation, eccentricity and normalized central moments can be computed. Another important feature that describes the morphology of a MCs cluster is the number of individual calcification particles in the cluster. This feature is very often employed for the characterization of MCs clusters and can easily be obtained from a segmentation of the individual MCs [28, 77, 86, 126]. Also, the MC coverage, which is defined by the ratio of the sum of the individual MC areas and the cluster area, is used to describe how densely packed a cluster is with MCs.

The location of the MCs cluster is another important aspect to be considered when analyzing the probability of malignancy of a breast lesion. According to the ACR, malignant lesions are more often located in the upper outer quadrant than other quadrants of the breast [7]. Hence several approaches prefer the computation of location-based features of the MCs clusters in the mammogram. For example in [86], It was used the relative distance of a cluster to the pectoral muscle and the breast edge as discriminative features. It is important to note that extracting features based on the location usually require a robust segmentation method for structures like the nipples, pectoral muscle, and breast boundary in the mammograms, which is a complex problem.

Morphology of an Individual Microcalcification

Usually, a set of statistics features such as: mean, standard deviations, minimum, maximum, or median are computed from an individual MC in a cluster. Many approaches considered the computation of the mean and standard deviations from previously computed shape descriptors like the areas, perimeters, circularities, rectangularities, orientations, and eccentricities of the MCs [77, 78, 86, 110, 126-128]. Also, the means and standard deviations of the individual normalized central moments as well as of the moments of the border pixels are used by some researchers [78, 126, 129, 130].

Veldkamp and Karssemeijer [86] employed a set of 16 image-based (intensity and shape) descriptors extracted from MCs lesions on ipsilateral images view (MLO and CC). The AUC-based classification performance of the kNN classifier was 0.83 for a dataset of 90 patient cases. Kallergi [126] employed 13 image-based descriptors extracted from the morphology of individual MCs and the distribution of the clusters. The best result was obtained when including the patient's age as input in the classification scheme, achieving an AUC of 0.98.

Zhang et al. [73] used two categories of features extracted from MCs in a two-step procedure to reduce the false positive rate. The set of descriptors included spatial and morphological features: average gray level of the foreground and background, standard deviation of the gray-level of the foreground and background, compactness, moment, and Fourier descriptor. Also, features related to the MCs cluster were added to the set of features. In the first step of the detection procedure was used only MCs features to reduce the false detection. In the second step were included two more MCs clusters features (cluster region size and cluster shape rate) to reduce the false detection rate. Experimental results using a back-propagation neural network showed that the method could reduce the false detection rate by 42% (3.15 per image).

Leichter in [131] analyzed the influence of two type of features in the diagnostic role. The selected features were: eccentricity (reflecting the geometry of clusters) and, the shape factor and number of neighbors (reflecting the shape of the individual MC). The analysis was performed using a dataset formed by 324 clustered of MCs (with biopsy-proven). According to the obtained classification result (AUC value of 0.87) by a linear discriminant analysis, it was possible to conclude that the cluster geometry feature was more effective in differentiating benign from malignant clusters than was the shape of individual MC.

Chan et al [132] compared two set of MCs features (morphological and texture) for discriminating between benign and malignant lesions. Morphological descriptors were related to size, contrast, shape of MCs and their variations within clusters. Meanwhile, texture descriptors were all derived from the spatial grey-level dependence matrices constructed at different distances and directions. The combined morphological and texture features achieved an AUC of 0.89, which increased to 0.93 when averaging discriminant scores from all views of the same cluster. This result was superior when comparing with the obtained result by using morphological features (0.79) or texture features (0.84) alone.

Spatial Distribution and Optical Density of Microcalcifications

Two of the most employed features for describing the spatial distribution of MCs inside a cluster are the mean and standard deviation of the computed distances between individual MCs [84, 133]. Other interesting features but used in less degree are the eccentricity and the normalized central moments of the MC centroids. The research of Leicheter [134] describes a more complex scenario for using the mean as a spatial distribution feature. In this case is used the two-dimensional Delaunay triangulation of the MCs centroids for obtaining the k-number of nearest neighbors of the MCs inside the cluster, then, the mean of these k-neighbors is obtained. In others approaches, the mean and variance of grey values and the contrast of individual MCs have been employed for describing the optical density of MCs [77, 86, 129, 133].

Texture of Microcalcifications

The texture features based on the Haralick's descriptors constitute a powerful set of image-based features, which have been widely used for describing MCs lesions [78, 84, 129, 132, 135-137]. They are extracted from the Gray-Level Co-occurrence Matrices (GLCM) and represent the second-order statistics of the grey levels in a ROI [138]. Also, the texture analysis based on the wavelet descriptors has demonstrated to be important for MCs characterization [84, 129].

Dhawan et al [84] used two set of texture features extracted from GLCM and wavelet from ROIs containing MCs lesions. They reported an obtained AUC of 0.86 in the classification of 191 “difficult to diagnose” cases. Soltanian-Zadeh et al [129] compared the performance of four features sets (GLCM based, shape, wavelet and multiwavelet features); the multiwavelet

features, which use multiple scaling functions and mother wavelets outperformed the other three features sets, achieving an AUC of 0.89.

Mohanty et al [137] proposed a new system for breast cancer classification based on the technique of the association rule mining. The system used a set of 26 features extracted from the first and second-order statistics of MCs lesions. These features were enough (according to the minimization of the classification error) for differentiating between normal and cancerous breast tissues.

Malar et al [70] used three different set of features extracted from the GLCM, Gabor filter bank and wavelet transformation, for the discrimination of MCs from the normal tissue. The method was validated using a dataset formed by 120 ROIs containing normal and MCs images. The results highlighted that extreme machine learning produced better classification accuracy (94%) when using wavelet features.

Yu et al. in [139] presented a two-stage method for detecting MCs in digital mammograms. The first stage used a wavelet filter according to the mean pixel value for the detection of MCs. Subsequently, in the second stage is used a Markov random field model to extract textural features from the neighborhood of every detected calcification. These textural features in combination with other three auxiliary features (the mean pixel value, the gray-level variance, and a measure of edge density) were used as inputs for both the Bayes and Feed Forward Back-Propagation (FFBP) neural network classifiers. The method was evaluated using 20 mammograms containing 25 areas of clustered MCs. As results, the method was able to reject false positive in a 98.9% of the cases with a sensitive of 92%, at 0.75 false positive per image.

AbuBaker et al. in [140] presented a study of the characteristics of true MCs compared to falsely detected MCs using first (mean, entropy, standard deviation, moment3, kurtosis) and second (angular second moment, contrast, absolute value, inverse difference, entropy, maximum probability) order statistical texture analysis techniques. These features were generated with the intention of reducing the false positive ratio on mammogram images. As result, it can successfully reduce the ratio of false positives by 18% without affecting the ratio of true positives (currently 98%).

The application of fractal geometry for MC analysis in mammography images have been also reported in the literature [141-143]. Its applicability is justified by the fact of being the MCs

clusters tiny bright spots with different size and shape embedded in a non-homogeneous background surrounding of breast tissue. This particular situation allows the opportunity of using fractal geometry analysis by considering the MCs cluster as a fractal normal background superimposed by a non-fractal foreground [144, 145].

Rangayyan and Nguyen in [143] demonstrated that the computation of the fractal dimension of MCs contours based on the grid method facilitates the discrimination between benign and malignant clusters. Also, the efficiency was superior when comparing with other shape factor methods such as: compactness, the spiculation index, fractional concavity, Fourier factor.

Table 3 Overview of most employed group of image-based descriptors for MCs detection/classification.

Descriptors	Description	References
Individual MC features	Features extracted from mammogram directly such as perimeter, area, compactness, elongation, eccentricity, thickness, orientation, direction, line, background, foreground, distance, and contrast. They are easy to extract and they originate from the experience of radiologists.	[58, 73, 75, 77, 86, 129, 132, 137, 146-149]
Grey Level Co-occurrence Matrix features	Features extracted from GLCM.	[70, 75, 78, 84, 129, 132, 135, 137, 140]
Wavelet features	Energy, entropy, and norm extracted from the wavelet transform sub-images.	[70, 84, 129, 139, 150, 151]
Border information features	Features extracted from MCs border information.	[78, 126, 129, 130]
Fractal dimension	Features extracted from fractal model of the image	[76, 141-145, 152-154]
Cluster features	Features used to describe the distribution of the MCs; area, perimeters, circularity, rectangularity, orientation, and eccentricity.	[77, 78, 86, 126-128, 133, 134, 155]

Mammographic Masses Descriptors

Similar to MCs lesions, most approaches to the feature extraction for mammographic masses are based on the lesion attributes that are used by radiologists in the clinician procedure. They characterize masses based on their shape (also called morphological or geometrical features), the characteristics of their margin, and their texture [7]. The standard approach is to compute margin, shape, and texture related features from the mass and its surrounding tissue and use them as inputs to a classifier to obtain a malignancy score. An overview of most employed group of image-based descriptors for masses detection/classification is shown in Table 4.

Shape and Margin of Masses

Most benign masses are homogeneous and possess well-defined edges; malignant tumors typically have fuzzy or ill-defined boundaries. Benign masses possess smooth, round, or oval shapes with possible macrolobulations, as opposed to malignant tumors which typically exhibit rough contours with microlobulations, spiculations, and concavities (see Figure 6) [7, 156]. Based on the segmentation of the mass contour, several studies have therefore focused on analyzing the margin and shapes of mammographic masses [28, 81, 157-159]. Similar to the approaches used to represent the morphology of individual Microcalcification particles; these include the area and the perimeter as well as the circularity, rectangularity, orientation, and eccentricity of the mass.

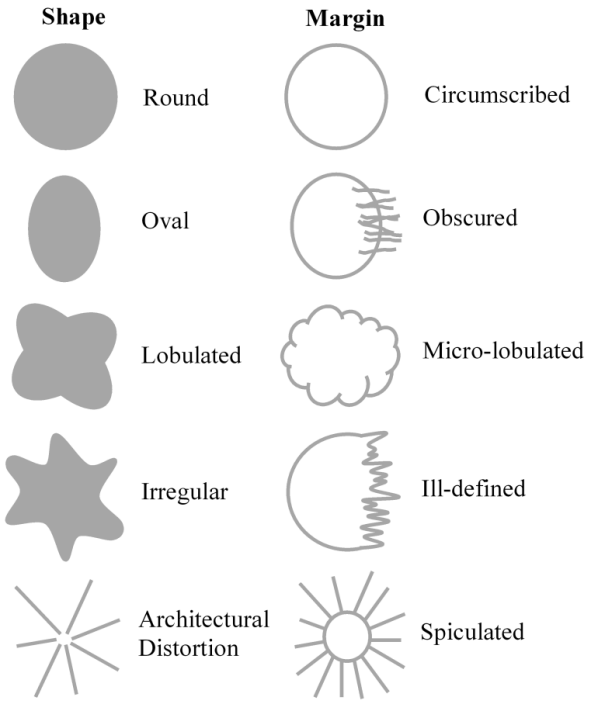

Figure 6 Characteristics of shape and margins of masses.

Rojas and Nandi [160] developed a mass classification method based on two automated segmentation methods: the dynamic programming based boundary tracking and constrained region growing. They simplified the initial mass contours (after segmented) by modelling the set of points as ellipses. Subsequently, a total of six features describing the mass margins were extracted for further classification. The features were: contrast between foreground and background regions, the variation coefficient of edge strength, two measures of the fuzziness

of mass margins, a measure of spiculation based on relative gradient orientation, and a measure of spiculation based on edge-signature information. As results, it was found there is a difference of 14% in the segmentation accuracy and a 4% of difference in the classification performance between both methods. Also, it was observed that the spiculation feature (based on edge-signature information) was clearly better than the remaining features; however, this feature is sensible to changes in the quality of the segmentation.

In [161], Liu et al. proposed a method for mass classification based on the combination of the level set segmentation and shape analysis. The method used as starting point the initial mass contour made by radiologists as input to the level set segmentation method in order to obtain the final contour. Then, a set of shape features were extracted from the segmented masses for further classification using the LDA and SVM classifiers. The evaluation of 292 ROIs from DDSM mammogram images highlighted the best area under the ROC curve of 0.8803 when using the Fourier descriptor of normalized accumulative angle feature.

Rangayyan et al. in [107] introduced two new shape factors, spiculation index and fractional concavity, and applied them for the classification of manually segmented mammographic masses. The combined use of the spiculation index, fractional concavity, and compactness yielded a benign-versus-malignant classification accuracy of 81.5%. Similar approach was presented by Guliato et al. [24], which developed a method that preserve the details of spicules and diagnostic by generating polygonal models of contours. The classification performance used a set of 111 contours representing 65 benign and 46 malignant masses was an AUC value of 0.94.

Zheng and Chan in [92] proposed an algorithm for masses detection based on the combination of several artificial intelligence methods. First, the fractal analysis was performed for the initial selection of suspicious regions. Then, it is applied a multi-resolution Markov random field algorithm for lesions segmentation. Finally, a classification based on the lesions shape is performed for reducing the proportion of false positive. The obtained results on 322 images from the Mini-MIAS databases highlighted a sensitive value of 97.3% with a 3.9 false positives per image.

Furthermore, features based on the normalized radial length and the normalized chord length has been used to represent the mass shape [79, 80, 85]. The normalized radial length is defined as the Euclidean distance of each pixel on the object contour to the object's centroid.

Meanwhile, the definition of the normalized chord length is defined as the Euclidean distance of pair of points on the object boundary.

Besides, in Zheng et al. [85] two features for describing masses margin have been proposed. The features are: the standard deviation and the skewness of the gradient strength of the mass contour. Spiculated margins are a symptom of malignant masses, thus, the texture analysis on bands close to the margin of a segmented mass is important. This idea is extended in the approach of Shi et al. [23], they developed a new feature (margin abruptness) that measures the margin sharpness by using line detection in rubber-band-straightening transform images. Moreover, in Mudigonda et al. [162] is proposed two features (to measure the sharpness) based on the image gradient in a band of pixels surrounding the mass contour.

Varela et al. [27] proposed a new method for describing the mass margins in order to improve the binary (benign and malignant) classification performance. The mass margin features used by this method aims to measure the sharpness of the margin and the presence of microlobulations. The AUC-based results using a dataset formed by 1076 biopsy proved masses from the DDSM database were 0.69, 0.76 and 0.75 for interior, border and outer mass segment respectively. Moreover, the classification performance using a combination of mass segments (interior, border and outer) was 0.81 for image-based and 0.83 for case-based evaluation. In this research was concluded that sharpness features perform better than microlobulation features for masses classification.

Huo et al [74] used a set of features extracted from the margins and density of masses for feeding three different machine learning classifiers. The best result (AUC value of 0.94) was obtained by using a hybrid method consisting of a step rule-based method with a spiculation measure followed by an ANN on a dataset formed by 95 masses. In another experiment, the same classification model was employed on a dataset of 110 masses and it attained an AUC value of 0.82 [163].

Texture of Masses

Similar to feature extraction for MCs, features based on the GLCM, gray-level run length metrics and wavelet decompositions have been popular for the characterization of masses [27] [162] [76, 164, 165]. However, in contrast to the diagnosis of MCs, in mass approaches, the

texture analysis is not always performed on the entire ROI; sometimes the analysis is carried out on a particular region within the ROI i.e. on bands of pixels close to the mass margin.

Mudigonda et al in [162] used texture features and two gradient-based measures to estimate the sharpness of a mass contour. On a database of 53 mass lesions they obtained AUC values of 0.73, 0.84 and 0.80 for sharpness, texture and combined feature spaces, respectively.

Wei et al. in [28] proposed a method for masses detection based on the combination of the gradient field analysis and the grey level information. The method used a clustering-based region growing algorithm for detecting the suspicious lesions. Then, a set of shape and texture descriptors were computed from detected lesions before feeding two MLCs: ruled-based and LDA. The reported case-based sensitive result on a mass (containing 110 cases) dataset, non-mass (containing 90 cases) dataset and a combination of them was 70%, 80%, and 90% at 0.72, 1.08 and 1.82 false positive per image respectively.

Bellotti et al. in [71] proposed a three-stage system for mass detection. In the first stage, a segmentation algorithm using a dynamical threshold is applied for detecting suspicious lesions. Then, a set of eight texture features (extracted from the GLCM at different angles) were computed from segmented lesions. In the last stage, a FFBP neural network classifier (trained with the gradient descent learning rule) was used for discriminating between normal masses and normal tissues. The system evaluation using a dataset containing 3369 mammography images (2307 negative cases and 1062 positive cases) reported an AUC-based classification performance of 0.783 (standard deviation of 0.008) by the proposed system.

Sahiner et al. in [80] combined morphological and texture features for describing mass lesions. The obtained classification results using a dataset formed by 249 images were an AUC value of 0.83, 0.84, and 0.87 when using morphological, texture, and a combination of both type of features respectively.

Alto et al. in [166] analyzed several image-based features in order to select masses lesions with similar constitution in terms of computed descriptors. The evaluation of the method was using the retrieval precision as a performance measure. The higher result (91%) was obtained when using the three most-effective features (fractional concavity, acutance and sum of entropy).

Mavroforakis et al. in [76] proposed a quantitative approach for masses classification by using linear and non-linear classification architectures. Also, the method is supported by the fractal analysis (calculated by the box-counting method) of the set of extracted texture features. The

evaluation on two datasets containing 130 digitized mammograms revealed that the best score (83.9%) was obtained by the SVM classifier using only texture features.

Ayres and Rangayyan [167-169] presented a method that analyzes the oriented texture on mammography images in order to detect architectural distortion. The method used the Gabor filters for obtaining the orientation field of the images and three maps models (node, saddle and spiral) for locating the place of the architectural distortion, being the node map the most prominent. The method was tested on two set of images, one containing 19 cases of architectural distortion and 41 normal mammograms, and the other containing 37 cases with architectural distortion. Sensitivity rates of 84% and 81% at 4.5 and10 false positives per image were reported for the two set of images respectively.

More recently, Moura and Lopez in [88] developed a new round-shape descriptor based on Histograms of Gradient Divergence (HGD) for masses classification. The HGD was compared against eleven group of image descriptors (extracted from Intensity statistics, Histogram measures, Invariant moments, Zernike moments, Haralick features, Grey-level run length, Grey-level difference matrix, Gabor filter banks, Histogram of oriented gradients, Wavelets and Curvelets) on benchmarking datasets extracted from two public available mammography databases. Obtained results using different machine learning classifiers revealed that the HGD was the best descriptor (or comparable to best) in 8 out of 12 scenarios, demonstrating promising capabilities to classify breast masses.

Table 4 Overview of most employed group of image-based descriptors for masses detection/classification.

Descriptors	Descriptions	References
Intensity features	Contrast measure of ROIs; Average grey level of ROIs (Mean); Standard derivation inside ROIs or variance; Skewness and Kurtosis of ROIs; Zernike moments.	[72, 75, 88, 160, 170]
Shape features	Margin spiculation and Sharpness; Area, circularity, convexity, rectangularity and perimeter measures; Acutance measure; Shape factor; Invariant moments; Furrier descriptor; Fractal analysis.	[23, 24, 72, 75, 76, 80, 92, 107, 160-163, 166, 170, 171]
Normalized radial length and the Normalized chord length	Boundary roughness, mean, entropy, area ratio, standard deviation, zero crossing count, mean, variance, skewness and kurtosis.	[79, 80, 85, 88]
Texture features from GLCM, Grey-level difference statistics and from Run-level statistics	Energy (or angular second moment); Correlation, inertia and entropy of co-occurrence matrix; Difference moment; Inverse difference moment; Sum average, sum entropy and difference entropy; Sum variance, difference average and information of correlation; Contrast, angular second moment, entropy and mean Short and long runs emphasis, grey-level and run length non-uniformity and run percentage.	[27, 71, 72, 76, 88, 162, 164, 165]

These image-based descriptors could improve diagnostic accuracy and led to the development of mammography-based CADx systems to increase both sensitivity and specificity [156]

2.3. Feature Selection Methods

Goal of the feature selection

The objectives of features selection are manifold, two of the most important are:

- to avoid overfitting and improve model performance, i.e. prediction performance in the case of supervised classification and better cluster detection in the case of clustering [61, 62].

- to provide faster and more cost-effective models, i.e. models with lower algorithmic complexity [61, 62].

Selection paradigms

Selecting the optimal feature subset for supervised learning problems requires an exhaustive search of all possible subsets of features of the chosen cardinality, which is not practical in most situations because the number of possible subsets given N features is 2^N-1 (the empty set is excluded), which means *NP*-hard algorithms [56]. Hence, in practical machine learning applications, usually a satisfactory instead of the optimal feature subset is searched. Feature selection techniques differ from each other in the way they incorporate this search in the added space of feature subsets in the model selection.

Regarding their classification, feature selection techniques can be structured into three paradigms, depending on how they combine the feature selection search with the construction of the classification model: filters (univariate and multivariate), wrappers and more recently hybrid methods. Filters methods are considered the earliest approaches to feature selection within machine learning and they use heuristics based on general characteristics of the data rather than a machine learning classifiers to evaluate the merit of features [56, 57]. Wrappers methods utilize machine learning classifiers as a black box to score subsets of features according to their predictive power. Finally, the Hybrid methods combine filter and wrapper methods as a unique model to perform feature selection. As consequences, filter methods generally present lower algorithmic complexity and are much faster than wrapper or hybrid methods [56, 57].

On the other hand, feature selection methods can be also categorized depending on search strategies used. Thus, the following search strategies are more commonly used [60, 172]:

- Forward selection: start with an empty set and greedily add features one at a time.
- Backward elimination: start with a feature set containing all features and greedily remove features one at a time.
- Forward stepwise selection: start with an empty set and greedily add or remove features one at a time.
- Backward stepwise elimination: start with a feature set containing all features and greedily add or remove features one at a time.
- Random mutation: start with a feature set containing randomly selected features, add or remove randomly selected features one at a time and stop after a given number of iterations.

2.3.1. Filter Paradigm

Filter techniques assess the relevance of features by looking only at the intrinsic properties of the data. In most cases a feature relevance score is calculated, and low-scoring features are removed. Afterwards, this subset of features is presented as input to the classification algorithm [56]. A generalized filter algorithm is showed in Table 5. For a given dataset *D*, the algorithm starts the search by using an initial subset S_0, which could be an empty set, a full set, or any randomly selected subset through the whole feature space and according to a particular search strategy. Subsequently, the initial subset S_0 is evaluated by an independent measure *M* and the result is stored in Ω_{best}. After that, a new features subset *S* is generated and evaluated (by the same *M* independent measure) for further comparison with the previous best one Ω_{best}. If it is found to be better, it is regarded as the current best subset. The search iterates until a predefined stopping criterion ε is reached. The algorithm outputs the last current best subset S_{best} as the final result.

Table 5 Pseudocode of the generalized filter algorithm.

Filter Algorithm	
input:	
$D(f_0, f_1, ..., f_{N-1})$	// initial dataset with *N* features
S_0	// an empty subset to start the search
ε	// a stopping criterion
output:	
S_{best}	// an optimal subset of features
begin	
$\Omega_{best} = eval(S_0, M);$	// evaluate S_0 by an independent measure *M*
do begin	
$S = generate(D);$	// generate a subset of feature for evaluation
$\Omega = eval(S, D, M);$	// evaluate the current subset *S* by an independent measure *M*
if $(\Omega > \Omega_{best})$	
$\Omega_{best} = \Omega;$	
$S_{best} = S;$	
end until (ε is reached);	
return $S_{best};$	
end	

From this algorithm, it is possible to vary the search strategies (*S*) and evaluation measures (*M*) to design different individual filter models. Since the filter models are independent of any classifiers, it does not inherit any bias and will be computationally efficient.

2.3.2. Wrapper Paradigm

Wrapper methods integrated the model hypothesis search and the features subset search in the same setup. As long as the search procedure is defined (for finding possible subset of features in the whole features space), other new subsets of features are generated and evaluated at the same time. The evaluation occurs by a specific MLC, which makes this method extremely dependent of the employed classifier. Therefore, the search procedure is wrapped around the classification model. However, as the space of feature subsets grows exponentially with the number of features, heuristic search methods such as deterministic and randomized search algorithms [50, 56] are more likely to be used for guiding the search of an optimal subset. Table 6 shows a simple pseudocode of the generalized wrapper algorithm.

Table 6 Pseudocode of generalized wrapper algorithm.

Wrapper Algorithm	
input:	
$D(f_0, f_1, ..., f_{N-1})$	// initial dataset with *N* features
S_0	// a subset from which to start the search
ε	// a stopping criterion
output:	
S_{best}	// an optimal subset of features
begin	
$\theta_{best} = eval(S_0, D, MLC);$	// evaluate S_0 by a MLC
do begin	
$S = generate(D);$	// generate a subset of feature for evaluation
$\theta = eval(S, D, MLC);$	// evaluate the current subset *S* by the classifier MLC
if $(\theta > \theta_{best})$	
$\theta_{best} = \theta;$	
$S_{best} = S;$	
end until (ε is reached);	
return $S_{best};$	
end	

The wrapper and filter algorithms are very similar. As it is shown in Table 6, the main different is the evaluation function. Filter methods used an independent measure (*M*) for the evaluation of each generated subset *S*, meanwhile wrapper methods evaluated its goodness (quality of mined results) by applying the MLC to the data with feature subset *S*. The application of different MLCs will produce different features selection results. Moreover, varying the model search strategies according to the function *generate(D)* and the machine learning classifier *(MLC)* can result in different wrapper methods. As an advantage, the

features subset selection is supervised by the employed classifier; thus, the final subset of features will provide better classification performances. However, this improvement has the inconvenient that they are more computationally expensive than the filter model.

2.3.3. Hybrid Paradigm

Hybrid methods combine filter and wrapper methods as a unique model for achieving the best performance using a particular MLC with a similar time complexity to a filter method. They use the filter methods for obtaining information about the ranking and thus, to guide the search for wrapper methods. These methods are more recent approach and constitute a promising direction in the feature selection field [52].

The hybrid model is proposed to handle large datasets [173]. A general hybrid algorithm uses an independent measure (filter method) and a MLC (wrapper method) to evaluate subset of features (see Table 7). The independent measure (*M*) selects the best subset of features according to a given cardinality and then, the MLC determines the best subset of features among all generated subsets (with different cardinalities).

Basically, the algorithm starts the search with an empty subset S_0 and tries to find the best subsets while is increased the cardinality. For each round, the best subset with cardinality *c* and the new generated subset *S* (by adding one feature from the remaining features) with cardinality *c+1* are evaluated using an independent measure (*M*) and then it is established a comparison between them. If the *S* subset with cardinality *c+1* is better, it becomes the current best subset of features S'_{best} at level *c+1*. At the end of each round, the *S* subset with cardinality *c* and the new S'_{best} subset with cardinality *c+1* are evaluated by a MLC for further comparison according to their mined result θ. If S'_{best} is better, the algorithm continues to find the best subset at the next level; otherwise, it stops and outputs the current best subset as the final best subset. The quality of results from a MLC provides a natural stopping criterion in the hybrid model.

Table 7 Pseudocode of generalized hybrid algorithm.

Hybrid Algorithm

input:

$D(f_0, f_1, ..., f_{N-1})$ // initial dataset with *N* features

S_0 // a subset from which to start the search

output:

S_{best} // an optimal subset of features

begin

$c_0 = card(S_0);$ // calculate the cardinality of S_0

$\Omega_{best} = eval(S_0, D, M);$ // evaluate S_0 by an independent measure *M*

$\theta_{best} = eval(S_0, D, MLC);$ // evaluate S_0 by a classifier MLC

for $c = c_0 + 1$ to *N* **begin**

for *i = 0* to *N - c* **begin**

$S = S_{best} \cup \{f_j\};$ // generate a subset of feature with cardinality *c* for evaluation

$\Omega = eval(S, D, M);$ // evaluate the current subset *S* by an independent measure *M*

if $(\Omega > \Omega_{best})$

$\Omega_{best} = \Omega;$

$S'_{best} = S;$

end

$\theta = eval(S'_{best}, D, MLC);$ // evaluate S'_{best} by a classifier MLC

if $(\theta > \theta_{best})$

$S_{best} = S'_{best};$

$\theta_{best} = \theta;$

else

break and **return** S_{best}

end

return $S_{best};$

end

2.3.4. Related Works

Koller and Sahami [101] proposed an algorithm for feature subset selection that uses backward elimination to eliminate predefined number of features. The idea is to select a subset of features that keeps the class probability distribution as close as possible to the original distribution that is obtained using all the features. The algorithm starts with all the features and performs backward elimination to eliminate a predefined number of features. The evaluation function selects the next feature to be deleted based on the Cross entropy measure. For each feature the algorithm finds a subset of *K* features such that, the feature is approximated to be conditionally independent of the remaining features. Setting *K* = 0 results

in a much faster algorithm that is equal to a simple filtering approach commonly used on text-data.

In the Relief algorithm [174] the main idea is to estimate quality of the features according to how well their values distinguish between examples that are similar. The feature score is calculated from a randomly selected subset of training examples, so that each example is used to calculate the difference in the distance from the nearest example of the same class and the nearest example of the different class. The nearest instances are found using the kNN algorithm. Some theoretical and empirical analysis of the algorithm and its extensions is provided in [175].

Almuallim and Dietterich [176] developed several feature subset selection algorithms including a simple exhaustive search and algorithms that use different heuristics. They based their feature subset evaluation function on conflicts in class value occurring when two examples have the same values for all the selected features. In the first approach (named FOCUS), all the feature subsets of increasing size are evaluated until a sufficient subset is encountered. Feature subset *Q* is said to be sufficient if there are no conflicts i.e. if there is no pair of examples that have different class values and the same values for all the features in *Q*. The second approach (called FOCUS-2) reduces the search space by evaluating only promising subsets. As both algorithms assume the existence of a solution (small set of features) their application on domains with a large number of input variables can be computationally infeasible. Due to this, heuristics searches are implemented on further versions of the algorithm.

Aijuan and Baoying in [177] proposed a multi-resolution approach to automated classification of mammograms using Gabor filters (with different frequencies and orientations). They applied the statistical t-test and its p-value for feature selection and weighting respectively. According to the experimental results, the statistical t-test reduced the feature space without degrading the classification performance.

Akay in [178] proposed a breast cancer diagnosis method based on the combination of the SVM classifier and the f-score feature selection method. The performance of the method is evaluated using classification accuracy, sensitivity, specificity, positive and negative predictive values, receiver operating characteristic curves and confusion matrix on different training-test partitions of the Wisconsin Breast Cancer Dataset. The results show that the

highest classification accuracy (99.51%) is obtained for the SVM model that contains five features.

Aha and Bankert in [179] used a wrapper approach for feature subset selection in instance-based learning. They proposed a new search strategy that performs beam search using a kind of backward elimination. Namely, instead of starting with an empty feature subset, their search randomly selects a fixed number of feature subsets and starts with the best among them.

Recently, the work of Chandrashekarand and Sahin [180] presents a survey of feature selection methods. They implemented the correlation criteria and mutual information methods from the filter paradigm, the sequential floating forward selection and a modified version of the genetic algorithm (named CHGA) methods from the wrapper paradigm. These methods were evaluated with the performance of a SVM and radial basis function network classifiers on seven datasets, including five from the UCI machine learning repository (Wisconsin breast cancer dataset, Diabetes, Ionosphere, Liver Disorder and Medical).

In [181], a set of three feature selection methods were developed for combining with a multilayer neural network and multiclass support vector machines. The developed methods used the backward elimination and direct search in selecting a subset of salient features. Also, in these classification models was employed the mutual information between class labels and classifier outputs as an objective function. The methods were evaluated on various artificial and real world datasets (including the Wisconsin Breast Cancer Diagnosis).

Lately, algorithms of the hybrid model [51, 55, 173, 182-184] are considered to handle data sets with high dimensionality. A number of algorithms that combines fuzzy logic and genetic programming in selecting relevant features for ANN and decision trees have been proposed [185, 186]. Rakotomamonjy in [187] proposed new feature selection criteria derived from SVMs and were based on the generalization error bounds sensitivity with respect to a feature. The effectiveness of these criteria was tested on several problems including medical datasets (Breast Cancer, Colom Cancer, Diabetes and Heart data).

Richeldi and Lanzi in [188] proposed a two-step feature selection method named ADHOC. First, the method identifies false features according to a previous constructed profile of each feature, then; a genetic algorithm is used for finding an important subset features. Other studies (e.g. ref [184], [55] and [189]) also use genetic algorithms in feature selection. In

[184], is combined a filter and wrapper method as a unique approach (hybrid) for feature selection. The filter method used the mutual information to guide the searching and ranking the features space. Then, a wrapper method based on a genetic algorithm is used for finding the most relevant subset of features.

2.3.5. Comparative Analysis

The earliest approaches to feature selection within machine learning were filter methods. Filter methods use heuristics based on general characteristics of the data rather than a learning algorithm to evaluate the merit of feature subsets.

Advantages of filter techniques are that they easily scale to very high-dimensional datasets [56], they are computationally simple and fast, and they are independent of the classification algorithm. The process of feature selection is often most useful in situations in which wrappers may overfit, i.e. with small training sets. As a result, feature selection needs to be performed only once, and then different classifiers can be evaluated [173]. A common disadvantage of filter methods is that they ignore the interaction with the classifier (the search in the feature subset space is separated from the search in the hypothesis space), and that most proposed techniques are univariate. This means that each feature is considered separately, thereby ignoring feature dependencies, which may lead to worse classification performance when compared to other types of feature selection techniques. In order to overcome the problem of ignoring feature dependencies, a number of multivariate filter techniques were introduced, aiming at the incorporation in some degree of feature dependencies.

Whereas filter techniques treat the problem of finding a good feature subset independently of the model selection step. Wrapper approaches (as advantages) include the interaction between feature subset search and model selection, and the ability to take into account feature dependencies. But, a common drawback of these techniques is that they have a higher risk of overfitting than filter techniques and are very computationally intensive, especially if building the classifier has a high computational cost [60].

On the other hand, hybrid models attempt to take advantage of the two previous models by exploiting their different evaluation criteria in different search stages. It means that hybrid approaches improve the classification performance of filter approaches by including a specific machine learning algorithm in the selection procedure, and improve the efficiency of wrapper

approaches by narrowing the searching space [190]. They also include the interaction with the classification model, while at the same time being far less computationally intensive than wrapper methods. Table 8 shows an overview of several feature selection techniques. For each feature selection type, it is highlighted a set of characteristics which can guide for the most favorable choice.

Table 8 A brief description of feature selection methods.

Paradigm	Advantages	Disadvantages	Methods
Filter	Univariate		
	-Fast -Scalable -Independent of the classifier	-Ignores feature dependencies -Ignores interaction with the classifier	-X quadratic [60, 75] -T-test [60, 97, 191] -Euclidean distance [60] -FOCUS [176] -RELIEF [75, 192] -F-test [193] -Information Gain (IG) [60, 75, 194] -Kolmogorov- Smirnov test (KS) [195]
	Multivariate		
	-Models feature dependencies -Independent of the classifier -Better computational complexity than wrapper methods	-Slower than univariate techniques -Less scalable than univariate techniques -Ignores interaction with the classifier	-Correlation-based feature selection (CFS) [46, 60] -Markov blanket filter (MBF) [101] -Fast correlation-based feature selection (FCBF) [47, 60]
Wrapper	Deterministic		
	-Simple -Interacts with the classifier -Models feature dependencies -Less computationally -Intensive than randomized methods	-Risk of over fitting -More prone than randomized algorithms to getting stuck in a local optimum (greedy search) -Classifier dependent selection	-Sequential forward selection [196, 197] -Sequential backward elimination[60, 197] -Beam search [60, 198] -Naïve Bayes [60]
	Randomized		
	-Less prone to local optima -Interacts with the classifier -Models feature dependencies	-Computationally intensive -Classifier dependent selection -Higher risk of overfitting than deterministic algorithms	-Simulated annealing [60, 199] -Randomized hill climbing [60, 199] -Genetic algorithms [196] -Estimation of distribution [60, 200]
Hybrid	-Independent measure to decide the best subset (filter methods) -Interacts with the classifier -Searching guided by filter methods -Models feature dependencies -Better accuracy than filter and wrapper methods	-Classifier dependent selection	-Fuzzy Random Forest ensemble (FRF-fs) [182] -Ant colony optimization and ANNs [183] -Hybrid genetic algorithm (HGA) [184] [55] -Boosting-based hybrid for feature selection (BBFS) [173] -Automatic discoverer of higher order correlations (ADHOC) [188]

2.4. Machine Learning Classifiers

In the daily practice of radiology, medical images from different modalities are read and interpreted by radiologists. Usually radiologists must analyze and evaluate these images comprehensively in a short time. But with the advances in modern medical technologies, the amount of imaging data is rapidly increasing.

Machine learning provides an effective way to automate the analysis and diagnosis for medical images. It can potentially reduce the burden on radiologists in the practice of radiology. Bishop and Nasrabadi in [201] defined machine learning as the study of computer algorithms which can learn complex relationships or patterns from empirical data and make accurate decisions. It is an interdisciplinary field that has close relationships with artificial intelligence, pattern recognition, data mining, statistics, probability theory, optimization, statistical physics, and theoretical computer science.

One of the most important advantages of machine learning is comparable performance to humans. In many radiology applications (e.g. mammography and colon CADe), CADe systems have shown comparable, or even higher, performance compared with well-trained and experienced radiologists and technologists [63-65]. In addition, a good machine learning predictor usually will give predictions with low bias and variance at any time. On the other hand, radiologists' performance may be affected by various factors: fatigue, emotion, reading time and environment, etc. In principle, machine learning-based computer systems will perform more consistently than human beings.

A variety of machine learning classifiers have been applied in different approaches to solve the problem of breast cancer detection/classification (see Table 9). The kNN is not only one of the most commonly employed classifiers in mammographic CADe systems [84-87], but also one of the simplest and most popular classifiers in general. The ANN seems to be the most commonly used type of classifiers in mammographic CADx systems [67-74]. SVM [76-78, 202, 203] and LDA [23, 28, 79-83] are also popular in both for CADe and CADx community. They performed very well in breast cancer detection/classification. Others less frequently classifiers applied in CADx systems include NB [70, 88-90], binary DT [90-92], logic programing models [204] and the fuzzy modeling methods [205-208]. However, the latter is very expensive in terms of Central Processing Unit (CPU) time consuming, because they are mainly based on rules. An example is the work of Ghazavi and Liao [209] where

three fuzzy modeling methods for breast cancer classification were used, achieving a satisfactory AUC value (0.9587) when using the fuzzy kNN algorithm in the Wisconsin breast cancer dataset, but the CPU time consumed was high. A brief description of most employed classifiers for breast cancer detection/classification (kNN, ANN, SVM and LDA) is given here:

2.4.1. k-Nearest Neighbors

The kNN classifier is a nonparametric technique called a 'lazy learning' because little effort goes into building the classifier and most of the work is performed at the time of classification [210]. It represents one of the simplest and most intuitive techniques in the field of statistical discrimination. It is a nonparametric method, where a new observation is placed into the class of the observation from the learning set that is closest to the new observation, with respect to the covariates used [211]. The determination of this similarity is based on distance measures. Formally this simple fact can be described as follows:

Let

$$L = \{(y_i, x_i), i = 1,2,..,n_L\} \qquad (1)$$

be a training or learning set of observed data, where $y_i \in \{1,...,c\}$ denotes class membership and the vector $x'_i = (x_{i1},..,x_{ip})$ represents the predictor values. The determination of the nearest neighbors is based on an arbitrary distance function $d(.,.)$ (usually the Euclidean distance). Then for a new observation (y,x) the nearest neighbor $(y_{(1)}, x_{(1)})$ within the learning set is determined by:

$$d(x, x_{(1)}) = \min_i (d(x, x_i)) \qquad (2)$$

and $\hat{y} = y_{(1)}$, the class of the nearest neighbor, is selected as prediction for y. The notation of x_j and y_j here describes the *j*th nearest neighbor of *x* and its class membership, respectively. Figure 7 shows a graphical illustration of the classification process by the kNN classifier using 3 and 7 *k*-neighbors.

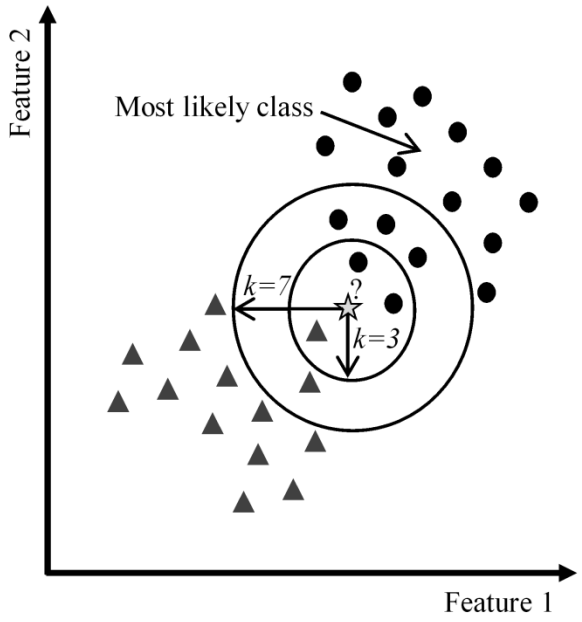

Figure 7 Possible classification of a new instance [26] by the kNN classifier using k=3 and 7 neighbors in a features space of two different classes of data (Triangle and Circle).

2.4.2. Artificial Neural Networks

ANNs are the collection of mathematical models that imitate the properties of biological nervous system and the functions of adaptive biological learning. They are made of many processing elements that are highly interconnected together with the weighted links that are similar to the synapses. Unlike linear discriminants, ANNs usually use non-linear mapping functions such as: linear, sigmoid, tangent-hyperbolic, step, multi-quadratic and Gaussian as decision boundaries. The advantage of ANNs is their capability of self-learning, and often suitable to solve the problems that are too complex to use the conventional techniques, or hard to find algorithmic solutions. It includes an input layer, an output layer and one or more hidden layers between them (according with the selected topology). Depending on the weight values of $w(j, i)$ and $w(k, j)$ the inputs are either amplified or weakened to obtain the solution in the best way. The weights are determined by training the ANN using the known samples. The ANN topologies vary according to the problem to be solved, for example, the most common structure for breast cancer classification is the three-layer back-propagation ANN. Figure 8 shows a graphical representation of a Feed Forward back-propagation ANN.

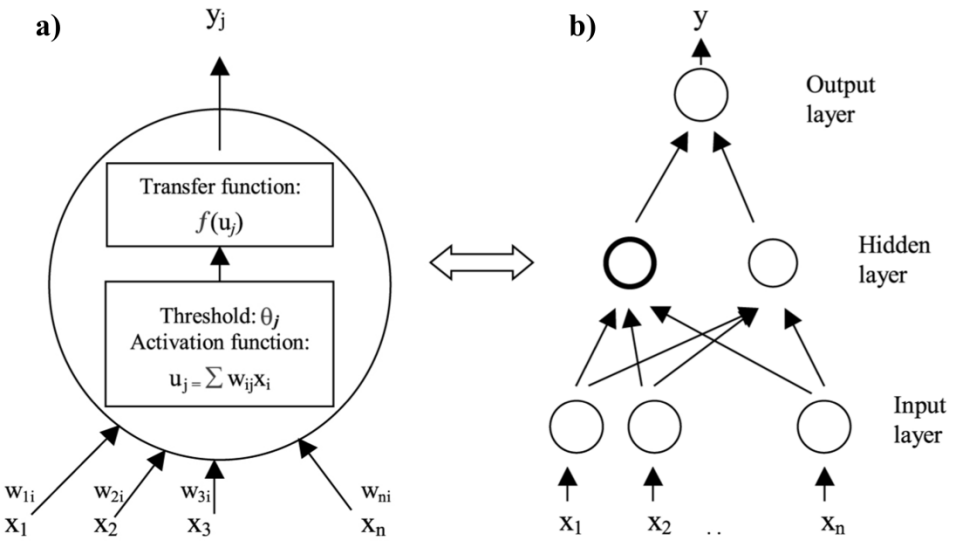

Figure 8 Graphical representation of; a) an artificial neuron, and b) a typical Feed-Forward ANN.

2.4.3. Support Vector Machines

SVMs are a set of kernel-based supervised learning methods used for classification and regression [212]. The kernel means a matrix which encodes similarities between samples (evaluated by a certain kernel function which is a weighting function in the integral equation used to calculate similarities between samples). In comparison with other classification methods, a SVM aims to minimize the empirical classification error and maximize the distances (geometric margin) of the data points from the corresponding linear decision boundary [77, 155]. For a binary classification problem, given training samples $\{(x_1, y_1),..,(x_n, y_n)\}, y_i \in \{-1,+1\}$, the optimization problem for learning a linear classifier in the feature space is defined as (hard margin):

$$\min_{w,b} \|w\|, \qquad (3)$$

subject to:

$$y_i[(w \cdot x_i) - b] \geq 1, i = 1,2,...,n, \qquad (4)$$

where $(w \cdot x_i)$ is the inner product of two vectors and refers to the mapping of the input vector x into a higher dimensional space for easily separated by a linear hyperplane from original space to feature space (see Figure 9). The matrix composed by inner products of samples in

feature space (after linear or non-linear mapping) is called the kernel matrix which describes the similarities between samples and serves as evidence when it maximizes the margin between two classes of samples. The above problem is a quadratic programming optimization problem and it is convex. The optimal (w,b) is a maximal margin classifier with geometric margin $\frac{1}{2}\|w\|^2$ if it exists. It can be applied to classify test samples once it is learned from the training set. Figure 9 shows an illustration of the SVM concept to map a non-linear problem to a linear separable one.

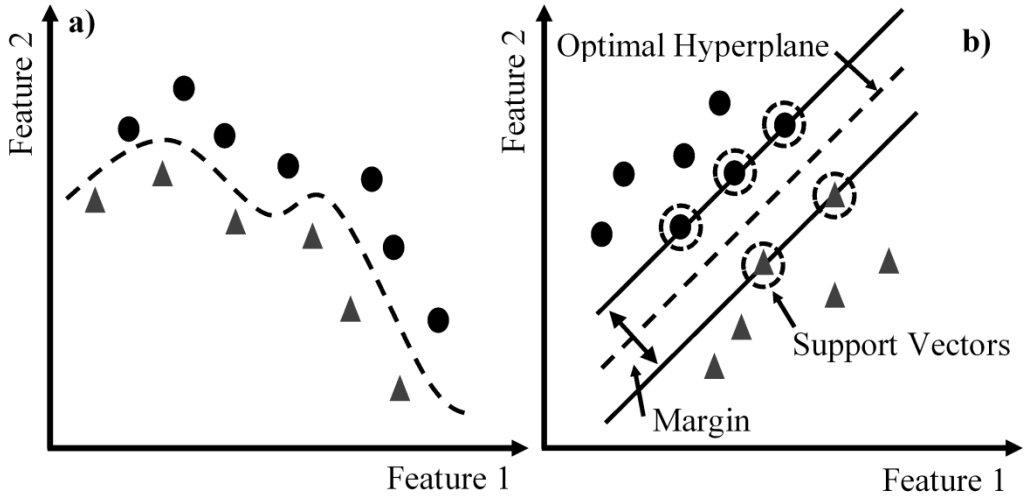

Figure 9 Illustration the concept of SVM to map: a) a nonlinear problem to (b) a linear separable one; Dashed line is the best hyperplane which can separated the two classes of data (Triangle and Circle) with maximum margin. Dashed circles represent the support vectors.

2.4.4. Linear Discriminant Analysis

LDA is a traditional method for classification [213, 214]. The main idea of this method is to construct the decision boundaries directly by optimizing the error criterion to separate the classes of objects. If there are n classes, and linear discriminant analysis classifies the observations as the following n linear functions:

$$g_i(x) = W_i^T * x - c_i, \quad 1 \le i \le n \qquad (5)$$

where W_i^T is the transpose of a coefficient vector, x is a feature vector and c_i is a constant as the threshold. The values of W_i^T and c_i are determined through the analysis of a training set. Once the values of W_i^T and c_i are determined, they can be used to classify the new

observations. The observation is abnormal if $g_i(x)$ is positive, otherwise it is normal. An illustration of LDA for 2D data projected to one dimensional line is shown in Figure 10.

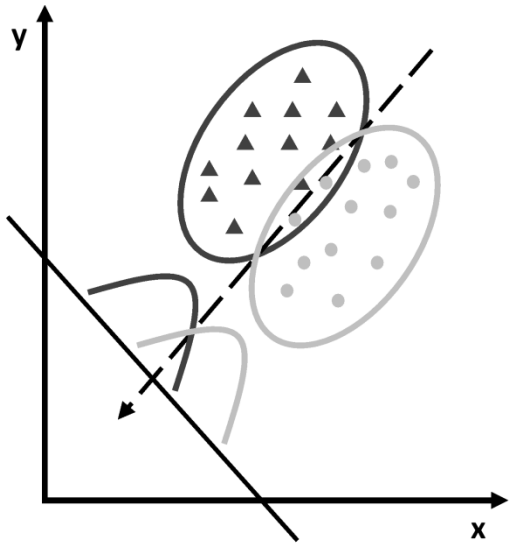

Figure 10 Best projection direction (dashed arrow) found by LDA. Two different classes of data (Triangle and Circle) with "Gaussian-like" distributions are shown in different ellipses. 1-D distributions of the two-classes after projection are also shown along the line perpendicular to the projection direction.

2.4.5. Related Works

Sahiner et al. [79] used a classification model based on the stepwise features selection method and the LDA classifier for masses classification. The method used a set of morphological and spiculation features computed from manual (by radiologists) and computer-based segmentation respectively. The evaluation on a dataset containing 249 films from 102 patients highlighted an AUC score of 0.89 (for manual segmentation) and 0.88 (for computer-based segmentation), respectively.

Similarly, in Shi et al. [23] is used a classification model based on the stepwise features selection method and the LDA classifier for masses classification. The evaluation on the primary data set (427 biopsy-proven masses: 909 ROIs, 451 malignant and 458 benign) from multiple mammographic views was an AUC value of 0.83. This result was improved when including the patients age in the classification model, attaining an AUC score of 0.85 (for view-based) and 0.87 (for case-based). Moreover, an independent evaluation using a masses dataset extracted from the DDSM (132 benign and 197 malignant ROIs) achieved a view-based AUC value of 0.84.

Jesneck et al. in [82] evaluated mammographic and sonographic features using both LDA and ANN models to differentiate benign from malignant lesions. The high classification performance obtained with cross validation (AUC value of 0.92 and 0.90 for LDA and ANN, respectively) in a dataset including 803 breast mass lesions (296 malignant, 507 benign) corroborated that combining mammographic and sonographic descriptors in a CADx model can result in high classification and generalization performance.

Gupta et al in [83] compared the performance of CADx systems based on BI-RADS descriptors from single or ipsilateral mammographic image view. They used a set of image-based descriptors computed from segmented masses on the ipsilateral mammographic image views of 115 patient cases (extracted from the DDSM). Also, it was included the BI-RADS and the patient age information as a feature in the classification model. The CADx system using the BI-RADS descriptor with image-based features from the ipsilateral mammographic image view performed better than using the same descriptors extracted from the mammographic single view, attaining an AUC value of 0.92.

Medjahed et al. in [215] used the kNN algorithm with both types of Euclidean distance and Manhattan for the classification of 683 clinical cases of “fine needle aspiration” (458 benign and 241 malignant) extracted from the Wisconsin Breast Cancer dataset. Despite the time consuming respect to others distance measurement, these distances were effective in terms of classification and performance (98.70% for Euclidean distance and 98.48% for Manhattan with k = 1). These results were not significantly affected even when k = 1 is increased to 50.

Salama et al. in [89] presented a comparison among different classifiers: decision tree, Multi-Layer Perception, Naive Bayes, sequential minimal optimization, and Instance Based for kNN on three different databases of breast cancer (Wisconsin Breast Cancer (original), Wisconsin Breast Cancer (diagnostic) and Wisconsin Breast Cancer (pronostic)). Despite the well classification accuracy obtained by the kNN classifier (94.44%, 95.96% and 64.44% respectively), the sequential minimal optimization classifier was the best among all.

In Christobel [90], the performance of the DT C4.5, NB, SVM and kNN classifiers were compared to find the best classifier in the Wisconsin Breast Cancer dataset. The SVM classifier proved to be the most accurate classifier with an accuracy value of 96.99% respect to 94.56% for C4.5, 95.99% for NB and 95.13% for kNN classifiers.

Kramer and Aghdasi [216] used a set of texture and wavelet features, which were validated by using a kNN classifier. The classification accuracy using a dataset formed by 40 images of Nijmegen database [106] was satisfactory (100%). Moreover, in Kramer and Aghdasi [217] is compared the performances of both popular classifiers the kNN and ANN. According to the obtained results the ANN was better than the kNN classifier. Zadeh et al. [218] used a set of shape and texture features with a kNN classifier for MCs classification. The classification model was validated by using a dataset containing 74 malignant and 29 benign MCs clusters extracted from the Nijmegen database [106]. The obtained results by each set of features were an AUC values of 0.82 with k=7 for shape features and 0.72 with k=9 for texture features, which were much worse than the obtained results in previous work [216].

Ping et al. in [67] proposed a classification model based on a neural genetic algorithm (as a features selector) and ANN classifier for the classification of small breast abnormalities. The method used a combination of image-based features (intensity statistics) and human extracted features from mammograms. The reported accuracy results were 90.5% rate for calcification cases and 87.2% for mass cases with difference feature subsets.

Malar et al. in [70] proposed a variety of feed forward neural network classifier, which contains only one layer in its configuration (called Extreme Learning Machine). In this approach, the reported learning speed is thousand times faster than any conventional feed forward neural network. The performance of the proposed classifier for MCs detection was higher (AUC value of 0.94) when comparing to other machine learning classifiers such as: SVM, NB and Bayes Net.

Bellotti et al. in [71] used an ANN to classify masses as negative and positive case. The performance evaluation reported in a dataset with 3369 mammographic images, which included 2307 negative cases and 1062 positive cases (diagnosed at least by one expert radiologist) was an AUC value of 0.783 and standard deviation of 0.008 for the ROI based classification compared with 80% sensitivity of mass detection by expert radiologists (4.23 false positives per image).

Yunfeng et al. in [219] described several linear fusion strategies, in particular the majority vote, simple average, weighted average, and perceptron Average, which were used to combine a group of component multilayer perceptron with optimal architecture for the classification of breast lesions. They used in their experiments the criteria of mean squared

error, absolute classification error, relative error ratio, and ROC curve to concretely evaluate and compare the performances of the four fusion strategies. The experimental results demonstrated that the weighted average and perceptron average strategies achieved better diagnostic performance compared to the majority vote and simple average methods.

In a similar research [68], the perceptron average strategy outperformed the other fusion strategies for imbalanced input features. From these results of fusion strategies, the authors stated the advantages of fusing the component networks, and provided a particular broad sense perspective about information fusion in neural networks.

Verma in [220] investigated multiple clusters based ANN with a training algorithm based on the random weights (It utilizes six input nodes to represent each input feature) to find out whether or not multiple clusters have any impact on classification of ROIs in digital mammograms. The experimental results showed that the multiple clusters for each class strategy wilt three clusters per class achieved the best classification accuracy (96%) in a dataset of 100 ROIs (50 benign and 50 malignant). The authors concluded that the multiple clusters per class improved the classification accuracy. Also, it was found that the accuracy increases with the increase of number of clusters per class.

López et al. in [221] developed a new method to classify correctly (as benign or malignant) six different types of breast cancer abnormalities on mammography images. The method used two different topologies of ANN as classifiers: FFBP and learning vector quantization classifiers. The classification performance (based on the true positives) reported using a dataset extracted from the publicly available database (Mini-MIAS [111]) was 97.5% for the FFBP and 72.5% for the LVQ. In a similar research, López et al. [222] developed a new CADx system, which used a FFBP neural network and included a new model of ANN; the generalized regression neural network for the classification of six different pathological lesions (calcifications, well-defined/circumscribed masses, spiculated masses, ill-defined masses, architectural distortions and asymmetries). The system performance was confirmed in an experimental dataset formed by 100 features vectors extracted from the publicly available database Mini-MIAS [111]. Like in previous work [221], the obtained result of the FFBP neural network (94%) outperformed the generalized regression neural network (80%) of true positives.

Ferreira et al. in [202], provided a methodology to produce machine learning classifiers that predict mass density and predict malignancy from a reduced set of annotated mammography findings The generated classifiers were validated using a dataset containing 348 masses cases (biopsy-proven). The best result for predicting mass density was achieved with the SVM classifier, attaining an accuracy value of 81.3%. This result was superior when comparing to the obtained expert annotation (70 %.). Also, for predicting the malignancy, the best result was provided by a SVM classifier, obtaining an accuracy score of 85.6% with a positive predictive value of 85%. In this approach, it was possible to predict malignancy in the absence of the mass density attribute, because they used a developed mass density predictor.

Table 9 Overview of most employed machine learning classifiers for breast cancer detection/classification.

Classifier	Details	References
kNN	A nonparametric method, where a new observation is placed into the class of the observation from the learning set that is closest to the new observation, with respect to the covariates used.	[85, 88-90, 129, 215-218]
ANN	Construct non-linear mapping function as a decision boundary.	[27, 67-74, 77, 78, 89, 126, 139, 145, 217, 219-222]
SVM	Construct linear decision boundaries by minimizing the empirical classification error and maximizing the distances (geometric margin) of the data points.	[76-78, 88, 90, 160, 161, 202, 203, 223]
LDA	Construct decision boundaries by optimizing certain criteria to classify cases into one of mutually exclusive classes.	[23, 28, 79-83, 141, 161, 166]
NB	A classifier based on probabilistic models with strong (naïve) independence assumptions. In spite of its oversimplified assumptions.	[70, 88-90, 139]
DT	A binary decision tree recursively using a threshold to separate mammogram data into two classes each time.	[90-92]

2.5. CADe and CADx systems in Breast Cancer

CADe and CADx systems which integrate diagnostic imaging with several machine learning techniques such as: image processing, pattern recognition, and artificial intelligence. It can be defined as a diagnosis that is made by a radiologist who uses the output from computerized analysis of medical images as a “second opinion” in detecting (CADe) and classifying (CADx) lesions with subsequent diagnostic decisions [221, 222].

These systems represent a valuable resource for both, research scientists and medical specialists (radiologists) because of the associated demanding research topics and potential clinical applications. For research scientists, there are several interesting research topics in CADe and CADx systems, such as high efficiency, high lesion classification performance, high accuracy lesion detection algorithms, including the detection of calcifications and

masses, architectural distortion, bilateral asymmetry, etc. Radiologists, on the other hand, are paying attention to the effectiveness of clinical applications of these systems [224].

Actually both CADe and CADx systems are divided in two categories depending of mammography type: the first group is based on the conventional SFM, where the films are scanned, digitized, and saved on the computer for additional examination and the second group is based on FFDM, which is expected to provide a higher signal-to-noise ratio, a higher detection quantum efficiency, a wider dynamic range, and a higher contrast sensitivity than the first one type of mammography [28]. Although FFDM technology is expected to be superior to the conventional SFM technology, the results obtained in a recent study show, that there is no difference in the accuracy between FFDM and SFM for asymptomatic women [225].

The most important requirement for CADe systems is to expose clearly that the accuracy and efficiency of the screening mammograms interpretation is better than the conventional method. On the other hand, CADx systems have been focused in the used techniques to improve their performance in the diagnosis of lesions. Although the significance progress; the CADe and CADx systems for breast cancer is still an active research field, particularly in regard to the detection/classification of subtle abnormalities in mammography images. An overview of a representative selection of Breast Cancer CADe and CADx systems is presented in Table 10.

CADe and CADx systems for screen field and full field digital mammography

Helvie et al. in [226] conducted a pilot prospective clinical trial of a noncommercial CADe system developed at the University of Michigan for screening mammography. A total of 2389 screening cases were read by 13 qualified radiologists in two academic institutions. The most prominent result reported here was the reasonable increment in the call back rate from 14.4% to 15.8% when using CADe systems.

Birdwell et al. [227] evaluated the usefulness of a CADe system by comparing the detection result with and without the CADe. They performed 165 interventions on a set of 8682 cases and were detected 29 cancers in the following way: 21 cancers were detected by both the CADe and the radiologists, 6 cancers were detected only by the radiologists and 2 cancers were detected only by the CADe system. Also, it was reported that radiologists reading using a CADe system resulted in an increment of the detection (7.4%) and the recall rate (7.6%).

One interesting observation in the above two studies was that the radiologists' call-back rate for the study cases increased even before the CADe marks were displayed, indicating that they might become more vigilant when they were aware that their reading would be compared with a second reading.

Hadjiiski et al. in [41] evaluated the influence of CADx systems on radiologists' characterization of masses. A total of 8 experts (radiologists and breast imaging fellows) evaluated (with and without CADx system) 253 masses cases (138 malignant and 115 benign). The AUC average for the radiologists' estimation of the likelihood of malignancy was 0.79 without CADx and 0.84 with CADx system. This improvement was statistically significant at $p=0.005$. Moreover, according to the BI-RADS assessment, it was estimated that each radiologist reduced the number of unnecessary biopsies (average of 0.7% less) and correctly recommended 5.7% additional biopsies.

Destounis et al. in [228] evaluated the role of CADe in reducing the false negative rate of findings on screening mammograms (normal and double reading). As result, the CADe system correctly detected 71% of the 52 findings read as negative in previous screening year. This result highlights the importance of CADe system for reducing false positive rate.

Butler et al. [229] studied the influence of CADe system on the detection of suspicious breast cancers. The system was able to correctly detect 87% of findings, which were located in a wrong place. This result corroborates that CADe systems can aid to the radiologists.

Marx et al. in [230] proposed an experiment with 5 radiologists and 185 patients for analyzing the performance of CADx systems. As result, they observed an increase in the call-back rates (5% to 7%) when patient cases were analyzed by the CADx system. Also, it was observed a reduction in the number of recommended unnecessary biopsies from 12 to 34%.

Baker et al. in [231] studied the consistency of a commercial CADe system by scanning 10 times the mammograms and evaluating the prompts from the CADe system. He concluded that there was an inconsistency in the CADe analysis for the breast cancers detected at screening; however, the CADe system was reasonably consistent in the overall number of cancers identified at different runs. Greater variability was observed for the false positive marks compared to true positive marks.

Two commercial CADe schemes were compared by Gur et al. [232] on 219 patients. The obtained accuracy detection rate for masses lesions varied from 67% to 72%. They reported that this difference between both systems was not statistically significant. However, the difference in the false positive rate was statistically significant, ranging from 1.08 to 1.68 per four view examinations.

McLoughlin et al. in [233] developed a method for noise equalization in FFDM images and showed that the proposed square root noise model improved the performance of their CADe algorithm for detection of MCs clusters on FFDM images.

Multiview and Multimodal CADe/CADx systems

Besides the inclusion of temporal change information into CADe and CADx systems as discussed in previous section, the incorporation of information from multiple mammographic views as well as from complementary modalities (e.g., breast sonography, breast MRI, and breast elastography) are important topics of current and future CADe and CADx research. In breast cancer screening, usually the two standard mammography views CC and MLO are acquired. Often an additional view, like the special view mammograms (e.g. spot compression or spot compression magnification views) is also available. Radiologists of course consider the appearance of a lesion in all available mammographic views, as well as in the images acquired using complementary modalities, in their diagnosis. Hence, CADe and CADx approaches should probably do so as well. While several CADe and CADx systems published so far consider information from the standard CC and MLO views (e.g. in [23, 86, 148]), systems that include lesion features from additional views or even from additional modalities are rare.

Huo et al. in [170] investigated the use of special view mammograms in the CADx of mammographic masses. Their results, AUC value of 0.95 using the special views, AUC value of 0.78 and AUC value of 0.75 using the CC and MLO views, respectively, indicate that the CADx of special view mammograms significantly improves the classification of masses. However, the AUC performance that was achieved when all three views were used (AUC value of 0.95) was not higher than when only the special view mammograms were used (AUC value of 0.95). This indicates that the CC and MLO views might not add significant diagnostic information to a system that already includes spot compression or spot compression magnification views.

Horsch et al. [43, 234] proposed multimodal CADx approaches that incorporates information from mammograms and breast sonography. They found that the system's performance significantly improved when lesion features from both modalities were combined. However, classification performance depended on specific methods for combining features from multiple images per lesion (mean, minimum, or maximum). They achieved an AUC maximum value of 0.95 for the multimodal system.

Velikova et al. [235] proposed a Bayesian network framework for breast cancer detection at a patient level. The method performs a multi-view mammographic analysis based on causal-independence models and context modeling over the whole breast represented as links between the regions detected by a single-view CAD system in the two breast projections. The method was validated using a dataset formed by 1063 patient cases (385 with breast cancer). The reported results show that the proposed multi-view modeling leads to significantly better performance in discriminating between normal and cancerous patients. Also, it was demonstrated the potential of using multi-view system for selecting the most suspicious cases.

Table 10 Overview of a representative selection of Breast Cancer CADe/CADx systems.

Author	Year	System	Number of Lesions	Type of Lesion	Setup	AUC value
Salfity et al. [236]	2003	CADe	131	MCs	Multiview	0.93
Kallergi et al. [126]	2004	CADx	100	MCs	Singleview	0.98
Lim and Er [164]	2004	CADx	343	Masses	Singleview	0.87
Timp and Karssemeijer [237]	2004	CADe	1210	Masses	Multiview	0.74
Leichter et al. [131]	2004	CADx	324	MCs	Singleview	0.87
Soltanian-Zadeh et al. [129]	2004	CADx	103	MCs	Singleview	0.89
Drukker et al. [234]	2005	CADx	100	Masses	Multimodal	0.92
Papadopoulos et al. [77]	2005	CADe	105/25	MCs	Singleview/ Multiview	0.79/ 0.81
Wei et al. [148]	2005	CADe	386	MCs	Multiview	0.85
Varela et al. [27]	2006	CADx	1076	Masses	Singleview	0.81
Delogu et al. [25]	2007	CADx	226	Masses	Singleview	0.78
Karahaliou et al. [26]	2007	CADx	100	MCs	Singleview	0.96
Guliato et al. [24]	2008	CADx	111	Masses	Singleview	0.94
Shi et al. [23]	2008	CADx	427	Masses	Multiview	0.85

Note that direct comparisons of the AUC values are not reasonable as the systems have been evaluated on different databases

2.6. Conclusions

This chapter describes current developments and status in the five critical areas in which the thesis contributions are inserted: (1) Breast Cancer supporting repositories; (2) Clinical and image-based descriptors for breast cancer; (3) Feature selection methods; (4) Machine learning classifiers; and (5) CAD methods in breast cancer. In summary, principal achieved conclusions about related areas are presented:

1. The public BCDR, BancoWeb LAPIMO, DDSM and IRMA mammographic image databases provide greatest opportunities for development new breast cancer analysis methods, due to the well documented ground-truth about lesions.

2. Image-based descriptors originated from the experience of radiologists such as: perimeter, area, compactness, elongation, eccentricity, orientation, direction and contrast evidenced to be very significant for MCs detection/classification. Also, texture features from the GLCM, wavelet features and features extracted from MCs clusters provided satisfactory classification performances.

3. Shape-based descriptors constituted the most important group of image-based descriptor for masses detection/classification. They described the mass lesions according to their shape and margin (characteristics described in the BI-RADS atlas). Also, texture features from the GLCM and intensity features are commonly used.

4. Clinical descriptors presented in the BI-RADS lexicon demonstrated to be useful for breast cancer classification. They consistently improve the classification performance when combined with image-based descriptors.

5. There are evidences that filter methods are faster and with lower computational cost than wrapper or hybrid methods. However, they ignore feature dependencies and ignore interaction with the classifier; thus, the classification performance tends to decrease.

6. It was observed that many researchers in the field of feature selection still consider filter feature selection approaches. However wrapper or hybrid models tend to be the most promising future lines of work for the scientific community.

7. ANNs, SVMs, kNNs and LDAs classifiers are the most employed machine learning classifiers for breast cancer detection/classification. They appear consistently in most developed CAD systems. Therefore, it is possible to conclude they are trustworthy classifiers for breast cancer analysis.

CHAPTER 3

Experimental Methodologies

This chapter underlines materials and methods employed in the experimental design such as: datasets description; considered clinical and image-based descriptors; exploration of several machine learning classifiers and features selection methods; and the experimentation with a new feature selection method we named *RMean*. The experimental design was divided in two different moments (experiments) in order to analyze the selection of features and its relevance in the context of Breast Cancer classification with mammography images. The first experiment addresses the issue of variable selection within a feature space containing clinical and image-based descriptors extracted from segmented lesions in both MLO and CC mammography images. Meanwhile, the second experiment aims to gather experimental evidence of features relevance, as well as finding a Breast Cancer classification scheme that provides the high AUC-based performance. Discussion of results also is presented in this chapter.

3.1. Datasets

In this thesis were considered two public repositories as the principal resource for datasets creation: the Breast Cancer Digital Repository (BCDR), which is the first Portuguese breast cancer database, with anonymous cases from medical historical archives supplied by Faculty of Medicine "Centro Hospitalar São João" at University of Porto, Portugal [30, 34] and the Digital Database for Screening Mammography version created (in compliance with all restrictions of DDSM) by the Image Retrieval in Medical Applications (IRMA) project (courtesy of TM Deserno, Dept. of Medical Informatics, RWTH Aachen, Germany) [115, 116]. These public repositories were selected because they provide the highest number of annotated mammograms with biopsy-proven diagnostic. Although both repositories differ in term of image resolution, number of grey levels, number of cases and the included observations of radiologists; They include for each case, the density of the breast (BI-RADS scale) and the contour of the lesions in one or two mammograms per breast (MLO and CC), which is an important information for further computation of image-based descriptors.

3.1.1. BCDR

BCDR is composed of 1734 patient cases subdivided in two different repositories: (1) a Film Mammography-based Repository (BCDR-FM) and (2) a Full Field Digital Mammography-based Repository (BCDR-DM).

The BCDR-FM is formed by 1010 (998 female and 12 male) patients cases, including 1125 studies, 3703 MLO and CC mammography incidences and 1044 identified lesions clinically described (820 already identified in MLO and/or CC views). Thus, a total of 1517 segmentations were manually made and BI-RADS classified by specialized radiologists. The MLO and CC images are grey-level (8 bits) digitized mammograms in TIFF format with a resolution of 720 (width) by 1168 (height) pixels.

The BCDR-DM is composed by 724 (723 female and 1 male) patients cases, including 1042 studies, 3612 MLO and/or CC mammography incidences and 452 lesions clinically described (already identified in MLO and CC views). Thus, a total of 818 segmentations were manually made and BI-RADS classified by specialized radiologists. The MLO and CC images are grey-level (14 bits) mammograms with a resolution of 3328 (width) by 4084 (height) or 2560

(width) by 3328 (height) pixels, depending on the compression plate used in the acquisition (according to the breast size of the patient).

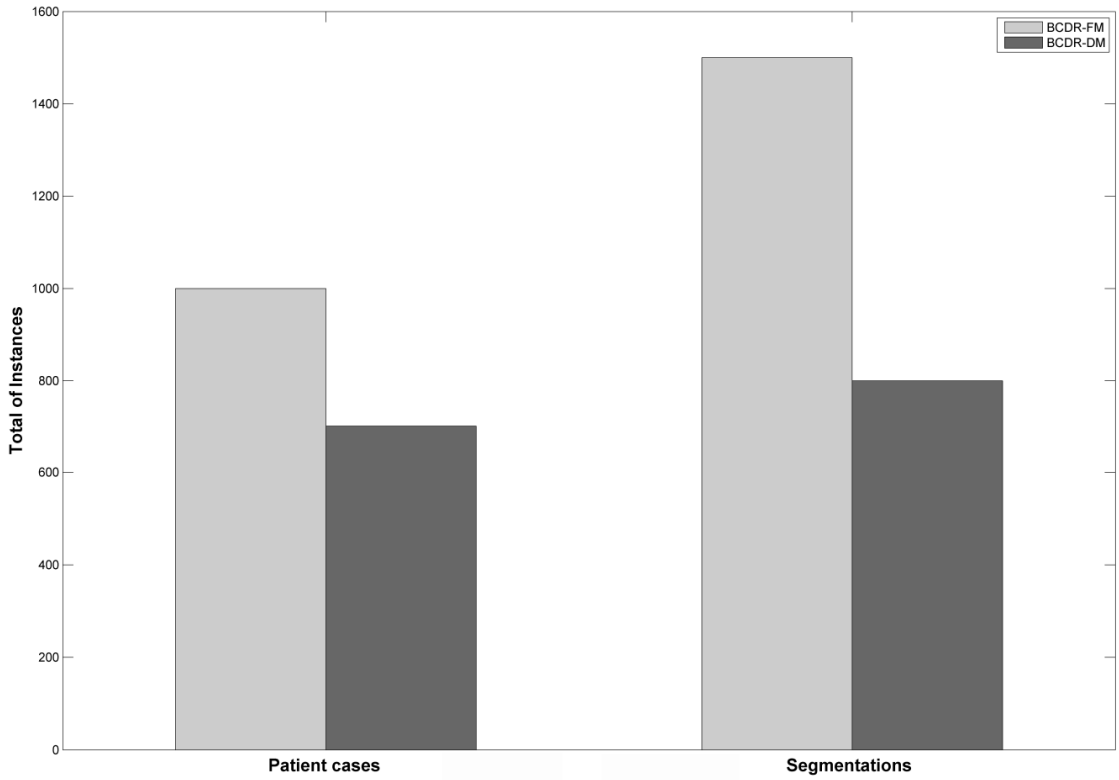

Figure 11 Distribution of patient cases and segmentations on the BCDR-FM and BCDR-DM respectively.

Although the BCDR-DM seems to be a high quality repository, it is still under construction and presents lesser number of patient cases and segmentations than the BCDR-FM (see Figure 11). Therefore, for convenience, we only considered extracting the experimental datasets from the BCDR-FM.

According to the features space to be analyzed it were created different datasets as follow (see Table 11 for more detailed information):

- MCs dataset representing segmented lesions in only one view (MLC or CC) including or not clinical features.
- Masses dataset representing segmented lesions in only one view (MLC or CC) including or not clinical features.
- MCs with Masses dataset representing lesions segmented in only one view (MLC or CC) including or not clinical features.

- MCs dataset representing segmented lesions in an ipsilateral image view (MLC and CC), including or not clinical features.
- Masses dataset representing segmented lesions in an ipsilateral image view (MLC and CC), including or not clinical features.
- MCs with Masses dataset representing lesions segmented in an ipsilateral image view (MLC and CC), including or not clinical features.
- MCs with Masses balanced dataset (same number of instances per class) formed from the BCDR-F01 (biopsy-proven diagnostic dataset).
- MCs with Masses unbalanced dataset (with more benign than malignant instances per class) formed from the BCDR-F01 (biopsy-proven diagnostic dataset).
- MCs with Masses unbalanced dataset (with more malignant than benign instances per class) formed from the BCDR-F01 (biopsy-proven diagnostic dataset).

3.1.2. DDSM

The DDSM database is composed by 2620 patient cases divided into three categories: normal cases (12 volumes), cancer cases (15 volumes) and benign cases (14 volumes) [112]; each case may have one or more associated Pathological Lesion (PL) segmentations, usually in MLO and CC image views of the same breast. In addition to the PL segmentations and density of the breast, the DDSM dataset also includes the subtlety of the lesion (an integer number ranging between 1 and 5). Regarding the observations of the radiologists about the lesions, DDSM stores if there are masses or calcifications and characterizes the shape and margins of masses as well as the type and distribution of calcifications using keywords of the BI-RADS glossary.

Due to the substantial volume of information, we considered only 582 segmentations representing two volumes of cancer (vol. 1 and 2) and benign (vol. 1 and 5) cases. These volumes correspond to the scanner LUMISYS, which provides the highest resolution in the database (50 microns). The produced images have an average size of 3,118 (width) by 5,001 (height) pixels and 3,600 grey levels in LJPG format. For better suitability, the images used in this thesis were obtained from the IRMA project where the original LJPEG images of DDSM were converted to 16 bits PNG format [115, 116].

According to the number of pathological lesions segmentations it was created three datasets with different configurations (see Table 11 for more detailed information):

- MCs with Masses balanced dataset using the same number of instances per class (benign and malignant).
- MCs with Masses unbalanced dataset using more benign than malignant instances per class.
- MCs with Masses unbalanced dataset using more malignant than benign instances per class.

Table 11 Description of experimental datasets extracted from both repositories.

Name	Repository	Type of Lesion	Features vectors	View	Total of features	Clinical features	Image-based features
DS1.Mi.C(+)	BCDR-FM	MCs	381	Single	39	Yes	Yes
DS1.Ma.C(+)	BCDR-FM	Masses	168	Single	39	Yes	Yes
DS1.All.C(+)	BCDR-FM	MCs and Masses	549	Single	39	Yes	Yes
DS2.Mi.C(+)	BCDR-FM	MCs	76	Ipsilateral	64	Yes	Yes
DS2.Ma.C(+)	BCDR-FM	Masses	173	Ipsilateral	64	Yes	Yes
DS2.All.C(+)	BCDR-FM	MCs and Masses	249	Ipsilateral	64	Yes	Yes
DS1.Mi.nC(+)	BCDR-FM	MCs	381	Single	24	No	Yes
DS1.Ma.nC(+)	BCDR-FM	Masses	168	Single	24	No	Yes
DS1.All.nC(+)	BCDR-FM	MCs and Masses	549	Single	24	No	Yes
DS2.Mi.nC(+)	BCDR-FM	MCs	76	Ipsilateral	48	No	Yes
DS2.Ma.nC(+)	BCDR-FM	Masses	173	Ipsilateral	48	No	Yes
DS2.All.nC(+)	BCDR-FM	MCs and Masses	249	Ipsilateral	48	No	Yes
BCDR1	BCDR-F01(*)	MCs and Masses	362	Single	23	No	Yes
BCDR2	BCDR-F01(*)	MCs and Masses	281	Single	23	No	Yes
BCDR3	BCDR-F01(*)	MCs and Masses	281	Single	23	No	Yes
DDSM1	DDSM	MCs and Masses	582	Single	23	No	Yes
DDSM2	DDSM	MCs and Masses	491	Single	23	No	Yes
DDSM3	DDSM	MCs and Masses	491	Single	23	No	Yes

(+) Included the *Area fraction* image-based descriptor; (*) Biopsy-proven dataset available online at: http://bcdr.inegi.up.pt/information/downloads

From Table 11, it is possible to read that most of the experimental datasets were extracted from the BCDR-FM, including those datasets which employed clinical features and ipsilateral image view analysis respectively. This fact is associated to the good relationship between images quality and annotated specialized information (by radiologists) in the BCDR.

3.1.3. Considered Clinical and Image-based Descriptors

Clinical features, according to the ACR [7, 156] were related to morphological and localization of pathological lesions in mammography images and represented the patient associated metadata. Meanwhile image-based descriptors included intensity statistics, shape and texture features, computed from segmented pathological lesions in both MLO and CC mammography views. The intensity statistics and shape descriptors were selected according to the radiologist's experience (similar to the clinician procedure) and the ACR (BI-RADS-Mammography atlas), which described in detail how to detect/classify pathological lesions. Additionally, texture descriptors were the Haralick's descriptors extracted from the grey-level co-occurrence matrices [138].

The BCDR is a well-documented repository with a total of 15 clinical features annotated by the observation of radiologists and 23 pre-computed image-based descriptors from segmented lesions. These set of clinical features is bigger than the existing set of clinical features in the IRMA repository, which is limited to a few features per segmentation, such as: density, lesion type and BI-RADS category.

Therefore, we considered clinical features extracted from the BCDR and are listed below:

- Density (f_1): means the mammographic density, ordinally scaled with values 1, 2, 3 and 4 representing the density degree of 1..24%, 25..49%, 50..74% and 75..100% respectively. The risk of breast cancer increases as the density increases [238].
- Breast location (f_2): identified the breast under study (0 for left and 1 for right breast).
- Right – top (f_3) or bottom (f_4) quadrant: means the pathological lesion location.
- Left – top (f_5) or bottom (f_6) quadrant: means the pathological lesion location.
- Axillary (f_7), Central (f_8), Retroareolar (f_9): means the pathological lesion location.
- Mammography nodule (f_{10}): means the presence or not of a nodule.

- Mammography calcification (f_{11}): means the presence or not of a calcification.
- Mammography microcalcification (f_{12}): means the presence or not of a microcalcifications.
- Mammography axillary adenopathy (f_{13}): means the presence or not of an axillary adenopathy.
- Mammography architectural distortion (f_{14}): means the presence or not of an architectural distortion.
- Mammography stroma distortion (f_{15}): means the presence or not of architectural distortion.

Besides, image-based descriptors in the BCDR were computed from the lesions contour, which is stored in Cartesian coordinates. However, in the IRMA database the lesions contour was stored using a chain-code technique making more difficult the computation of any descriptors. Thus, it was necessary implementing a MATLAB (version R2011a) interface to compute the same image-based descriptors (see Figure 12).

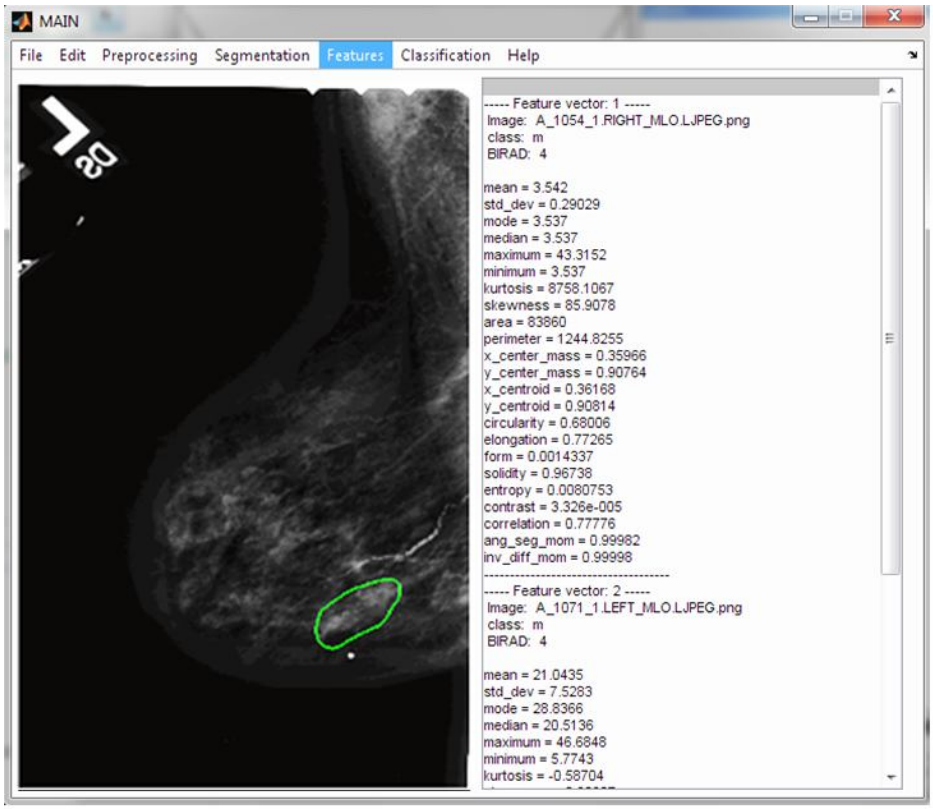

Figure 12 A screenshot of the developed MATLAB interface for the automatic computation of image-based descriptors. An example using the patient number A_1054_1 of the IRMA repository.

The mathematical formulations of implemented image-based descriptors are presented below:

- Skewness:

$$f_{16} = \frac{\frac{1}{n}\sum_{i=1}^{n}(x_i - \bar{x})^3}{\left(\sqrt{\frac{1}{n}\sum_{i=1}^{n}(x_i - \bar{x})^2}\right)^3} \quad (6)$$

with x_i being the i^{th}-value and $\bar{x}$ the sample mean.

- kurtosis:

$$f_{17} = \frac{\frac{1}{n}\sum_{i=1}^{n}(x_i - \bar{x})^4}{\left(\frac{1}{n}\sum_{i=1}^{n}(x_i - \bar{x})^2\right)^2} - 3 \quad (7)$$

with x_i being the i^{th}-value and $\bar{x}$ the sample mean.

- Area fraction (f_{18}): is the percentage of non-zero pixels in the image or selection.

- Circularity:

$$f_{19} = 4\pi \frac{area}{perimeter^2} \quad (8)$$

- Perimeter:

$$f_{20} = length\ (E) \quad (9)$$

with $E \subset O$ being the edge pixels.

- Elongation:

$$f_{21} = m / M \quad (10)$$

with m being the minor axis and M the major axis of the ellipse that has the same normalized second central moments as the region surrounded by the contour.

- Standard deviation:

$$f_{22} = \sqrt{\frac{1}{n-1}\sum_{i=1}^{n}(x_i - \bar{x})^2} \tag{11}$$

with x_i being the grey level intensity of the i^{th} pixel and $\bar{x}$ the mean of intensity.

- Roughness:

$$f_{23} = \frac{(perimenter)^2}{4\pi * area} \tag{12}$$

- Minimum (f_{24}) and Maximum (f_{25}): The minimum and maximum intensity value in the region surrounded by the contour.

- Shape:

$$f_{26} = \frac{perimeter \ * Elongation}{8 * area} \tag{13}$$

- X centroid:

$$f_{27} = \frac{min(x) + max(x)}{2} \tag{14}$$

with x being the set of X coordinates of the object's contour.

- Entropy:

$$f_{28} = -\sum_{i=1}^{L}\sum_{j=1}^{L} p(i,j)\log\big(p(i,j)\big) \tag{15}$$

with $p(i,j)$ being the probability of pixels with grey-level i occur together to pixels with grey-level j.

- X center mass (f_{29}) and Y center mass (f_{30}): Normalized X and Y coordinates of the center of mass of O.

- Energy:

$$f_{31} = \sum_{i=1}^{L}\sum_{j=1}^{L} p(i,j)^2 \tag{16}$$

with L being the number of grey-levels, and p being the grey-level co-occurrence matrix and, thus, $p(i,j)$ is the probability of pixels with grey-level i occur together to pixels with grey-level j.

- Median:

$$f_{32} = \begin{cases} MED = \dfrac{n+1}{2}, & if\ length(X)\ is\ odd \\ MED = \dfrac{X(\frac{n}{2}) + X(\frac{n}{2}+1)}{2}, & if\ length(X)\ is\ even \end{cases} \tag{17}$$

with X being the set of intensities.

- Contrast:

$$f_{33} = \sum_{i}\sum_{j} (i-j)^2\, p(i,j) \tag{18}$$

with $p(i,j)$ being the probability of pixels with grey-level i occur together to pixels with grey-level j.

- Correlation:

$$f_{34} = \frac{\sum_{i}\sum_{j} (ij)\, p(i,j) - \mu_x \mu_y}{\sigma_x \sigma_y} \tag{19}$$

with μ_x, μ_y, σ_x and σ_y being the means and standard deviations of the marginal distribution associated with $p(i,j)$.

- Mean:

$$f_{35} = \frac{1}{n}\sum_{i=1}^{n} x_i \tag{20}$$

with n being the number of pixels inside the region delimited by the contour and x_i being the grey level intensity of the i^{th} pixel inside the contour.

- Homogeneity:

$$f_{36} = \sum_i \sum_j \frac{1}{1+(i-j)^2}\, p(i,j) \tag{21}$$

with $p(i,j)$ being the probability of pixels with grey-level i occur together to pixels with grey-level j.

- Area:

$$f_{37} = |O| \tag{22}$$

with O being the set of pixels that belong to the segmented lesion.

- Y centroid:

$$f_{38} = \frac{min(Y) + max(Y)}{2} \tag{23}$$

with Y being the set of Y coordinates of the object's contour.

- Statistical mode (f_{39}): Most frequent intensity value in a segmented ROI (lesion).

3.2. Feature Selection

As it was mentioned in previous chapter, there are many potential benefits of features selection, i.e. facilitating data visualization and data understanding, reducing the measurement and storage requirements, reducing training and utilization times, defying the curse of dimensionality to improve prediction performance [56, 60]. However, these advantages come at a certain price, as the search for a subset of relevant features introduces an additional layer of complexity in the modeling task; the one of finding an optimal subset of relevant features [61, 62]. This is not practical in most situations because the number of possible subsets given N features is 2^N-1 (the empty set is excluded), which means *NP*-hard algorithms [56]. Therefore, in practical machine learning applications, usually a satisfactory instead of the optimal feature subset is searched.

We considered the application of four traditional features selection methods and another one developed from our own initial exploration made in this area (we named *RMean*). All employed methods belong to the filter paradigm, because its execution is a one step process without any data exploration (search) involved and are also independent of classifiers [239]. In addition, these methods use different evaluation function, which provides important information about the nature of each feature (dependence with respect to the class) in the features space. Typically, an evaluation function tries to measure the discriminating ability of a feature or a subset of features to distinguish the different class labels. Thus, an optimal subset chosen using one evaluation function may not be the same as that which uses another evaluation function [240].

The selected methods were:

- CHI2 discretization [96]: This method consists on a justified heuristic for supervised discretization. Numerical features are initially sorted by placing each observed value into its own interval. Then the chi-square statistic is used to determine whether the relative frequencies of the classes in adjacent intervals are similar enough to justify merging. The extent of the merging process is controlled by an automatically set chi-square threshold. The threshold is determined through attempting to maintain the fidelity of the original data.

- IG method: The IG measurement normalized with the symmetrical uncertainty coefficient [98] is a symmetrical measure in which the amount of information gained about *Y* after observing *X* is equal to the amount of information gained about *X* after observing *Y* (a measure of feature-feature intercorrelation). This model is used to estimate the value of an attribute *Y* for a novel sample (drawn from the same distribution as the training data) and compensates for information gain bias toward attributes with more values.

- 1Rule [241]: This method estimates the predictive accuracy of individual features building rules based on a single feature (can be thought of as single level decision trees). As we used training and test datasets, it is possible to calculate a classification accuracy for each rule and hence each feature. Then, from classification scores, a ranked list of features is obtained. Experiments with choosing a selected number of the highest ranked features and using them with common machine learning algorithms showed that, on average, the top three or more features are as accurate as using the original set. This approach is unusual due to the fact that no search is conducted.

- Relief [174]: This method uses instance based learning to assign a relevance weight to each feature. Each feature weight reflects its ability to distinguish among the class values. The feature weight is updated according to how well its values distinguish the sampled instance from its nearest hit (instance of the same class) and nearest miss (instance of opposite class). The feature will receive a high weight if it differentiates between instances from different classes and has the same value for instances of the same class. For nominal features it is defined as either 1 (the values are different) or 0 (the values are the same), while for numeric features the difference is the actual difference normalized to the interval [0..1].

3.3. Exploring Classifiers

In this thesis, the problem of breast cancer classification is modeled as a two-class (binary) classification problem with two discrete values: benign and malignant respectively. Therefore, the discrimination between samples of two classes may be formulated as a supervised learning problem, which is defined as the prediction of the value of a function for any valid input after training a MLC using examples of input and target output pairs [125].

Several MLCs have been used in Breast Cancer CADx systems. We used five of the most employed: FFBP neural network, SVM, LDA, kNN, NB and DT J48, which are implemented and available on Weka version 3.6 [242]. For all MLC with the exception of the NB (which are parameterless), 10-fold cross validation method [243] was applied on the training set for optimizing the classifiers' parameters. A brief description and parameters configuration of employed MLCs is given here:

- The FFBP neural network is a particular model of ANN, which provides a nonlinear mapping between its input and output according to the back-propagation error learning algorithm. This model has demonstrated to be capable of approximating an arbitrarily complex mapping within a finite support using only a sufficient number of neurons in few hidden layers [244]. We used this classifier with the following parameters: neurons on hidden layers were determined according to the equation *(attributes + number of classes)/2*; one output layer associated with the binary classification (benign or malignant); the sigmoid function was used as transfer function for all layers and the number of iterations (epochs) were optimized in the range of 100 to 1000 epochs (with an interval increment of 100 units).

- The SVM classifier, which is based on the definition of an optimal hyperplane, which linearly separates the training data. In comparison with other classification methods, a SVM aims to minimize the empirical risk and maximize the distances (geometric margin) of the data points from the corresponding linear decision boundary [77, 244]. The SVM classifier was used with the following settings: the regularization parameter *C* (cost) was optimized in the range of 10^{-3} to 10^{3} and the kernel type was based on a linear function, which provided better results respect to others kernel such as: radial basis, polynomial and sigmoid function (from our experimental experience).

- LDA is a traditional method for classification [213]. The basic idea is to try to find an optimal projection (decision boundaries optimized by the error criterion), which can maximize the distances between samples from different classes and minimize the distances between samples from the same class. We used LDA for binary classification, thus, observations were classified by the following linear function:

$$g_i(x) = W_i^T x - c_i \qquad 1 \le i \le 2 \qquad (24)$$

where W_i^T is the transpose of a coefficient vector, x is a feature vector and c_i is a constant as the threshold. The values of W_i^T and c_i are determined through the analysis of a training set. Once these values are determined, they can be used to classify the new observations (smallest $g_i(x)$ is preferred).

- The kNN classifier is a nonparametric technique called a 'lazy learning' because little effort goes into building the classifier and most of the work is performed at the time of classification. The kNN assigns a test sample to the class of the majority of its *k*-neighbors; that is, assuming that the number of voting neighbors is $k=k_1+k_2+k_3$ (where k_i is the number of samples from class i in the *k*-sample neighborhood of the test sample, usually computed using the Euclidean distance), the test sample is assigned to class m if $k_m = \max(k_i), \quad i = 1,2,3$ [210]. We used the kNN classifier including the estimation of an optimal value *k* for the size of the neighborhood varying from 1 to 20, and the contribution of each neighbor was always weighted by the distance to the instance being classified.

- The NB classifier is based on probabilistic models with strong (Naive) independence assumptions, which assumes that a class variable depends of the set of input features [245]. This classifier can be trained based on the relative frequencies shown in the training set to get an estimation of the class priors and feature probability distributions. For a test sample, the decision rule will be picking the most probable hypothesis, which is known as the maximum a posteriori decision rule using the above model.

- The DTJ48 classifier. This model is a standard tree, which has the useful characteristic of generating tree-based models that human experts can easily interpret [244], where non-terminal nodes represent tests on one or more attributes and terminal nodes reflect decision outcomes. The Classification algorithm in DTJ48 is inductively learned constructing a model from the pre-classified dataset. Each data item is defined by values of the attributes. Due to this, the classification may be viewed as a mapping from a set of features to a particular class. The DTJ48 classifier was used with a confidence factor varying from 10^{-2} to 10^2 (with an interval increment of 0.1 units) and 2 leaf per node (to guarantee the binary model).

3.4. The *RMean* Method

RMean is an ensemble method based on the mean criteria and it is supported on the filter paradigm [4, 246]. It considers that an optimal subset of features is always relative to a certain evaluation function, thus, the use of different evaluation function provides important information about the nature of each feature (dependence with respect to the class) in the features space [240].

The *RMean* method used as input four feature selection methods with different evaluation function from the filter paradigm: CHI2 discretization [96] based on the chi-square statistic function, IG [98] based on the information measure, 1Rule [241] based on rules as evaluation functions and Relief [174] based on the distance measure. These four methods were applied on the experimental datasets under analysis to produce four different ranking of features (one by each applied feature selection method). Then the mean position of each feature along the four features ranking was computed. Finally, a new ranking was created using the mean position of features as indexing criterion. Table 12 shows a pseudo-code describing the developed *RMean* method.

Table 12 The *RMean* method

RMean		
input:		
	$D(F_1, F_2, ..., F_N)$	// A training dataset with *N* features
output:		
	R_{mean}	// Final ranking of features
1.	**Begin**	
2.	$R_{chi2} = eval(CHI2, D)$	// Application of CHI2 discretization method to the *D* dataset.
3.	$R_{IG} = eval(IG, D)$	// Application of IG method to the *D* dataset.
4.	$R_{1Rule} = eval(1Rule, D)$	// Application of 1Rule method to the *D* dataset.
5.	$R_{relief} = eval(relief, D)$	// Application of Relief method to the *D* dataset.
6.	$R_{mean} = (R_{chi2} + R_{IG} + R_{1Rule} + R_{relief})/4$	// Averaging the features position throughout resultant rankings from steps 2,3,4 and 5.
7.	$R_{mean} = sorting(R_{mean}, 'ascendant')$	// Sorting in ascendant way the resultant ranking from the step 6.
8.	**End**	

3.5. Experimental Setup

Two different experiments were piloted in order to analyze the selection of features, as well as its relevance in the context of breast cancer classification with mammography images. The first experiment addressed the issue of feature selection within a feature space containing clinical and image-based descriptors extracted from segmented lesions in both MLO and CC mammography images [75, 247]. Meanwhile, the second experiment aimed to gather experimental evidence of features relevance, as well as finding a breast cancer classification scheme that provides the high AUC-based performance [4].

Once both experiments are a multistep modeling procedure, the application of the k-fold cross validation method [243] to the entire sequence of modeling steps guarantee reliable results [248]. We applied ten times 10-fold cross validation before features ranking (to avoid giving an unfair advantage to predictors) and classification steps respectively (to prevent overfitting of classifiers to the training set [243]) (see Figure 13 and 14 step 2 and 3). Thus, no sample appears simultaneously in training and test (disjoint test partitions). In this way, individual classifiers will be trained on different training sets, leading to different representations of the input space. Testing on these different input space representations leads to diversity in the resultant classifications for individual samples.

The overall procedure of the first experiment:

- Applying the CHI2 discretization [96], IG [98], 1Rule [241] and Relief [103] methods on DS1.Mi.C, DS1.Ma.C, DS1.All.C, DS1.Mi.nC, DS1.Ma.nC, DS1.All.nC, DS2.Mi.C, DS2.Ma.C, DS2.All.C, DS2.Mi.nC, DS2.Ma.nC and DS2.All.nC datasets to produce different ranking of features (see Figure 13 step 1 and 2).
- Creating several ranked subsets of features using increasing quantities of features. The top *N* features of each ranking (resultant from the previous step) was used for feeding different classifiers, with *N* varying in the following way (from our experimental experience): for all dataset derived from the single view (DS1), *N* varied from 5 to the total number of features of the dataset (with increments of 5) and for all dataset derived from the ipsilateral view (DS2), *N* varied from 10 to the total number of features of the dataset, with increments of 10, as it is shown in Figure 13 step 3.

- Classifying the generated ranked subsets of features using FFBP neural network [244], SVM [77, 244], and DTJ48 [75] classifiers for a statistical comparative analysis of AUC scores, all comparisons were using the Wilcoxon statistical test [249-251] (see Figure 13 step 3).
- Analyzing the relevance of features by the separation of all features ranking into four ranking groups: Single and Multiview Ranking including Clinical features and, Single and Multiview Ranking without including Clinical features. For each group, it was computed the total of features to be analyzed by averaging the size of the features subset in each winner scheme. Finally, the feature relevance was decided by averaging its position throughout all features ranking within the group under analysis.

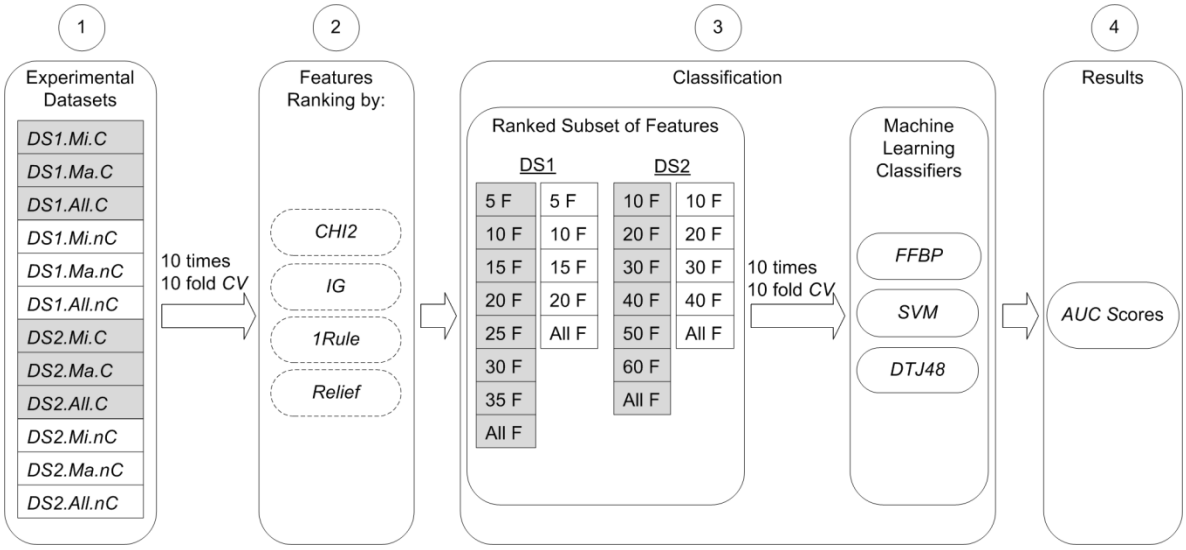

Figure 13 Flowchart of the first experiment; filled box represents the presence of clinical features.

The overall procedure of the second experiment:

- Applying the CHI2 discretization [96], IG [98], 1Rule [241], Relief [103] and *RMean* [4, 246] methods on DS2.Mi.C and DS2.Ma.C datasets to produce different ranking of features (see Figure 14 step 1 and 2).
- Creating several ranked subsets of features using increasing quantities of features. The top *N* features of each ranking (resultant from the previous step) were used for feeding different classifiers, with *N* varying from 10 to the total number of features of the dataset, with increments of 10 (from our experimental experience) as it is shown in Figure 14 step 3.

- Classifying the generated ranked subsets of features using FFBP neural network [244], SVM [77, 244], LDA [213, 214], kNN [210] and NB [245] classifiers for a statistical comparative analysis of AUC scores, all comparisons were using the Wilcoxon statistical test [249-251] (see Figure 14 step 3).
- Discovering features with higher importance for MCs and masses classification throughout (1) the validation of selected features as the most appropriate ranked subset of features for breast cancer classification and (2) the selection of features with higher importance inside each dataset.

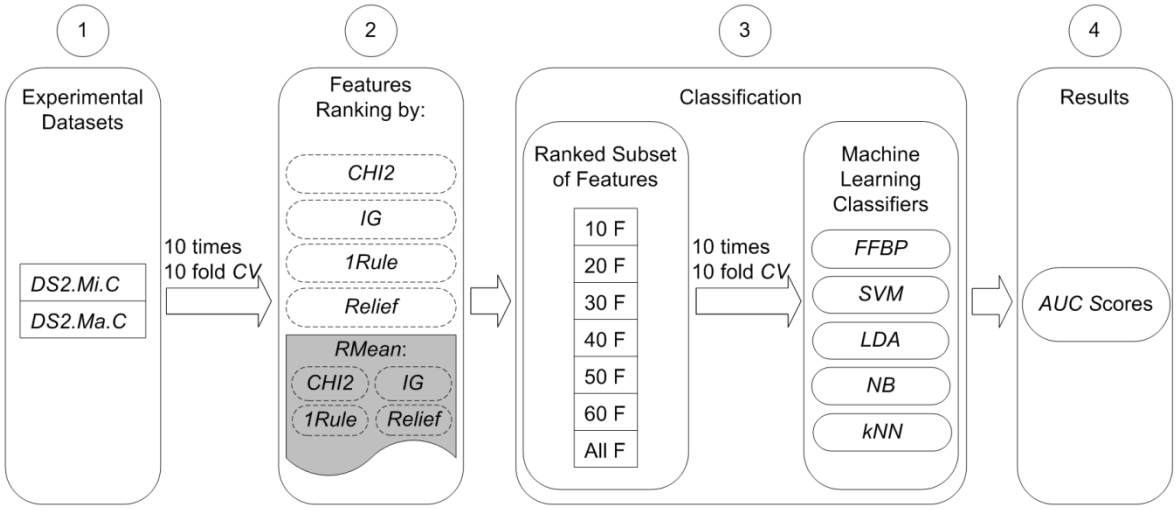

Figure 14 Flowchart of the second experiment; filled box means the developed *RMean* method.

3.6. Results and Discussions

In this section, the empirical evaluation and discussion of results will be presented according to the experimental setup section: first and second experiment respectively.

3.6.1. First Experiment

In this experiment, a total of 300 ranked subsets of features containing clinical and image based features were classified using FFBP neural network, SVM and DTJ48 classifiers in order to gather experimental evidences of variable selection within a feature space containing clinical and image-based descriptors extracted from segmented lesions in both MLO and CC mammography images. The obtained results showed reliable performances in the

classification of MCs, masses and both lesions together in the same dataset (see Figures 15, 16, 17, 18, 19 and 20).

Classification of Microcalcifications

Particular results for MCs classification illustrated that the best combination for DS1.Mi.C dataset was formed by the DTJ48 classifier and the IG method with a total of 20 features (see Figure 15 c). The reached AUC of 0.91 was significantly superior ($p<0.05$) to others satisfactory results such as: the obtained by the FFBP neural network classifier and the CHI2 discretization method with 25 features, attaining an AUC value of 0.88 (see Figure 15 a, and the SVM classifier with the CHI2 discretization method using a total of 20 features, achieving an AUC value of 0.893 (see Figure 15 b). Table 13 shows the AUC-based statistical comparison among these combinations.

Table 13 The AUC-based statistical comparison among the three best combinations on DS1.Mi.C dataset

Classification Model	**Number of Features**							
	5	**10**	**15**	**20**	**25**	**30**	**35**	**39**
FFBP neural network / CHI2 discretization	0.805	0.86	0.795	0.863	0.888	0.845	0.835	0.835
SVM / CHI2 Discretization	0.807	0.843	0.873	0.893	0.87	0.845	0.855	0.83
DTJ48 / IG method	0.86	0.88	0.893	**0.91**$^{(*)}$	0.888	0.898	0.878	0.87

$^{(*)}$ Statistically superior among all values at $p<0.05$; Bold value means the higher AUC score; Underlying value means the selected one scheme.

The most prominent results for the MCs dataset without the inclusion of clinical features (DS1.Mi.nC) were obtained using the schemes formed by the CHI2 discretization method with 5 features in conjunction with: the FFBP neural network and SVM classifiers, attaining AUC value of 0.8344 and 0.8301 respectively (see Figure 15 d, and e).

Table 14 The AUC-based statistical comparison among the three best combinations on DS1.Mi.nC dataset

Classification Model	**Number of Features**				
	5	**10**	**15**	**20**	**24**
FFBP neural network / CHI2 discretization	**0.8344**$^{(+)}$	0.7822	0.7497	0.7792	0.7768
SVM / CHI2 Discretization	0.8301$^{(+)}$	0.8156	0.7035	0.7807	0.7454
DTJ48 / CHI2 Discretization	0.8031	0.7506	0.7365	0.8207	0.7835

$^{(+)}$ No significant difference among them at $p<0.05$; Bold value means the higher AUC score; Underlying score means the selected one scheme.

From Table 14 it is possible to analyze that two classification schemes could be considered as appropriate for MCs classification on datasets without including clinical features. According

to the Wilcoxon statistical test [249, 250], they do not present significant difference in the performances ($p<0.05$). However, it was selected as the best scheme the combination which used the SVM classifier. Because it is a classification model less complex than the combination using the FFBP neural network classifier.

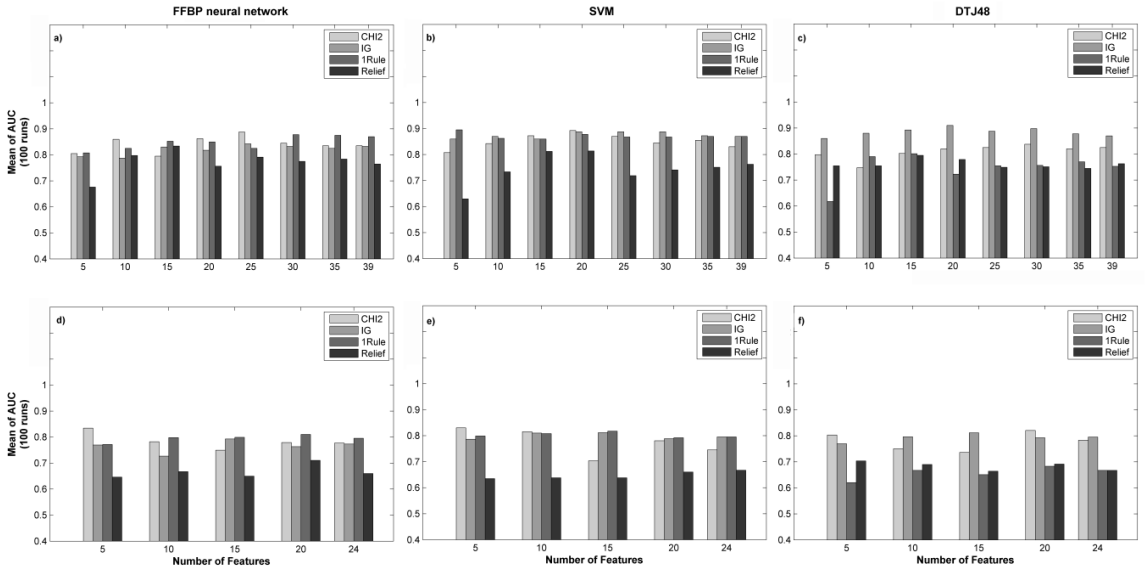

Figure 15 The mean of AUC scores (on 100 runs) of different classification schemes on DS1.Mi.C (first row) and DS1.Mi.nC (second row) datasets.

For the MCs dataset using clinical features and image-based descriptors extracted from both MLO and CC image view (DS2.Mi.C), the results highlighted three combinations with the same performance (AUC value of 0.7604): the FFBP neural network classifier and the 1Rule method using 30 features; the SVM classifier and the IG method with 50 features and the DTJ48 classifier with the IG method using 50 features (see Figure 16 a, b, c).

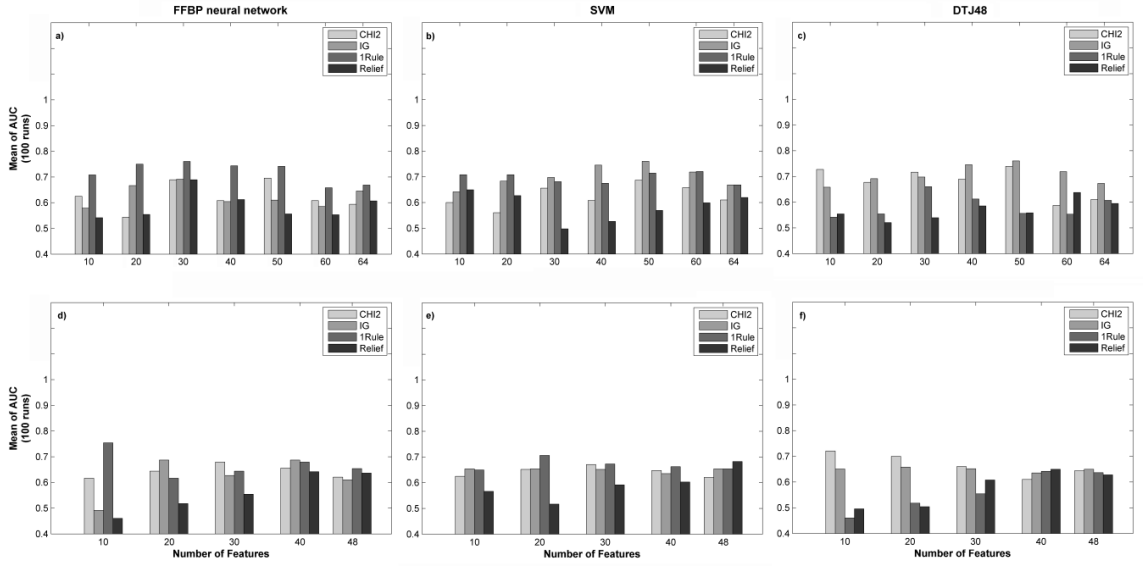

Figure 16 The mean of AUC scores (on 100 runs) of different classification schemes on DS2.Mi.C (first row) and DS2.Mi.nC (second row) datasets.

This result was statistically superior to the remaining schemes (see Table 15). However, it is reasonable to consider the first combination (the FFBP neural network classifier and the 1Rule method with 30 features) as the most appropriate scheme for MCs classification in this dataset, due to the fact of reaching this performance using a fewer number of features than the other two combinations (50 features).

Table 15 The AUC-based statistical comparison among the three best combinations on DS2.Mi.C dataset

Classification Model	**Number of Features**						
	10	**20**	**30**	**40**	**50**	**60**	**64**
FFBP neural network / 1Rule method	0.7083	0.75	**0.7604**$^{(+)}$	0.7438	0.7417	0.6583	0.6688
SVM / IG method	0.6417	0.6833	0.6979	0.7458	**0.7604**$^{(+)}$	0.7188	0.6688
DTJ48 / IG method	0.6583	0.6917	0.6979	0.7458	**0.7604**$^{(+)}$	0.7188	0.6729

$^{(+)}$ No significant difference among them at $p<0.05$; Bold value means the higher AUC score; Underlying value means the selected one scheme.

Besides, the classification results on DS2.Mi.nC dataset underlined as the best combination, the scheme formed by the FFBP neural network classifier and the 1Rule method using 10 features, attaining an AUC value of 0.754 (see Figure 16 d, e and f). In this dataset, only a few classification schemes provided AUC values superior to 0.70 (low classification performance). As it can read in Table 16, the best classification result statistically overcomes the remaining classification schemes.

Table 16 The AUC-based statistical comparison among the three best combinations on DS2.Mi.nC dataset

Classification Model	Number of Features				
	10	**20**	**30**	**40**	**48**
FFBP neural network / 1Rule method	**0.7542**(*)	0.6167	0.6438	0.6792	0.6542
SVM / 1Rule method	0.65	0.7063	0.6729	0.6625	0.6542
DTJ48 / CHI2 Discretization	0.7208	0.7	0.6604	0.6104	0.6438

(*) Statistically superior among all values at $p<0.05$; Bold value means the higher AUC score; Underlying value means the selected one scheme.

Classification of Masses

Several classification results, when using clinical features on masses, were superior to an AUC value of 0.80 in the DS1.Ma.C dataset, which are globally considered as acceptable results (see Figure 17 a, b and c). The higher AUC score of 0.9539 belongs to the classification scheme formed by the SVM classifier and the CHI2 discretization method using 25 features (see Figure 17 b). However, this result was not statistically superior ($p<0.05$) to obtained results by the combinations of the FFBP neural network classifier and the CHI2 discretization method with 20 features (AUC value of 0.9496), and the combination of the SVM classifier with the CHI2 discretization method using 20 features, which had also a good performance result (AUC value of 0.9485). Therefore, both combinations using 20 features could be considered as most appropriated classification schemes for masses classification in the DS1.Ma.C dataset. In this case, it was preferred the selection of the scheme formed by the SVM classifier and the CHI2 discretization method using 20 features, due to the fact of being a less complex classification model. The table 17 shows the best classification schemes for DS1.Ma.C dataset and the statistical comparison among all of them.

Table 17 The AUC-based statistical comparison among the three best combinations on DS1.Ma.C dataset.

Classification Model	Number of Features							
	5	**10**	**15**	**20**	**25**	**30**	**35**	**39**
FFBP neural network / CHI2 discretization	0.8673	0.9015	0.9175	0.9496(+)	0.9426	0.9301	0.9256	0.9259
SVM / CHI2 Discretization	0.8666	0.9027	0.9325	<u>0.9485</u>(+)	**0.9539(+)**	0.9305	0.9289	0.9383
DTJ48 / IG method	0.8005	0.8712	0.9102	0.9254	0.9195	0.9349	0.9377	0.9300

(+) No significant difference among them at p<0.05; Bold value means the higher AUC score; Underlying value means the selected one scheme.

The masses classifications performances in the dataset without including clinical features (DS1.Ma.nC) resulted in worse AUC scores with respect to the dataset including clinical features (see Figure 18). Only classification schemes using the CHI2 discretization and IG methods provided an AUC value superior to 0.80. The higher result in the DS1.Ma.nC dataset was obtained by the combination of the SVM classifier and the CHI2 discretization method with 15 features, attaining an AUC value of 0.8672 (see Table 18).

Table 18 The AUC-based statistical comparison among the three best combinations on DS1.Ma.nC dataset.

Classification Model	Number of Features				
	5	**10**	**15**	**20**	**24**
FFBP neural network / CHI2 discretization	0.8601	<u>0.8658</u>(+)	0.8585	0.8603	0.8487
SVM / CHI2 Discretization	0.8576	0.83	**0.8672(+)**	0.8589	0.8536
DTJ48 / CHI2 Discretization	0.8031	0.8096	0.845	0.8634(+)	0.86

(+) No significant difference among them at p<0.05; Bold value means the higher AUC score; Underlying value means the selected one scheme.

From Table 18, the higher AUC value obtained by the SVM classifier and the CHI2 discretization method did not overcome statistically others combinations such as: the FFBP neural network and DTJ48 classifiers with the same CHI2 discretization method using 10 and 20 features respectively. In this case, it was preferred the combination which used the smaller number of features as the most appropriate classification scheme for masses classification in the DS1.Ma.nC dataset.

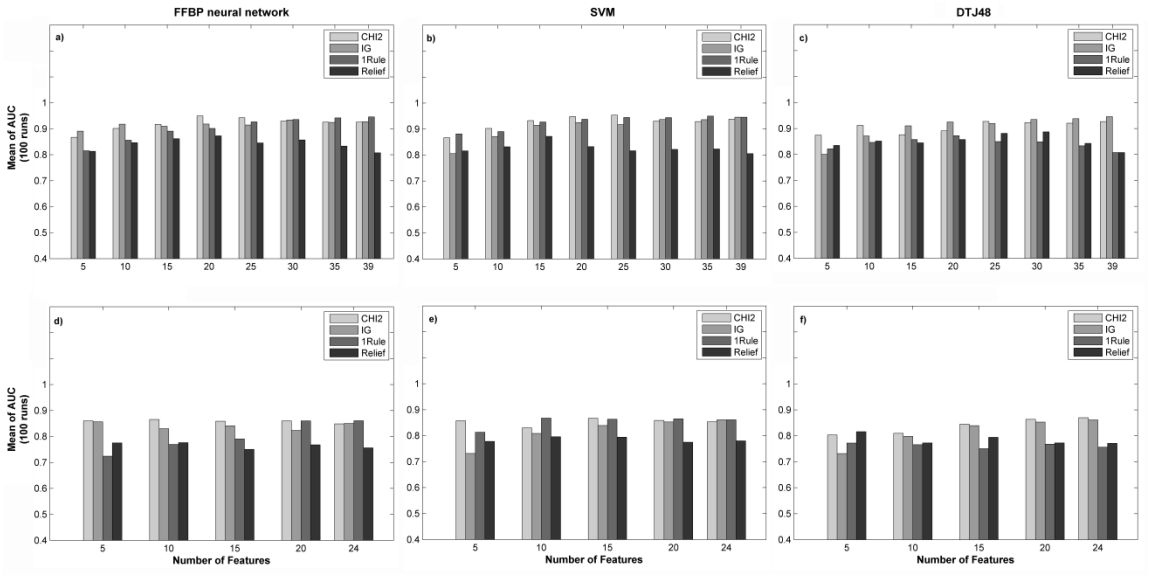

Figure 17 The mean of AUC scores (on 100 runs) of different classification schemes on DS1.Ma.C (first row) and DS1.Ma.nC (second row) datasets.

The best performance using DS2.Ma.C dataset was reached by the SVM classifier and the 1Rule discretization method with 30 features, reaching an AUC value of 0.9649 (see Figure 18 b). This higher result was almost statistically superior to the remainder classification scheme. Only one combination using the same classifier and feature selection method with 40 features provided not significantly difference between them (see Table 19). However, the most appropriate classification scheme for masses classification using the DS2.Ma.C dataset is the combination which used smaller number of features without affecting the classification performance (see Table 19).

Table 19 The AUC-based statistical comparison among the three best combinations on DS2.Ma.C dataset.

Classification Model	**Number of Features**						
	10	**20**	**30**	**40**	**50**	**60**	**64**
FFBP neural network / IG method	0.9495	0.9103	0.9325	0.9373	0.9398	0.9523	0.9307
SVM / 1Rule method	0.9213	0.94	**0.9649**$^{(+)}$	0.9609$^{(+)}$	0.9589	0.9595	0.9374
DTJ48 / IG method	0.8598	0.9136	0.9511	0.9502	0.946	0.9406	0.9374

$^{(+)}$ No significant difference among them at $p<0.05$; Bold value means the higher AUC score; Underlying value means the selected one scheme.

On the other hand, the best classification score using the DS2.Ma.nC dataset was acquired by the FFBP neural network classifier in aggregation to the IG method with 40 features, attainment an AUC value of 0.8899 (see Figure 18 d). This classification result was the highest AUC value using the DS2.Ma.nC dataset, but it was not significantly different to the combination formed by the SVM classifier and the 1Rule method using 40 features, which reached an AUC value of 0.8863 (see Table 20).

Table 20 The AUC-based statistical comparison among the three best combinations on DS2.Ma.nC dataset.

Classification Model	**Number of Features**				
	10	**20**	**30**	**40**	**48**
FFBP neural network / IG method	0.8004	0.854	0.8794	**0.8899**$^{(+)}$	0.8742
SVM / 1Rule method	0.8394	0.863	0.8655	0.8863$^{(+)}$	0.8643
DTJ48 / IG method	0.7316	0.8041	0.8275	0.8719	0.8643

$^{(+)}$ No significant difference among them at $p<0.05$; Bold value means the higher AUC score; Underlying value means the selected one scheme.

From Table 20, there are two combinations that can be used as the most appropriate classification schemes for masses classification using the DS2.Ma.nC dataset. In this case, the computation time and the simplicity of the classification model were the key for selecting the scheme formed by the SVM classifier and the 1Rule method with 40 features.

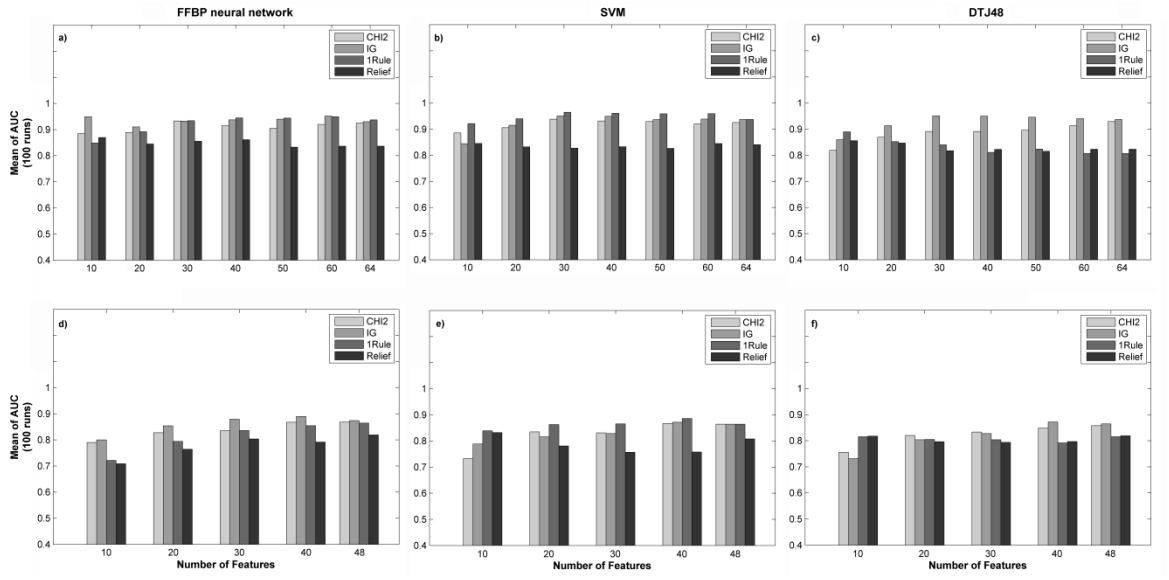

Figure 18 The mean of AUC scores (on 100 runs) of different classification schemes on DS2.Ma.C (first row) and DS2.Ma.nC (second row) datasets.

Classification of All Lesions (Masses and Microcalcifications together)

The classification results on datasets containing both lesions point as the winner combination the SVM classifier and the CHI2 discretization method with 30 features in the DS1.All.C dataset, attaining an AUC value of 0.934 (see Figure 19 b). This result was almost the winner (in terms of AUC value) when comparing to the rest of the classification results. Two other combinations provided similar satisfactory classification performance: the FFBP neural network and SVM classifiers in conjunction with the CHI2 discretization method using 35 features. However, as it can be observed from Table 21, these combinations reached the best classification performance with more features (35 features). Therefore, the selected combination with 30 features constituted the best classification scheme for DS1.All.C dataset.

Table 21 The AUC-based statistical comparison among the three best combinations on DS1.All.C dataset.

Classification Model	**Number of Features**							
	5	**10**	**15**	**20**	**25**	**30**	**35**	**39**
FFBP neural network / IG method	0.9055	0.9109	0.9113	0.9164	0.9149	0.9227	0.9279$^{(+)}$	0.9260
SVM / CHI2 Discretization	0.8562	0.8533	0.8957	0.8984	0.9122	**0.934**$^{(+)}$	0.928$^{(+)}$	0.9264
DTJ48 / CHI2 Discretization	0.8626	0.8768	0.9037	0.9226	0.92	0.9254	0.9270	0.9256

$^{(+)}$ No significant difference among them at $p<0.05$; Bold value means the higher AUC score; Underlying value means the selected one scheme.

The best classification result for the DS1.All.nC dataset was obtained by the combination of the SVM classifier and the CHI2 discretization method with 20 features; attaining an AUC score of 0.843 (see Figure 19 e). This result statistically surpasses the remaining classification schemes (see Table 22). Therefore, it could be considered as the most appropriated classification scheme for this dataset.

Table 22 The AUC-based statistical comparison among the three best combinations on DS1.All.nC dataset.

Classification Model	Number of Features				
	5	**10**	**15**	**20**	**24**
FFBP neural network / CHI2 discretization	0.7957	0.81	0.8209	0.831	0.821
SVM / CHI2 Discretization	0.7806	0.8149	0.8188	**0.843**$^{(*)}$	0.8305
DTJ48 / CHI2 Discretization	0.7743	0.7969	0.8054	0.823	0.8173

$^{(*)}$ Statistically superior among all values at $p<0.05$; Bold value means the higher AUC score; Underlying value means the selected one scheme.

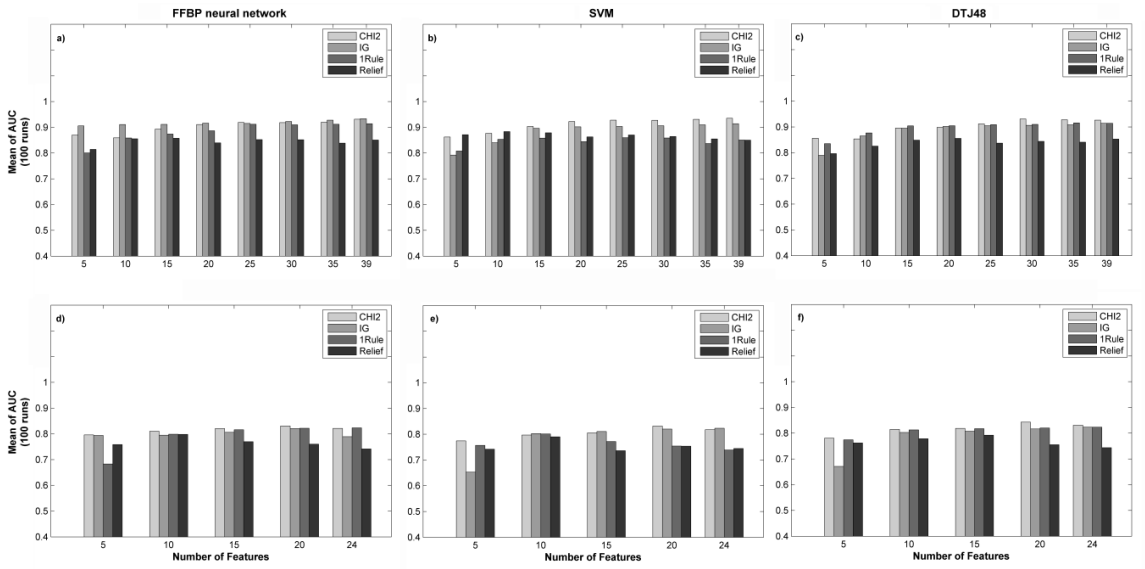

Figure 19 The mean of AUC scores (on 100 runs) of different classification schemes on DS1.All.C (first row) and DS1.All.nC (second row) datasets.

The higher classification result in the DS2.All.C dataset was obtained by the combination of the SVM classifier and the 1Rule method with 30 features, stretching an AUC value of 0.8874 (see Figure 20 b). According to the statistical test, this result was not the best classification scheme. Two others combinations using a smaller set of features demonstrated to be statistically similar in terms of classification performance (see Table 23). Thus, the most appropriated classification scheme in this dataset was the one formed by the SVM classifier and the 1Rule method using 20 features (AUC value of 0.8812), which provided a less complex classification model.

Table 23 The AUC-based statistical comparison among the three best combinations on DS2.All.C dataset.

Classification Model	Number of Features						
	10	**20**	**30**	**40**	**50**	**60**	**64**
FFBP neural network / IG method	0.844	0.8832$^{(+)}$	0.8443	0.8631	0.8572	0.8581	0.8401
SVM / 1Rule method	0.8731	<u>0.8812</u>$^{(+)}$	**0.8878**$^{(+)}$	0.8739	0.8698	0.86	0.8526
DTJ48 / IG method	0.8423	0.8495	0.8594	0.8629	0.8591	0.8535	0.8526

$^{(+)}$ No significant difference among them at $p<0.05$; Bold value means the higher AUC score; Underlying value means the selected one scheme.

The best classification result in the DS2.All.nC dataset was obtained by the combination of the SVM classifier and the CHI2 discretization method using a total of 40 features (see Figure 20 e). This classification scheme provided the highest AUC value (0.8409) among all combinations and also was statistically superior to the remainder results. Therefore, this combination constituted the most appropriated classification scheme in this dataset (see Table 24).

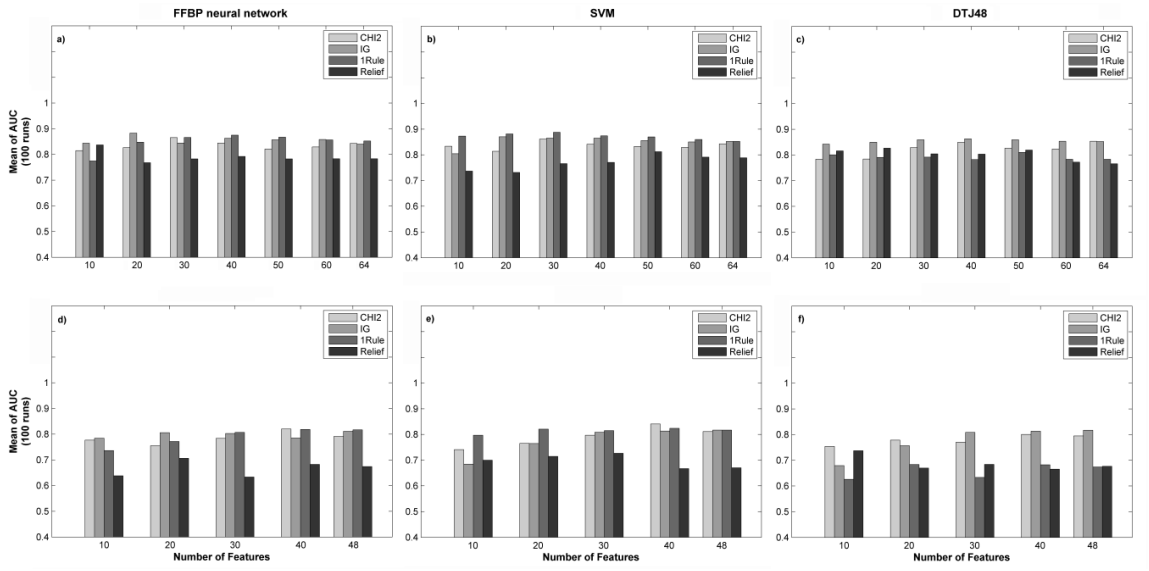

Figure 20 The mean of AUC scores (on 100 runs) of different classification schemes on DS2.All.C (first row) and DS2.All.nC (second row) datasets.

Table 24 The AUC-based statistical comparison among the three best combinations on DS2.All.nC dataset.

Classification Model	Number of Features				
	10	**20**	**30**	**40**	**48**
FFBP neural network / CHI2 discretization	0.7771	0.7555	0.7837	0.8204	0.7914
SVM / CHI2 discretization	0.741	0.7652	0.7969	**0.8409**$^{(*)}$	0.8111
DTJ48 / IG method	0.6796	0.757	0.8084	0.8135	0.8168

$^{(*)}$ Statistically superior among all values at $p<0.05$; Bold value means the higher AUC score; Underlying value means the selected one scheme.

Feature Relevance Analysis

The results listed in the previous section clearly provide experimental evidence that optimal classification performance depends upon the appropriate choice of a classifier together with a ranked subset of features and, the combination of clinical with image-based features increase the classification performance substantially for all cases. Therefore, it was our intention to find out the most important features in the whole features space.

The relevance of features was determined by the separation of 48 ranking of features (one by each employed feature selection method on every experimental dataset) into four ranking groups: Single View Ranking including Clinical features (SVRC), Single View Ranking without including Clinical features (SVRNC), Multi View Ranking including Clinical features (MVRC) and Multi View Ranking without including Clinical features (MVRC). For each group, the total of features to be analyzed was computed by averaging the size of features subset in each winner scheme. Finally, the relevance of feature was decided by averaging its position along all rankings within the group under analysis.

Relevance within SVRC and MVRC groups

The SVRC group is formed by the ranked features extracted from DS1.Mi.C, DS1.Ma.C and DS1.All.C datasets respectively and the total of features to be analyzed is approximately 25. Therefore, we considered only the top 25 features of each ranking for features relevance analysis in this group. Figure 21 shows the distribution of the average position for each selected feature.

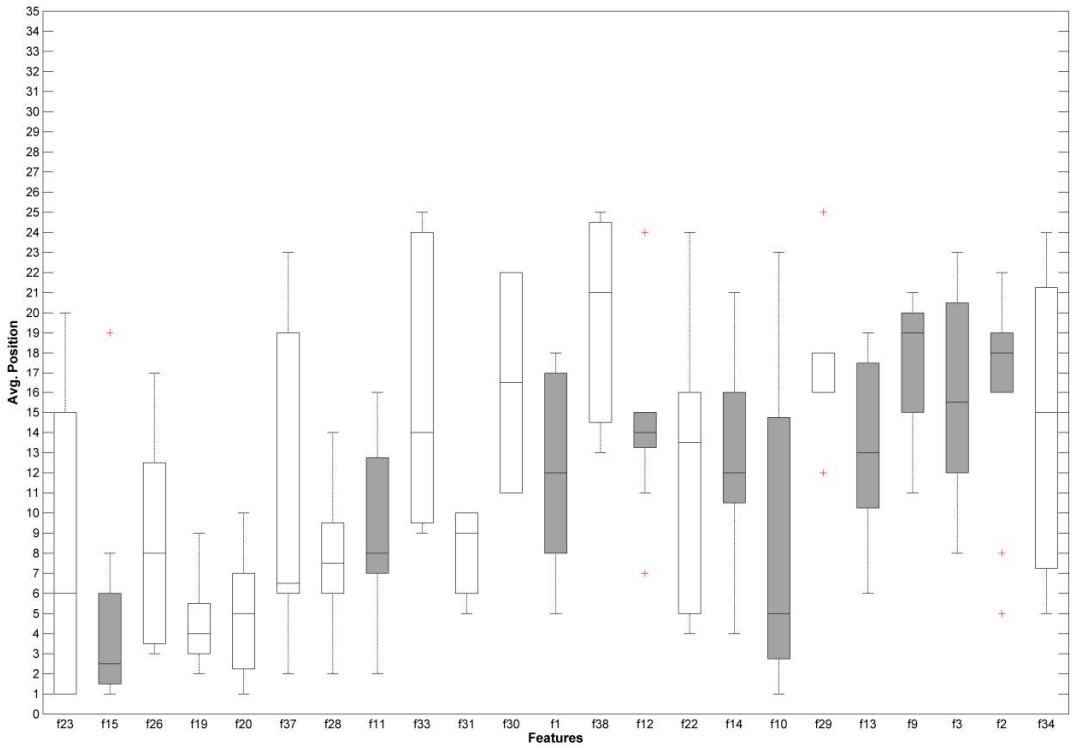

Figure 21 Distribution of the average position for each selected clinical (filled box) and image-based (white box) features within the SVRC group.

The top clinical and image-based feature within this group was the Mammography stroma distortion (f_{15}) and Circularity (f_{19}) with average positions of 2.5 and 4 respectively (see Figure 21, f_{15} and f_{19}). Even with a slight difference between them, the Mammography stroma distortion (f_{15}) clinical feature was the most consistent. Also, the presence of other clinical (43%) and image-based (57%) features such as: Mammography calcification (f_{11}), Density (f_1), Mammography microcalcification (f_{12}), Mammography architectural distortion (f_{14}), Mammography nodule (f_{10}), Mammography axillary adenopathy (f_{13}), Retroareolar (f_9), Right top quadrant (f_3), breast location (f_2), Roughness (f_{23}), Shape (f_{26}), Perimeter (f_{20}), Area (f_{37}), Entropy (f_{28}), Contrast (f_{33}), Energy (f_{31}), Y center mass (f_{30}), Y centroid (f_{38}), standard deviation (f_{32}), X center mass (f_{29}) and Correlation (f_{34}) contributed to the classification performances.

On the other hand, the MVRC group contains the ranked features extracted from DS2.Mi.C, DS2.Ma.C and DS2.All.C datasets respectively and the total of features to be analyzes is 27. Therefore, only 27 features were considered for relevance analysis. Similar to SVRC group, the relevance analysis in this group highlighted as the top clinical and image-based features, the Mammography stroma distortion (f_{15}) and Circularity (f_{19}) features with average positions

of 2 and 4 respectively (see Figure 22). The f_{15} feature like in SVRC group appears as the most consistent feature inside the group. The rest of clinical and image-based features selected in this group were: Roughness (f_{23} and f_{23*}), Perimeter (f_{20*} and f_{20}), Circularity (f_{19*}), Entropy (f_{28}), Mammography calcification (f_{11}), Area (f_{37*} and f_{37}), Density (f_1), Y center mass (f_{30} and f_{30*}), Contrast (f_{33*} and f_{33}), Y centroid (f_{38} and f_{38*}), Standard deviation (f_{22}), Energy (f_{31} and f_{31*}), Shape (f_{26} and f_{26*}), Mammography microcalcification (f_{12}), Mammography axillary adenopathy (f_{13}), Elongation (f_{21}) and Mammography nodule (f_{10}). In contrast with the SVRC group, the best classification performances and the equilibrium of features representation (22% for clinical against to a 78% for image-based) in this group were considered lower. These particular differences could be associated to the double presence of image-based features (see Figure 22, features with asterisk) in the features vectors.

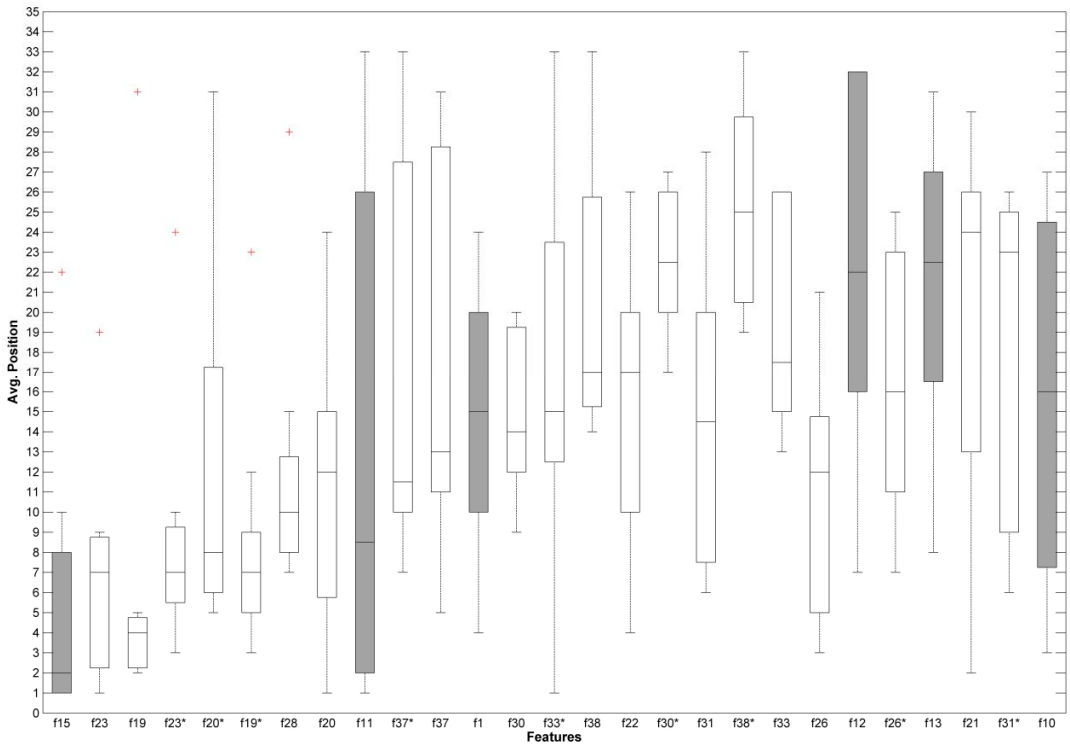

Figure 22 Distribution of the average position for each selected clinical (filled box) and image-based (white box) features within the MVRC group. Features with asterisk (*) represent a computed feature in the collateral view (MLO and CC).

Relevance within SVRNC and MVRNC groups

The SVRNC group is formed by the ranked features extracted from DS1.Mi.nC, DS1.Ma.nC and DS1.All.nC datasets respectively and the total of features to be analyzed is approximately 12. Therefore, only the top 12 features were considered for feature relevance analysis in this group. Figure 23 shows the distribution of the average position for each selected feature.

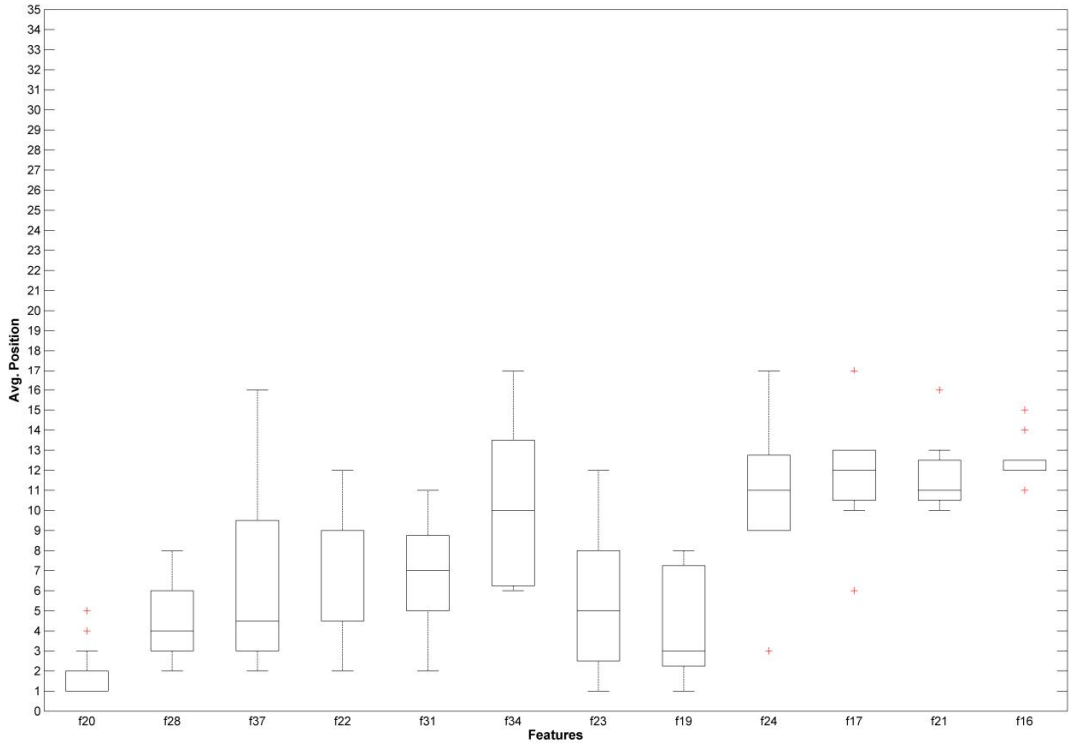

Figure 23 Distribution of the average position for each selected image-based features within the SVRNC group.

The Perimeter (f_{20}) feature (see Figure 23) was ranked as the top image-based feature within the group, only two feature selection methods (1Rule and Relief) does not considered it as the best feature, although it was ranked on the top 5. Also, the presence of other image-based features such as: Entropy (f_{28}), Area (f_{37}), Standard deviation (f_{22}), Energy (f_{31}), Correlation (f_{34}), Roughness (f_{23}), Circularity (f_{19}), Minimum (f_{24}), Kurtosis (f_{17}), Elongation (f_{21}) and Skewness (f_{16}) contributed to the classification performances.

The MVRNC group was created by the set of ranked features generated from DS2.Mi.nC, DS2.Ma.nC and DS2.All.nC datasets respectively and the total of features to be analyzed in this group is 30. The relevance analysis highlighted the Circularity (f_{19}) as the best feature in this group, with an average position of 2. The remaining contributions were provided by

features like: Perimeter (f_{20}), Entropy (f_{28}), Shape (f_{26}) and Roughness (f_{23}), which were rated in the top 10 inside this group (see Figure 24). Despite classifications performances inside this group may be considered as acceptable (0.7542, 0.8863 and 0.8404), those results were less impressive than classifications performances achieved in others group such as: SVRC and MVRC respectively.

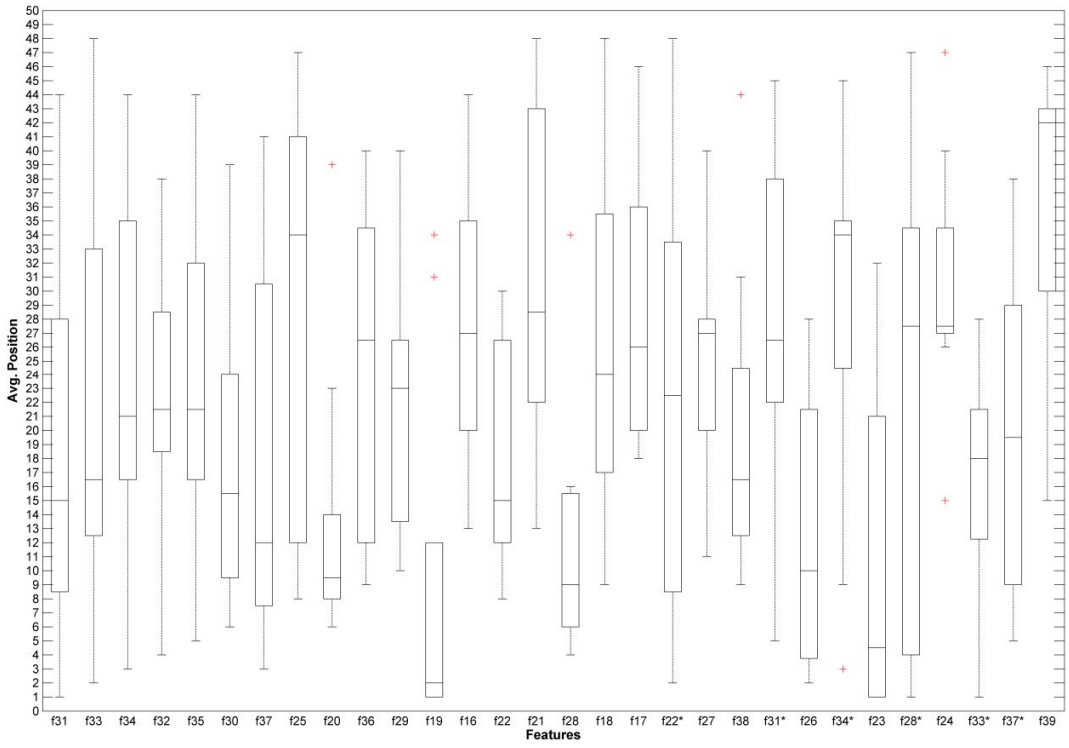

Figure 24 Distribution of the average position for each selected image-based features within the MVRNC group.

An overall perspective on image-based features relevance highlights the Circularity (f_{19}), Perimeter (f_{20}), Area (f_{37}), Entropy (f_{28}), Energy (f_{31}) and Standard deviation (f_{22}) which were selected as equally significant in the four groups. Also, additional features such as: Contrast (f_{33}), X center mass (f_{29}) and Y center mass (f_{30}), Y centroid (f_{38}), Correlation (f_{34}) and Elongation (f_{21}) demonstrated to be important appearing consistently on three groups.

3.6.2. Second Experiment

In this experiment, a total of 350 ranked subsets of features containing clinical and image-based features were analyzed. The produced subsets of features were applied for feeding five machine learning classifiers: FFBP neural network, SVM, NB, LDA and kNN in order to offer experimental evidences of features relevance within a features space extracted from both the MLC and CC mammography image view, as well as finding a breast cancer classification scheme that provides the highest performance.

The combination of CHI2 discretization, IG, 1Rule, Relief and *RMean* methods with the FFBP neural network, SVM, NB, LDA and kNN classifiers provided reliable results to classify pathological lesions in both microcalcifications and masses datasets. As it is shown in Figure 25 and 26, the NB and SVM classifiers provided the best AUC scores for DS2.Mi.C and DS2.Ma.C datasets respectively.

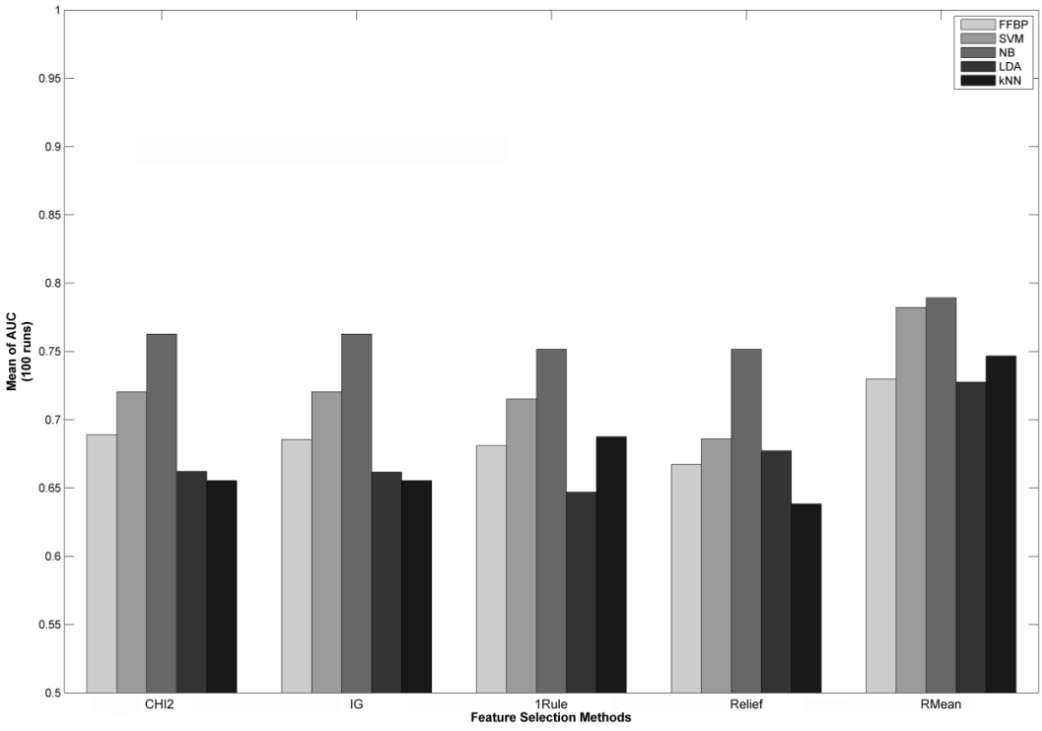

Figure 25 Performance evaluation of five MLCs on MCs dataset.

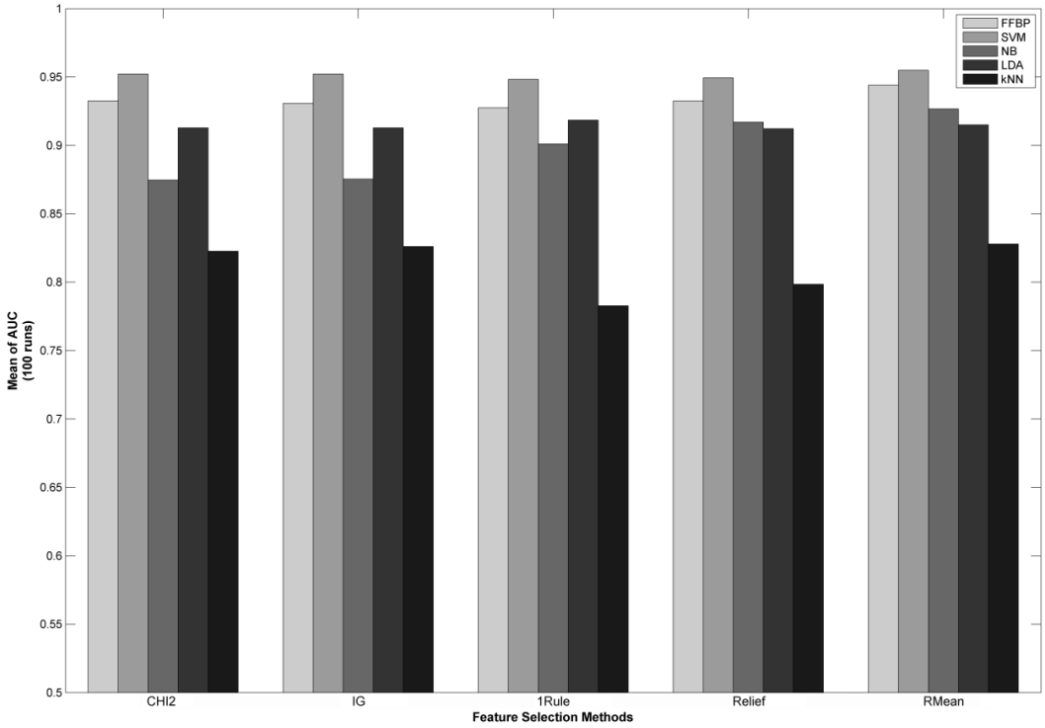

Figure 26 Performance evaluation of five MLCs on masses dataset.

Performance Evaluation

Classification results for MCs datasets illustrated that all machine learning classifiers provided the best AUC score when using the *RMean* method. The higher AUC score was obtained by the combination of the NB classifier and the *RMean* method with a total of 20 features, achieving an AUC score of 0.7893 with standard deviation of 0.16. Table 25 shows the best classification performance on DS2.Mi.C dataset and the number of features employed by each combination.

Table 25 The best classification performance based on AUC scores for the DS2.Mi.C dataset.

Pairs (FSM/MLC)	**CHI2**		**IG**		**1Rule**		**Relief**		***RMean***	
	AUC	**NF**	**AUC**	**NF**	**AUC**	**NF**	**AUC**	**NF**	**AUC**	**NF**
FFBP neural network	0.6890	30	0.6856	30	0.6810	30	0.6673	60	**0.7298**	**10**
SVM	0.7204	20	0.7204	20	0.7152	30	0.6860	60	**0.7823**	**20**
NB	0.7628	60	0.7628	60	0.7516	60	0.7516	60	**0.7893**	**20**
LDA	0.6621	10	0.6617	10	0.6469	10	0.6773	10	**0.7275**	**10**
kNN	0.6554	50	0.6554	50	0.6875	20	0.6383	20	**0.7467**	**10**

NF - means the number of features employed by each subset of features

From Table 25, it is possible to observe that *RMean* method increased the classification performance based on AUC scores for all schemes ($p<0.05$). The same trend of results was

not achieved with other schemes such as: the kNN classifier in conjunction with the CHI2 discretization, IG and Relief methods, which presented the worst AUC scores (0.6554, 0.6554 and 0.6383 respectively). Also, it is interesting to consider that these important results were obtained with no more than 20 features.

According to obtained AUC scores, the best classification scheme was formed by the NB classifier and the *RMean* method with 20 features (AUC score of 0.7893), which represented an AUC numerical difference of: 0.0595, 0.007, 0.0618 and 0.0426 respect to the FFBP neural network, SVM, LDA and kNN classifiers respectively. However, the statistical comparison revealed there is a significant difference in most cases ($p<0.05$); only the scheme formed by the SVM classifier and the *RMean* method using 20 features provided no significant difference on AUC performances. Therefore, it is possible to consider both combinations as appropriate MCs classification schemes (see Table 26).

Table 26 The statistical comparison based on the Wilcoxon Statistical Test for the DS2.Mi.C dataset.

Dataset	**Best scheme**	**AUC**		**Other winner scheme**	**AUC**		**Wilcoxon**
		Mean	**SD**		**Mean**	**SD**	**(α= 0.05)**
DS2.Mi.C	NB+*RMean*+20F	0.7893	0.16	FFBP+*RMean*+10F	0.7298	0.18	p<0.01
				SVM+*RMean*+20F	**0.7823**	**0.17**	**p=0.8109**
				LDA+*RMean*+10F	0.7275	0.18	p<0.01
				kNN+*RMean*+10F	0.7467	0.16	p<0.01

SD - Standard Deviation; F - Features.

In the case of masses classification, almost all machine learning classifiers provided the best AUC score when using the *RMean* method, only the LDA classifier reached a higher AUC score using another features selection method (see Table 30). The most important AUC score was obtained by the combination of the SVM classifier and the *RMean* method with a total of 30 features, for an AUC score of 0.9549 with standard deviation of 0.05. Table 27 shows the best classification performance on DS2.Ma.C dataset and the number of features employed by each combination.

Table 27 The best classification performance based on AUC scores for the DS2.Ma.C dataset.

Pairs (FSM/MLC)	CHI2		IG		1Rule		Relief		*RMean*	
	AUC	NF	AUC	NF	AUC	NF	AUC	NF	AUC	NF
FFBP neural network	0.9326	20	0.9307	60	0.9274	60	0.9324	50	**0.9440**	**10**
SVM	0.9522	50	0.9522	50	0.9483	40	0.9494	50	**0.9549**	**30**
NB	0.8747	10	0.8754	10	0.9011	30	0.9170	10	**0.9267**	**10**
LDA	0.9128	40	0.9128	40	**0.9185**	**30**	0.9122	20	0.9150	40
kNN	0.8226	20	0.8261	20	0.7827	20	0.7985	10	**0.8279**	**30**

NF- Number of Features

From Table 27, it is possible to perceive that the *RMean* method increased the classification performance based on AUC scores for most schemes ($p<0.05$), which is globally considered as good result. In contrast to the MCs classification, the number of selected features by each scheme was superior on masses classification. Only two combinations reached high AUC scores with the minimum number of features.

The best result based on AUC scores belongs to the scheme formed by the SVM classifier and the *RMean* method with 30 features (AUC score of 0.9549), which represents an AUC numerical difference of: 0.0109, 0.0282, 0.0364 and 0.127 with respect to the FFBP neural network, NB, LDA and kNN classifiers respectively. According to the Wilcoxon statistical test [249, 250] most of these numerical differences were statistically significant ($p<0.05$), only one scheme presented no significant AUC difference (see Table 28). Therefore, both combinations were considered as appropriate masses classification schemes. Table 28 shows results of the statistical comparison between the best classification scheme and others winner schemes.

Table 28 The statistical comparison based on the Wilcoxon Statistical Test for the DS2.Ma.C dataset.

Dataset	Best scheme	AUC		Other winner scheme	AUC		Wilcoxon
		Mean	SD		Mean	SD	(α= 0.05)
DS2.Ma.C	SVM+*RMean*+30F	0.9549	0.05	**FFBP+*RMean*+10F**	**0.9440**	**0.05**	**p=0.1256**
				NB+*RMean*+10F	0.9267	0.06	p<0.01
				LDA+1Rule+30F	0.9185	0.07	p<0.01
				kNN+*RMean*+30F	0.8279	0.09	p<0.01

SD - Standard Deviation; F- Features

Classification process on DS2.Mi.C and DS2.Ma.C datasets highlighted two winner schemes for MCs and masses datasets respectively, in which the *RMean* method provided ranked subsets of features with higher discriminant potential.

Features Relevance Analysis

The results listed in Table 26 and 28 provided statistical evidences on selecting the most appropriate classification scheme for MCs and masses datasets. From these results, two combinations resulted as the best classification performances per dataset. Thus, the features relevance analysis was conducted using these winner schemes and the following procedure: (1) corroborating of selected features in the best classification scheme as the most appropriate features subset for pathological lesions classification, and (2) determining features with higher importance inside each dataset.

Features Subset Validation

The validation of selected features subsets and its impact in the classification performance was based in the non-parametric Wilcoxon statistical test [249, 250] as the principal metric. In this process we compared AUC performances between the best scheme and the same combination using fewer features, and the key issue is to know how many features subsets could be reduced without affecting the classification performance. Table 29 shows the statistical results after applying the process of features subset validation.

Table 29 Results of the feature subset validation process.

Dataset	**Best scheme**	**AUC**		**Same scheme with**	**AUC**		**Wilcoxon**
		Mean	**SD**	**fewer features**	**Mean**	**SD**	**(α= 0.05)**
DS2.Mi.C	(1) NB+*RMean*+20F	0.7893	0.16	NB+*RMean*+10F	0.7395	0.20	p<0.01
	(2) SVM+*RMean*+20F	0.7823	0.17	SVM+*RMean*+10F	0.7775	0.17	p=0.8109
DS2.Ma.C	(3) SVM+*RMean*+30F	0.9549	0.05	SVM+*RMean*+10F	0.9271	0.06	p<0.01
	(4) FFBP+*RMean*+10F	0.9440	0.05	N/A	N/A	N/A	N/A

SD- Standard Deviation; F- Features; N/A – Not Applicable

After completing the comparison, for MCs dataset (DS2.Mi.C) only one scheme provided clear evidence of features subset reduction. From Table 29 it can be observed there is no significant difference with respect to the obtained AUC scores between one of the most appropriate schemes (scheme 2) and the same scheme using a more compact features subset. Therefore, it was possible to reduce the features subset from 20 to 10 features without affecting the consistency of the classification performance.

For the masses dataset (DS2.Ma.C), it was impossible the features subset reduction on one of the most appropriate schemes (see Table 29 scheme 3) because there is statistical evidence on

classification performance degradation. However, the scheme formed by the FFBP neural network and the *RMean* method guaranteed the use of minimal quantity of features for classifying masses. This means that selected features could be considered as the most relevant features subset.

Features with Higher Importance

In the previous section, we showed how to determine if selected features subsets constitute the most important extracted subset from the features space. From both DS2.Mi.C and DS2.Ma.C datasets were extracted features subsets with a minimum number of features without affecting the classification performance, which infers that selected features were relevant for MCs and masses classification.

The most relevant features subset for MCs classification was composed by three clinical and seven image-based features: Perimeter (f_{20}), Standard deviation (f_{22} and f_{22*}), Entropy (f_{28} and f_{28*}), Mammography stroma distortion (f_{15}), Density (f_1), Energy (f_{31} and f_{31*}) and Right bottom quadrant (f_4). Clinical features like f_{15} and f_4 were selected as relevant due to its great capacity of discriminating between masses and MCs. The f_{15} feature means the presence of architectural distortion that is a particular classification of masses. Meanwhile the f_4 feature means the location of the lesion, mostly used for MCs [7, 156]. As MCs are smaller and brighter than masses, image-based features are very useful. For example, the f_{20} feature (top ranked feature for MCs) will take smaller value than the f_{20} feature extracted from masses lesions and constitutes a discriminant feature between masses and MCs. In general, image-based features (intensity statistics, size, shape, etc.) are likely more employed for MCs classification [7, 156].

The most relevant subset of features for masses classification was formed by four clinical and six image-based features: Mammography stroma distortion (f_{15}), Circularity (f_{19} and f_{19*}), Roughness (f_{23} and f_{23*}), Shape (f_{26} and f_{26*}), Mammography calcification (f_{11}), Mammography nodule (f_{10}) and Density (f_1). Clinical features like f_{15} and f_{10} were considered strong features for masses classification because of the presence of architectural distortion and/or nodules constitutes a particular masses classification. On the other hand, selected image-based features were all associated to the shape and topology of masses. For example, the f_{19} and f_{19*} features (circularity features extracted from MLO and CC image view) are measurements related to the mass shape classification [7, 156]. Also, the f_{23} and f_{23*}

(roughness features extracted from MLO and CC image view) are features associated to lesions shape and topology. Generally when roughness value is near to zero means regular contours, which is representative of benign masses, otherwise it is an indicative signal for malignant masses or MCs (usually irregular contours is an indicative signal of malignant lesions [7, 156]).

3.6.3. Global Discussion of Experiments

As it was designed in the experimental setup section, all results were separated in two moments. The first one explored four traditional feature selection methods and three popular machine learning classifiers using a massive features space, which included clinical and image-based features extracted from single and ipsilateral pathological lesions segmentations in mammography images. Meanwhile the second moment was aimed to find classification schemes with less number of features and higher AUC-based performance for MCs and masses classification.

Following obtained results in the first experiment, the Table 30 summarizes the best classification schemes per dataset and the statistical comparison between AUC performances.

Table 30 The best classification scheme per dataset and the statistical comparison at $p<0.05$.

Dataset	Classification Scheme	AUC value	NF
DS1.Mi.C	DTJ48 classifier / IG method	**0.91**	**20**
DS1.Mi.nC	SVM classifier / CHI2 discretization method	**0.8301**	**5**
DS2.Mi.C	FFBP neural network classifier / 1Rule method	0.7604	30
DS2.Mi.nC	FFBP neural network classifier / 1Rule method	0.7542	10
DS1.Ma.C	SVM classifier / CHI2 discretization method	0.9485	20
DS1.Ma.nC	FFBP neural network classifier / CHI2 discretization method	0.8658	10
DS2.Ma.C	SVM classifier / 1Rule method	**0.9649**	**30**
DS2.Ma.nC	SVM classifier / 1Rule method	**0.8863**	**40**
DS1.All.C	SVM classifier / CHI2 discretization method	**0.934**	**30**
DS1.All.nC	SVM classifier / CHI2 discretization method	$0.843^{(+)}$	20
DS2.All.C	SVM classifier / 1Rule method	0.8812	20
DS2.All.nC	SVM classifier / CHI2 discretization method	$0.8309^{(+)}$	40

NF- Number of Features; $^{(+)}$ No significant difference among them at $p<0.05$; Underlying value means the selected one scheme.

From Table 30, it is possible to observe that the best classification schemes for MCs lesions were obtained on datasets with single image view (DS1.Mi.C and DS1.Mi.nC). These results

were significantly superior to the obtained results by the classification schemes on ipsilateral image view datasets (DS2.Mi.C and DS2.Mi.nC). The AUC value of 0.91 obtained by the DTJ48 classifier and the IG method with 20 features in the DS1.Mi.C dataset represents a significant performance increment of 0.15 (with $p<0.005$) respect to the best AUC score of 0.760 obtained by the FFBP classifier and the 1Rule method with 30 features on DS2.Mi.C dataset. Meanwhile, the AUC value of 0.8301 obtained by the SVM classifier and the CHI2 discretization method using 5 features in the DS1.Mi.nC dataset constituted a significant increment of 0.076 (with $p<0.05$) in the classification performance respect to the classification result reached by the FFBP neural network classifier and the 1Rule method using 10 features on DS2.Mi.nC dataset (0.7542).

In the case of masses classification (see Table 30), the best classification performances were obtained on ipsilateral image view datasets (DS2.Ma.C and DS2.Ma.nC). These results were significantly superior to the obtained results by the classification schemes on datasets with single image view (DS1.Ma.C and DS1.Ma.nC). The AUC value of 0.9649 obtained by the SVM classifier and the 1Rule method with 30 features in the DS2.Ma.C dataset represents a slight significant performance increment of 0.16 (with $p<0.005$) respect to the best AUC score of 0.9485 obtained by the SVM classifier and the CHI2 discretization method with 20 features on DS1.Ma.C dataset. Meanwhile, the AUC value of 0.8863 obtained by the SVM classifier and the 1Rule method using 40 features in the DS2.Ma.nC dataset constituted a significant increment of 0.021 (with $p<0.05$) in the classification performance respect to the classification result reached by the FFBP neural network classifier and the CHI2 discretization method using 10 features on DS1.Ma.nC dataset (0.8658).

On the other hand, for all lesions together, the best classification schemes were obtained on datasets using the single image view (DS1.All.C and DS1.All.nC). The AUC value of 0.934 obtained by the best classification scheme (SVM classifier and the CHI2 discretization with 30 features) in the DS1.All.C dataset represented a significant improvement of 0.053 in the AUC value against to the obtained result by the best scheme in the DS2.All.C dataset (SVM classifier and the 1Rule with 20 features), which stretched an AUC value of 0.8812. Also, the best classification scheme (SVM classifier and the CHI2 discretization method with 20 features) in the DS1.All.nC dataset provided an AUC value of 0.843 against to a 0.8409 reached by the best classification scheme (SVM classifier and the CHI2 discretization method with 40 features) in the DS2.All.nC dataset. These results were not significantly different ($p=0.089$) in term of classification performance. However, the classification scheme using a

fewer number of features constituted a less complex classification model and it was preferred (see Table 30).

The statistical difference in AUC performances between single and ipsilateral image view datasets could be explained by the fact of MCs lesions being smaller and brighter than masses lesions [7]. Thus, image-based features extracted from intensity statistics and shapes of segmented MCs in one image view could be considered sufficient for MCs classification. In contrast, masses lesions tend to be obscured and confused with the surrounding tissues. As they are very often characterized by its shape and margin [7], the use of more image-based descriptors extracted from texture, shape and margin of segmented masses on both MLO and CC image view could facilitate its classification.

In terms of features representation it was concluded that the inclusion of clinical features always improved the classification performance for all classification schemes. The balance of features participation between clinical and image-based descriptors was 43% (clinical) against 57% (image-based) for MCs classification and 22% (clinical) against 78% (image-based) for masses classification. These results explained why the best masses classification schemes were obtained using subsets of features extracted from segmented lesions in the ipsilateral image view (image-based descriptors computed from MLO and CC image view).

Regarding the features selection methods and machine learning classifiers, it is possible to observe that the best classification model was formed by the CHI2 discretization features selection method and the SVM classifier; they consistently appeared as the most prominent combination. Other combinations that performed well were: the 1Rule method and SVM classifier; the CHI2 discretization method and FFBP neural network. Finally, all of these combinations could be considered as appropriate classification schemes for breast cancer classification.

Despite the important results reported in the first experiment, it was detected a critical limitation:

- The mean of the number of employed features by the best classification schemes is still elevated: for single image view datasets using clinical features was around 23.33 features (60%); for single image view datasets without using clinical features was around 11.66 features (49%); for ipsilateral image view datasets with clinical features was around 26.66 features (42%) and for ipsilateral image view datasets without clinical features was around 30 features (63%).

Following this limitation, the second experiment provided experimental results of a new developed feature selection method (*RMean*) using MCs and masses ipsilateral image view datasets with clinical features.

The *RMean* method was able to provide ranked subsets of features with no more than 20 features, which increased statistically ($p<0.05$) the classification performance for all classification schemes in the MCs dataset (see Table 25). The same trend of results was obtained in the majority of classification schemes for the masses dataset. Only the LDA classifier considered another feature selection method (1Rule) instead the developed *RMean* method (see Table 27). However, as it is shown in Table 27 there is no significant difference of performance between them.

According to the statistical results presented in the Table 30, it was possible reducing the number of features employed by the best classification scheme on MCs and masses datasets. Both classification schemes were condensed from 20 to 10 features without affecting the classification performance. This means that the developed *RMean* method provides competitive subsets of features with higher discriminant power.

Regarding performance of the *RMean* method, these results were expected since the *RMean* method is based on the combination of four different feature evaluation functions, which mean that an unfairly underrated feature by any feature selection method could have a chance to be ranked as an important feature in the final ranking (output). However, the *RMean* is an univariate filter feature selection method which presents two important drawbacks: (1) it is an individual evaluator of features and it ignores the feature dependencies and, (2) it is dependent of data normalization (since CHI2 and IG method are based on statistical test) and samples sizes, which mean it is vulnerable to unbalanced training data.

Concerning relevant features, the overlay analysis between the features subset selected in the MVRC group of the first experiment ($f_{15,}$ $f_{19,}$ f_{23}, f_{23*}, f_{20*}, f_{19*}, f_{28}, f_{20}, f_{11}, f_{37*}, f_{37}, f_1, f_{30}, f_{33*}, f_{38}, f_{22}, f_{30*}, f_{31}, f_{38*}, f_{33}, f_{26}, f_{12}, f_{26*}, f_{13}, f_{21}, f_{31*}, f_{10}) and the features subsets selected by the developed *RMean* method in the second experiment (f_{20}, f_{22}, f_{22*}, f_{28}, f_{28*}, f_{15}, f_1, f_{31}, f_{31*}, f_4 for DS2.Mi.C dataset and f_{15}, f_{19}, $f_{19*,}$ f_{23}, $f_{23*,}$ f_{26}, $f_{26*,}$ f_{11}, f_{10}, f_1 for DS2.Ma.C dataset) highlighted that the *RMean* method was agreed on 70% and 100% of selected features for MCs (DS2.Mi.C) and masses (DS2.Ma.C) datasets respectively. Although a direct comparison between both experiments is not equitable, these results show the competence of the developed *RMean* method on selecting relevant features.

The most relevant clinical features were mammographic stroma distortion (f_{15}) and density (f_1) appearing persistently on every winner classification scheme. As it was mentioned before, the f_{15} feature is related to the presence of mammographic architectural distortion, which is a particular classification of masses. Meanwhile, the f_1 is a feature divided in four ranges depending on how dense breast tissue can be and where the low density is preferred for lesions detection/classification [7, 156]. In addition, the most relevant image-based features were perimeter (f_{20}) and circularity (f_{19}) for MCs and masses classification respectively. As MCs lesions are smaller than masses the perimeter feature will take smaller value than the perimeter feature extracted from masses lesions. Thus, it constitutes a strong feature for the discrimination between masses and MCs lesions. Similar situation occur with the circularity feature, which is a particular measurement for masses classification [7]. This feature is strongly related to the margin of the mass and its diagnosis, e.g. values nearest to zero, means the margin of the mass is turning into more irregular, and the possibility of being malignant will be higher.

3.7. Conclusions

As result of the proposed experimental methodology, we arrived to the following conclusions:

1. The classification performances on single view datasets (derived from DS1) were statistically favorable for MCs classification; semi favorable for all lesions (together) classification, and not favorable for masses classification.

2. The inclusion of clinical features always improved the classification performance for all classification schemes.

3. The combination of the CHI2 discretization method and SVM classifier produced the best feature selection method and machine learning classifier in the first experiment, due to its consistently participation in all profitable classification schemes.

4. The number of features employed by the best classification schemes in the first experiment was high. This situation provides us an open door for the improvement the features selection.

5. The *RMean* method resulting of the ensemble of the others four experimented methods achieved a high performance when compared to each other's method alone and according to the Wilcoxon statistic test was the best performed method for selecting relevant features, appearing consistently on all succeeds combinations for MCs and masses classification.

6. The *RMean* method improved the performance of mammography-based machine learning classifiers with respect to each single feature selection method, attaining AUC scores of 0.7775 and 0.9440 for MCs and masses datasets respectively.

7. The most relevant clinical features were *Mammograhpy Stroma Distortion* (f_{15}) and *Density* (f_1). They appeared consistently in all successful classification schemes.

8. The most relevant image-based features were the *Perimeter* (f_{20}) for MCs classification and *Circularity* (f_{19}) for masses classification. They were ranked as the top image-based features for the discrimination between MCs and masses lesions.

CHAPTER 4

The *uFilter* Method

This chapter addresses theoretical and implementation details of the *uFilter* feature selection method, as well as the experimental methodology for its evaluation in breast cancer databases. Also, it is describes a formal framework for understanding the proposed algorithm, which is supported on the statistical model/theory of the non-parametric Mann- Whitney U test [252]. The *uFilter* improved the Mann Whitney U-test for reducing dimensionality and ranking features in binary classification problems. It is an univariate filter method that solves some difficulties remaining on previous methods (including the *RMean*), such as: it is effective in ranking relevant features independently of the samples sizes (tolerant to unbalanced training data) and it does not need any type of data normalization. The performance results are presented and discussed in three ways: (1) a head-to-head statistical comparison between the *uFilter* method and its theoretical basis method, (2) a global comparison between the *uFilter* method with other four well-known features selection methods and, (3) a head-to-head statistical comparison of the *uFilter* method against the *RMean* method. Also, we analyzed the relevance of feature based on the Pearson correlation [253] as a complementary step to the *uFilter* method to determine and eliminate redundant features from relevant ones, and thus to produce the final subset.

4.1. Introduction

Devijver and Kittler define feature selection as the problem of "*extracting from the raw data the information which is most relevant for classification purposes, in the sense of minimizing the within-class pattern variability while enhancing the between-class pattern variability*" [254]. Guyon and Elisseeff consider that "*feature selection addresses the problem of finding the most compact and informative set of features, to improve the efficiency or data storage and processing*" [57].

During the last decade parallel efforts from researchers in statistics, machine learning, and knowledge discovery have been focused on the problem of feature selection and its influence in MLCs. The recent advances made in both sensing technologies and machine learning techniques make it possible to design recognition systems, which are capable of performing tasks that could not be performed in the past [57]. Feature selection lies at the center of these advances with applications in the pharmaceutical industry [255, 256], oil industry [257, 258], speech recognition [259, 260], pattern recognition [56, 102], biotechnology [261, 262] and many other emerging fields with significant impact in health systems for cancer detection [28, 129, 222, 263].

In contrast to other dimensionality reduction techniques like those based on projection (e.g. principal component analysis) or compression (e.g. using information theory), feature selection techniques do not alter the original representation of the variables, but merely select a subset of them. Thus, they preserve the original semantics of the variables, hence, offering the advantage of interpretability by a domain expert [264].

As it was mentioned in previous chapters, feature selection techniques are structured in three categories: filter (univariate and multivariate), wrapper and more recently, hybrid models, which combine filter and wrapper methods as a unique model. Wrappers are strictly dependent of MLCs for selecting relevant features. In opposite, filter methods use heuristics based on general characteristics of the data to evaluate the relevance of features. As result, filter methods present lower algorithm complexity and are much faster than wrapper or hybrid methods [4, 11].

Univariate filter methods, such as CHI2 [96], t-test [97], IG [98], Gain Ratio [99] and *RMean* [4, 246] present two main disadvantages: 1) ignoring the dependencies among features and 2)

assuming a given distribution (Gaussian in most cases) from which the samples (observations) have been collected. In addition, to assume a Gaussian distribution includes the difficulties to validate distributional assumptions because of small sample sizes. On the other hand, multivariate filters methods such as: Correlation based-feature selection [97, 100], Markov blanket filter [101], Fast correlation based-Feature selection [102], ReliefF [103, 104] overcome the problem of ignoring feature dependencies introducing redundancy analysis (models feature dependencies) at some degree, but the improvements are not always significant: domains with large numbers of input variables suffer from the curse of dimensionality and multivariate methods may overfit the data. Also, they are slower and less scalable than univariate methods [56, 57].

To overcome these inconveniences we developed the *uFilter* method. *uFilter* is an innovative feature selection method for ranking relevant features that assess the relevance of features by computing the separability between class-data distribution of each feature. The *uFilter* is an univariate filter method that solves some difficulties remaining on previous methods, such as: (1) it is effective in ranking relevant features independently of the samples sizes (tolerant to unbalanced training data); (2) it does not need any type of data normalization; and (3) the most important, it presents a low risk of data overfitting and does not incur the high computational cost of conducting a search through the space of feature subsets as in the wrapper or embedded methods.

4.2. The Mann - Whitney U-test

The Mann-Whitney U test is a non-parametric test (of the t-test) used to test whether two independent samples of observations are drawn from the same or identical distributions. The U test is based on the idea that the particular pattern exhibited when m number of *X* random variables and *n* number of *Y* random variables are arranged together in increasing order of magnitude provides information about the relationship between their parent populations [252]. The Mann-Whitney test criterion is based on the magnitude of the *Y's* in relation to the *X's* (e.g. the position of *Y's* in the combined ordered sequence). A sample pattern of arrangement where most of the *Y's* are greater than most of the *X's* or vice versa would be evidence against random mixing. This would tend to discredit the null hypothesis of identical distribution [265].

Foundation of the test

Hypothesis evaluated: Do two independent samples represent two populations with different median values (or different distributions with respect to the rank-orderings of the scores in the two underlying population distributions)?

Relevant Background Information

The Mann-Whitney U test is employed with ordinal (rank-order) data in a hypothesis testing situation involving a design with two independent samples. If the result of the Mann-Whitney U test is significant, it indicates there is a significant difference between the two sample medians, and as a result of the latter the researcher can conclude there is a high likelihood that the samples represent populations with different median values.

There are two versions of the Mann-Whitney U test, which were independently developed by Mann and Whitney [251] and Wilcoxon [266]. The first version is described here and is commonly identified as the Mann-Whitney U test, while the second version developed by Wilcoxon is usually referred as the Wilcoxon-Mann-Whitney test. Although they employ different equations and different tables, the two versions of the test yield comparable results. When the Mann-Whitney U test is employed, one of the following cases is true with regard to the rank-order data that are evaluated: (1) The data are in a rank-order format, since it is the only format in which scores are available; or (2) The data have been transformed into a rank-order format from an interval/ratio format, since the researcher has reason to believe that the normality assumption (as well as, perhaps, the homogeneity of variance assumption) of the t-test for two independent samples (which is the parametric analog of the Mann-Whitney U test) is saliently violated.

The Mann-Whitney U test undertakes the following assumptions [267]:

a) Each sample has been randomly selected from the population it represents.

b) The two samples are independent of one another.

c) The original variable observed (which is subsequently ranked) is a continuous random variable. In truth, this assumption, which is common to many nonparametric tests, is

often not adhered to, in that such tests are often employed with a dependent variable which represents a discrete random variable.

d) The underlying distributions from which the samples are derived are identical in shape.

The work of Maxwell and Delaney [268] point out the assumption of identically shaped distributions implies equal dispersion of data within each distribution. Because of this, they note that like the t-test for two independent samples, the Mann-Whitney U test also assumes homogeneity of variance with respect to the underlying population distributions. Because the latter assumption is not generally acknowledged for the Mann-Whitney U test, it is not uncommon for sources to state that violation of the homogeneity of variance assumption justifies use of the Mann-Whitney U test in lieu of the t-test for two independent samples.

It should be pointed out, that there is some empirical evidence which suggests that the sampling distribution for the Mann-Whitney U test is not as affected by violation of the homogeneity of variance assumption as is the sampling distribution for t-test for two independent samples. One reason cited by various sources for employing the Mann-Whitney U test is that by virtue of ranking interval/ratio data, a researcher will be able to reduce or eliminate the impact of outliers, which can dramatically influence variability (they can be responsible for heterogeneity of variance between two or more samples).

Null versus Alternative Hypotheses

Null hypothesis:

$H_0 : \theta_1 = \theta_2$. The median of the population Group 1 represents equals the median of the population Group 2 represents. With respect to the sample data, when both groups have an equal sample size, this translates into the sum of the ranks of Group 1 being equal to the sum of the ranks of Group 2 (i.e. $\sum R_1 = \sum R_2$. A more general way of stating this, which also encompasses designs involving unequal sample sizes, is that the means of the ranks of the two groups are equal (i.e. $\overline{R}_1 = \overline{R}_2$).

Alternative hypothesis:

1. $H_1 : \theta_1 \neq \theta_2$. The median of the population Group 1 represents does not equal the median of the population Group 2 represents. With respect to the sample data, when both groups have an equal sample size, this translates into the sum of the ranks of Group 1 not being equal to the sum of the ranks of Group 2 (i.e. $\sum R_1 \neq \sum R_2$). A more general way of stating this, which also encompasses designs involving unequal sample sizes, is that the means of the ranks of the two groups are not equal (i.e. $\overline{R}_1 \neq \overline{R}_2$). This is a non-directional alternative hypothesis and it is evaluated with a two-tailed test.

2. $H_1 : \theta_1 > \theta_2$. The median of the population Group 1 represents is greater than the median of the population Group 2 represents. With respect to the sample data, when both groups have an equal sample size (so long as a rank of 1 is given to the lowest score), this translates into the sum of the ranks of Group 1 being greater than the sum of the ranks of Group 2 (i.e. $\sum R_1 > \sum R_2$). A more general way of stating this, which also encompasses designs involving unequal sample sizes, is that the mean of the ranks of Group 1 is greater than the mean of the ranks of Group 2 (i.e. $\overline{R}_1 > \overline{R}_2$). This is a directional alternative hypothesis and it is evaluated with a one-tailed test.

3. $H_1 : \theta_1 < \theta_2$. The median of the population Group 1 represents is less than the median of the population Group 2 represents. With respect to the sample data, when both groups have an equal sample size (so long as a rank of 1 is given to the lowest score), this translates into the sum of the ranks of Group 1 being less than the sum of the ranks of Group 2 (i.e. $\sum R_1 < \sum R_2$) A more general way of stating this, which also encompasses designs involving unequal sample sizes, is that the mean of the ranks of Group 1 is less than the mean of the ranks of Group 2 (i.e. $\overline{R}_1 < \overline{R}_2$). This is a directional alternative hypothesis and it is evaluated with a one-tailed test.

Only one of the above mentioned alternative hypotheses is employed and consequently the null hypothesis is rejected.

Test Computations

Suppose we have a sample of n_x observations $\{x_1, x_2, ..., x_n\}$ in group 1 (i.e. from one population) and a sample of n_y observations $\{y_1, y_2, ..., y_n\}$ in group 2 (i.e. from another population). The Mann-Whitney test is based on a comparison of every observation x_i in the first sample with every observation y_j in the other sample. The total number of pairwise comparisons that can be made is $n_x n_y$ and the total number of observations is $N = n_x + n_y$.

The overall procedure for carrying the test is listed below:

1. Arrange all the *N* observations (scores) in order of magnitude (irrespective of group membership), beginning on the left with the lowest score and moving to the right as scores increase.

2. All *N* scores are assigned a rank. Moving from left to right, a rank of 1 is assigned to the score that is farthest to the left (which is the lowest score), a rank of 2 is assigned to the score that is second from the left (which, if there are no ties, will be the second lowest score), and so on until the score at the extreme right (which will be the highest score) is assigned a rank equal to *N* (if there are no ties for the highest score).

3. The ranks must be adjusted when there are tied scores present in the data. Specifically, in instances where two or more observations have the same score, the average of the ranks involved is assigned to all scores tied for a given rank (e.g. x_1 and y_1 are two observations having the same score of 0. Since the two scores of 0 are the lowest scores out of the total of *N* scores, in assigning ranks to these scores we can arbitrarily assign one of the 0 scores a rank of 1 and the other a rank of 2. However, since both of these scores are identical it is more equitable to give each of them the same rank. To do this, it is computes the average of the ranks involved for the two scores. Thus, the two ranks involved prior to adjusting for ties (i.e., the ranks 1 and 2) are added up and divided by two. The resulting value (1 + 2)/2 = 1.5 is the rank assigned to each of the subjects who is tied for 0).

It should be noted that any time each set of ties involves observations in the same group; the tie adjustment will result in the identical sum and average for the ranks of the two groups that

will be obtained if the tie adjustment is not employed. Because of this, under these conditions the computed test statistic will be identical regardless of whether or not one uses the tie adjustment. On the other hand, when one or more sets of ties involve observations from both groups, the tie-adjusted ranks will yield a value for the test statistic that will be different from that which will be obtained if the tie adjustment is not employed.

4. The sum of the ranks for each of the groups is computed: $\sum R_x$ and $\sum R_y$.

5. The values U_x and U_y are computed employing:

$$U_x = n_x n_y + \frac{n_x(n_x+1)}{2} - \sum R_x \qquad (25)$$

$$U_y = n_x n_y + \frac{n_y(n_y+1)}{2} - \sum R_y \qquad (26)$$

   Since the U values can never be negative, $n_x n_y = U_x + U_y$ equation confirms if they were correctly computed.

6. Calculate $U = \min(U_x, U_y)$. The smaller of the two values U_x versus U_y is designated as the obtained U statistic.

7. Use statistical tables for the Mann-Whitney U test to find the probability of observing a value of U or lower than the tabled critical value at the prespecified level of significance.

8. Interpretation of the test results (accept or reject the null hypothesis)

Additional Analytical Procedures

The normal approximation of the Mann-Whitney U statistic for large sample sizes

If the sample size employed in a study is relatively large (more than 20), the normal distribution can be employed to approximate the Mann-Whitney U statistic. Although sources do not agree on the value of the sample size which justifies employing the normal approximation of the Mann-Whitney distribution, they generally state that it should be employed for sample sizes larger than those documented in the exact table of the U

distribution contained within the source. Equation 27 provides the normal approximation of the Mann-Whitney U test statistic.

$$Z = \frac{U - \frac{n_x n_y}{2}}{\sqrt{\frac{n_x n_y (n_x + n_y + 1)}{12}}} \tag{27}$$

It should be noted that since the smaller of the two values U_x versus U_y is selected to represent U (see step 6 in the overall procedure), the value of Z will always be negative (unless $U_x = U_y$, in which case $Z = 0$). This is the case, since by selecting the smaller value U will always be less than the expected mean value $\overline{U} = \frac{n_x n_y}{2}$.

The correction for continuity for the normal approximation of the Mann-Whitney U test

The correction for continuity is generally not employed, unless the computed absolute value of Z is close to the prespecified tabled critical value. The correction, which reduces the absolute value of Z, requires that 0.5 be subtracted from the absolute value of the numerator of Equation 27. The continuity corrected version is formulated as:

$$Z = \frac{\left| U - \frac{n_x n_y}{2} \right| - 0.5}{\sqrt{\frac{n_x n_y (n_x + n_y + 1)}{12}}} \tag{28}$$

The absolute value of the continuity-corrected Z value will always be less than the absolute value computed when the correction for continuity is not used, except when the uncorrected value of $Z = 0$ (in which case it will have no impact on the result of the analysis).

Tie correction for the normal approximation of the Mann-Whitney U statistic

If there are an excessive number of ties in the data, an adjustment to the standard deviation should be introduced into Equation 27. Thus, the tie-corrected equation for the normal approximation of the Mann-Whitney U distribution is:

$$Z = \frac{U - \frac{n_x n_y}{2}}{\sqrt{\frac{n_x n_y (n_x + n_y + 1)}{12} - \frac{n_x n_y \left[\sum_{i=1}^{k} (l_i^{\,3} - l_i) \right]}{12(n_x + n_y)(n_x + n_y - 1)}}} \tag{29}$$

The only difference between Equations 28 and 29 is the term to the right of the element $\frac{n_x n_y (n_x + n_y + 1)}{12}$ in the denominator. The result of this subtraction reduces the value of the denominator, thereby resulting in the slight increase in the absolute value of *Z*. The term $\sum_{i=1}^{k} (l_i^3 - l_i)$ computes a value based on the number of ties in the data.

As $N = n_x + n_y$ is the total number of observations, substituting and reducing Equation 29:

$$Z = \frac{U - \frac{n_x n_y}{2}}{\sqrt{\frac{n_x n_y}{N(N-1)}\left[\frac{N^3 - N}{12} - \sum_{i=1}^{k} \frac{l_i^3 - l_i}{12}\right]}} \qquad (30)$$

4.3. The *uFilter* Method

We considered developing the new *uFilter* feature selection method based on the Mann-Whitney U-test [252], in a first approach, to be applied in binary class problems. The *uFilter* algorithm is framed in the univariate filter paradigm since it requires only the computation of *n* scores and sorting them. Therefore, its time execution (faster) and complexity (lower) are beneficial when is compared to wrapper or hybrid methods.

The principal advantage of the *uFilter* method against the Mann-Whitney U-test [252] is the way of computing the weight of each feature. The fact of the Mann-Whitney U test considering only one Z-indicator (the minimum between Equation 33 and 34) for the computation of the feature weight contributes to underrate the discriminative power of the feature by assigning a small value and, all those features in a dataset could unfairly regarded as irrelevant. In contrast, the *uFilter* method uses both Z-indicators for the computation of the feature weight (see Equation 38). Therefore, all those features underrated (irrelevant) at the bottom of the ranking (by the Mann-Whitney U-test) could have the opportunity to emerge based on its real discriminative power [269].

For better understanding the theoretical description of the developed method, we considered a binary class problem (benign and malignant class) with more than 25 instances per class and several tied observations, thus:

Let $F = \{f_1, f_2, ..., f_t\}$ a set of features with size *t*, and let $f_i = \{I_{c,1}, I_{c,2}, ..., I_{c,n}\}$ an ordered set of instances (in ascending way) with size *n* belonging to the i^{th} – feature under analysis, where $I_{c,j}$ represents the value of the feature f_i for an individual instance *j*, and *c* denotes the class value: Benign (*B*) and Malignant (*M*). Then, the *uFilter* performs a tie analysis in the f_i sequence according to the rule: if there are tie elements, their positions are updated by the resultant value of averaging the positions of tied elements. Then, the output sequence is saved in f'_i. Consequently, summation of benign (S_B) and malignant (S_M) instances positions in the f'_i sequence was defined by:

$$S_B = \sum_{j=1}^{n_B} f'_j \tag{31}$$

$$S_M = \sum_{j=1}^{n_M} f'_j \tag{32}$$

where n_B and n_M are the totals of benign and malignant instances respectively. Thus, *u*-values (according to the Equations 25 and 26) for each sample are computed as:

$$uB = n_B n_M + \frac{n_B(n_B+1)}{2} - S_B \tag{33}$$

$$uM = n_B n_M + \frac{n_M(n_M+1)}{2} - S_M \tag{34}$$

As the sample size exceeds 25 instances per class, the original Mann Whitney U Test selected the minimum between both computed *u* values (from Equations 27 and 28) for the calculation of the *Z*-indicator (see Equations 35 or 36). In this case, only one *Z*-indicator will be analyzed to accept or reject the null hypothesis at a given level of significance (alpha = 0.05). In contrast with the original Mann Whitney U Test, the proposed *uFilter* method computes both *Z*-indicators (one by each class) in the following way:

$$Z_B = \frac{uB - \bar{u}}{\sigma_u} \tag{35}$$

$$Z_M = \frac{uM - \bar{u}}{\sigma_u} \tag{36}$$

where $\bar{u}$ is the mean of the sample and the standard deviation is defined as:

$$\sigma_u = \sqrt{\frac{n_B n_M}{n(n-1)}\left(\frac{n^3 - n}{12}\right) - \sum_{i=1}^{k} \frac{l_i^3 - l_i}{12}} \qquad (37)$$

where k denotes the total of range having tied elements in f_i sequence and l_i means the quantity of elements within each $k^{th}-$ range. Finally, the score/weight of the feature f_i is calculated as the absolute value of the numerical difference between Z scores (see equation 38):

$$w_i = \left| Z_B - Z_M \right| \qquad (38)$$

The *uFilter* method is applied to the whole feature space and the output is the ranking of features established by sorting in descendant way the random sequence of weights (w). In this approach, higher values in Equation (38) are preferred, because it means the feature has better separability of class-data distributions and therefore higher discrimination power. Otherwise, the class-data distributions is overlapping and finding the decision boundary for future classifications becomes more difficult. Table 31 summarizes the *uFilter* steps.

Table 31 The *uFilter* algorithm

***uFilter* Algorithm**	
input:	
$D(f_1, f_2, ..., f_t)$	// a set of features with size t, where $f_i = \{I_{c,1}, I_{c,2}, ..., I_{c,n}\}$ is a set of instances with size n belonging to the $i^{th}-$feature under analysis, $I_{c,j}$ represents the value of the feature f_i for an individual instance j, and c denotes the class value (B or M)
output:	
w	// ranking of features
1. **begin**	
2. **for each** f_i	
3. **initialize:** $w_i = 0$;	// initial weight of the features
4. $sort(f_i, 'ascendant')$;	// arrange all the n instances (scores) in order of magnitude
5. $f'_i = avg(position\ \ of\ tied\ elements)$;	// compute the average of the ranks involved for all tied scores
6. Compute S_B and S_M ;	// compute the summatory of benign and malignant instances based on Equations (25) and (26)
7. Compute uB and uM ;	// compute u values based on Equations (27) and (28)
8. Compute Z_B and Z_M ;	// compute Z values based on equation (29) and (30)
9. $w_i = \left| Z_B - Z_M \right|$	// updating the weight of the feature based on equation (32)
10. **end for**	
11. **return** $sort(w, 'descendant')$;	
12. **end**	

4.4. Experimentation and Validation

This section outlines the experimental evaluation of the proposed *uFilter* method when compared to four well known (classical) methods and the developed *RMean* feature selection method on breast cancer diagnosis. The main goal is assessing the effectiveness (based on the AUC scores) in ranking relevant features when varying the features space conditions e.g. varying the samples sizes to analysis the tolerance to unbalanced training data.

The validation was carried out on six datasets: BCDR1, BCDR2 and BCDR3 formed from the BCDR and, DDSM1, DDSM2 and DDSM3 formed from the DDSM. These datasets are representing three different configurations: (1) two balanced datasets (same quantity of benign and malignant instances), (2) two unbalanced datasets containing more benign than malignant instances and (3) two unbalanced datasets holding more malignant than benign instances (see Chapter 3, Table 14 for more detailed information).

The BCDR1 dataset comprising 362 features vectors and the BCDR2 and BCDR3 datasets including a total of 281 features vectors (each one). Besides, the DDSM1 dataset holding 582 features vectors, and the DDSM2 and DDSM3 datasets involving a total of 491 features vectors respectively. Each dataset contains 23 image-based descriptors (including image intensity, shape and texture features) computed from segmented pathological lesions in both MLO and CC mammography image view (see Chapter 3 for the mathematical formulation of employed descriptors). Figure 27 shows a detailed description of employed datasets.

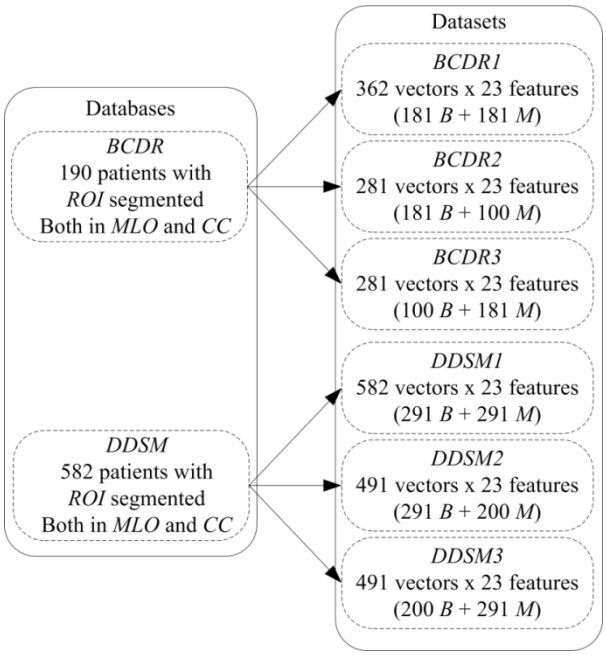

Figure 27 Datasets creation; *B* and *M* represent benign and malignant class instances.

Since this experiment is a multistep modeling procedure (similar to experiments defined in Chapter 3), we applied ten times the 10-fold cross validation method before to establish a ranking of features (to avoid giving an unfair advantage to predictors) and classification steps respectively (to prevent overfitting of classifiers to the training set [243]). Thus, no samples appear simultaneously in training and test (disjoint test partitions). In this way, individual classifiers will be trained on different training sets, leading to different representations of the input space. Testing on these different input space representations leads to diversity in the resultant classifications for individual samples.

The overall procedure for the *uFilter* evaluation is described by four main steps:

- Applying the classical Mann Whitney U-test (U-Test), the new proposed *uFilter* method [269], the developed *RMean* [4, 246] method and four well known feature selection methods: CHI2 discretization [96], IG [98], 1Rule [241] and Relief [103] to the six previously formed breast cancer datasets (see Figure 28 step 2).
- Creating several ranked subset of features using increasing quantities of features. The top *N* features of each ranking (resultant from the previous step) were used for feeding different classifiers, with *N* varying from 5 to the total number of features of the dataset, with increments of 5 (see Figure 28 step 3).

- Classifying the generated ranked subset of features using FFBP neural network [244], SVM [77, 244], LDA [213] and NB [245] classifiers for a comparative analysis of AUC scores. All comparisons were using the Wilcoxon statistical test [249, 251] to assess the meaningfulness of differences between classification schemes (see Figure 28 step 3).
- Selecting the best classification scheme on datasets (BCDR1, BCDR2, BCDR3, DDSM1, DDSM2 and DDSM3), and thus the best subset of features.

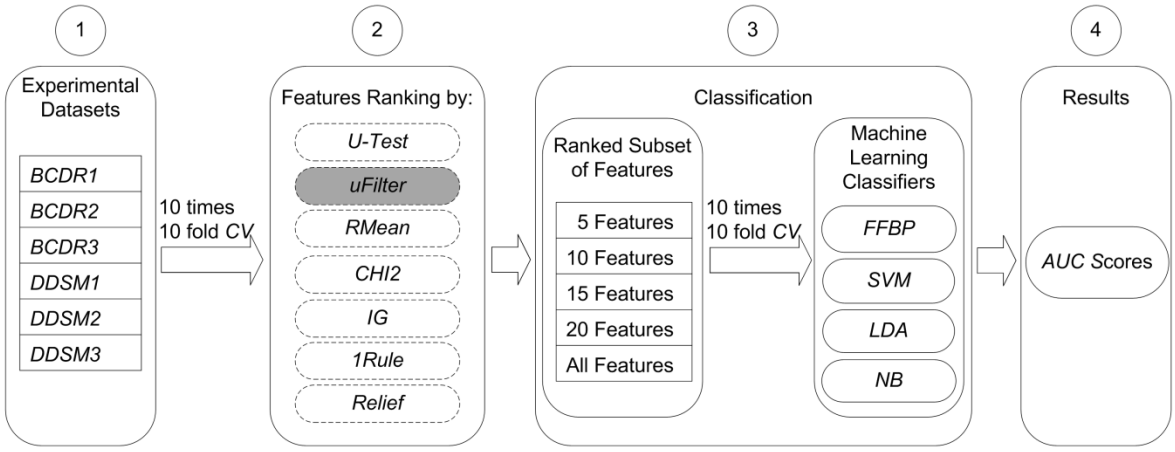

Figure 28 Experimental workflow.

In the last step of the experiment, we determined the feature relevance analysis using a two-step procedure involving (1) selecting the best subset of features for each dataset, and (2) performing a redundancy analysis based on the Pearson correlation [253], to determine and eliminate redundant features from relevant ones, and thus to produce the optimal subset of features.

In contrast to the work of Ghazavi and Liao [209], we decided to employ the correlation analysis as a complementary step to the *uFilter* procedure, instead to an evaluation function for features selection, because in real domains many features have high correlations and thus many are (weakly) relevant and should not be removed [270]. Also, some variables may have a low rank because they are redundant and yet be highly relevant [56].

4.5. Results and Discussions

4.5.1. Comparison between *uFilter* and U-Test Methods

The statistical comparison between *uFilter* and U-Test methods considered only features subsets formed by the top 10 features (empirical threshold) of each ranking. We used a total of 48 ranked subsets of features containing image-based features for feeding four machine learning classifiers. With this, a head-to-head statistical comparison based on the mean of AUC performances over 100 runs produced inspiring results. Figure 29 shows a boxplot graph representing the statistical comparison ($p<0.05$) based on the mean of AUC scores between both methods for all classification schemes.

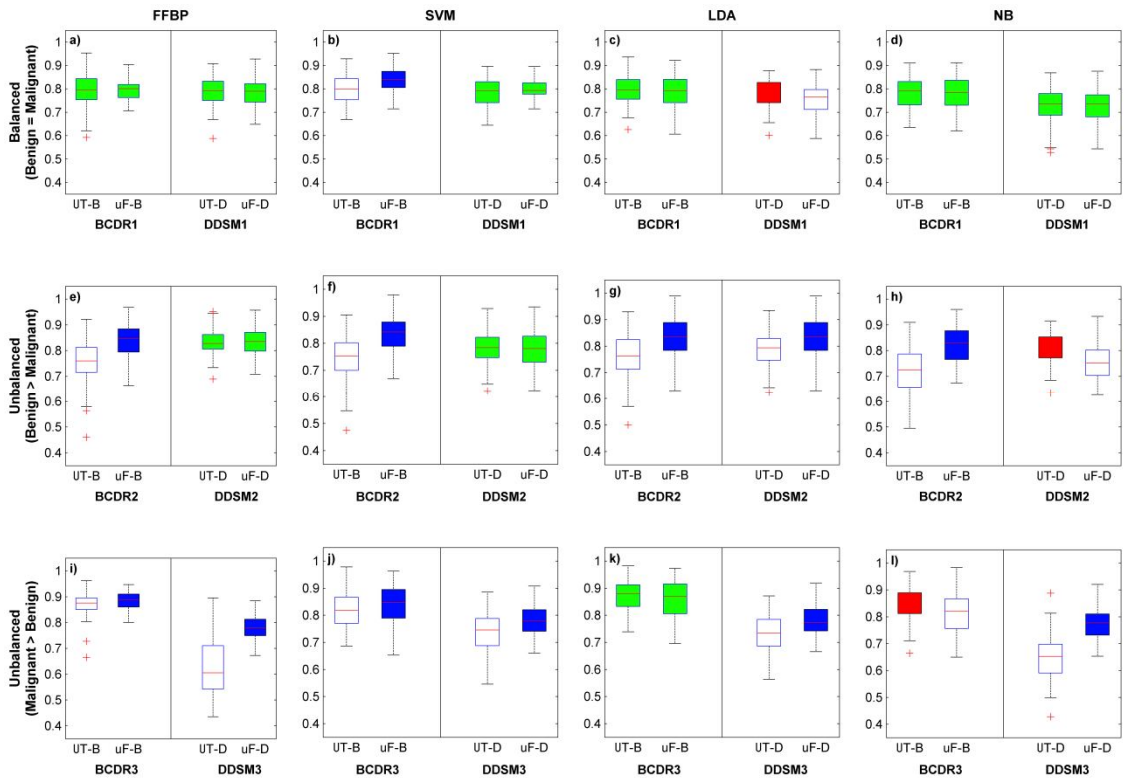

Figure 29 Head-to-head comparison between *uFilter* (uF) and U-Test (uT) methods using the top 10 features of each ranking; blue and red filled box represents significant difference ($p<0.05$) in the AUC performance.

Results on Balanced Datasets

The best classification scheme for BCDR1 dataset was formed by the *uFilter* method and the SVM classifier (see Figure 29 b). The AUC value of 0.8369 was statistically superior to the best AUC value (0.7995) obtained by the U-Test method when combined with the SVM classifier. Also, this combination was statistically better than the remaining classification schemes in the BCDR1 dataset (see Table 32).

For DDSM1 dataset, the best classification scheme was formed by the *uFilter* method and the SVM classifier, reaching an AUC score of 0.80. However, this result did not provide statistical evidence to be better than the combination of the U-Test method and the SVM classifier, which reached an AUC score of 0.7838 (see Figure 29 b). This combination statistically outperformed only three classification schemes for DDSM1 dataset (see Table 32).

Table 32 Summary of the Wilcoxon Statistical test among all classification schemes for BCDR1 and DDSM1 datasets.

Dataset	**Best scheme**	**AUC**	**Other scheme**	**AUC**	**Wilcoxon (α= 0.05)**
BCDR1	*uFilter*+SVM	0.8369	U-Test+SVM	0.7995	p<0.01
			uFilter+FFBP	0.8088	p<0.01
			U-Test+FFBP	0.7938	p<0.01
			uFilter+LDA	0.7906	p<0.01
			U-Test+LDA	0.7968	p<0.01
			uFilter+NB	0.7814	p<0.01
			U-Test+NB	0.7840	p<0.01
DDSM1	*uFilter*+SVM	0.80	U-Test+SVM	0.7838	p=0.1390
			uFilter+FFBP	0.7868	p=0.0986
			U-Test+FFBP	0.7925	p=0.5149
			uFilter+LDA	0.7567	p<0.01
			U-Test+LDA	0.7832	p=0.0624
			uFilter+NB	0.7277	p<0.01
			U-Test+NB	0.7288	p<0.01

Results on Unbalanced Datasets

The best classification scheme for BCDR2 dataset was formed by the *uFilter* method and the FFBP neural network, reaching an AUC score of 0.8350. This result was statistically superior to the obtained result by the combination of the U-Test method with the FFBP neural network, which provided an AUC score of 0.7578 (see Figure 29 e). In this dataset other classification schemes using the *uFilter* method stretched satisfactory results with no statistical difference respect to the best scheme (see Table 33).

Besides, for DDSM2 dataset the best classification performance was obtained by the combination of the *uFilter* and the FFBP neural network classifier; reaching AUC value of 0.8382 (see Figure 29 e). However, this result did not statistically outperform the obtained result by the combination of the U-Test method and the FFBP neural network (AUC value of 0.8308). The comparison among all classification schemes for DDSM2 dataset indicated that the best combination (higher AUC value) was almost statistically superior in all cases (see Table 33).

Table 33 Summary of the Wilcoxon Statistical test among all classification schemes for BCDR2 and DDSM2 datasets.

Dataset	**Best scheme**	**AUC**	**Other scheme**	**AUC**	**Wilcoxon (α= 0.05)**
BCDR2	*uFilter*+FFBP	0.8350	U-Test+FFBP	0.7578	p<0.01
			uFilter+SVM	0.8332	p=0.6086
			U-Test+SVM	0.7482	p<0.01
			uFilter+LDA	0.8296	p=0.5849
			U-Test+LDA	0.7613	p<0.01
			uFilter+NB	0.8219	p=0.1546
			U-Test+NB	0.7246	p<0.01
DDSM2	*uFilter*+FFBP	0.8382	U-Test+FFBP	0.8308	p=0.4923
			uFilter+SVM	0.7782	p<0.01
			U-Test+SVM	0.7844	p<0.01
			uFilter+LDA	0.8296	p=0.7031
			U-Test+LDA	0.7881	p<0.01
			uFilter+NB	0.7511	p<0.01
			U-Test+NB	0.8057	p<0.01

The best classification performance for BCDR3 dataset was provided by the combination of the *uFilter* method and the FFBP neural network classifier, accomplishment an AUC score of 0.8850 (see Figure 29 i). This result was statistically superior to the obtained result by the combination of the U-Test method and the FFBP neural network, which achieved an AUC score of 0.87. With the exception of the scheme formed by the U-Test method and the LDA classifier, which attained a similar AUC performance (0.8725), the best scheme statistically outperformed the remaining classification schemes (see Table 34).

In the DDSM3 dataset, the best classification scheme was formed by the combination of the *uFilter* method and the LDA classifier for an AUC value of 0.7819. This classification result showed significant difference with respect to the classification result provided by the combination of the U-Test method with the LDA classifier, which reached an AUC value of 0.7328 (see Figure 29 k). Also, the best combination statistically outperformed other obtained results using the U-Test method in the classification scheme, and does not indicated statistical evidences of being better than other *uFilter* combinations (see Table 34).

Table 34 Summary of the Wilcoxon Statistical test among all classification schemes for BCDR3 and DDSM3 datasets.

Dataset	**Best scheme**	**AUC**	**Other scheme**	**AUC**	**Wilcoxon (α= 0.05)**
BCDR3	*uFilter*+FFBP	0.8850	U-Test+FFBP	0.87	p<0.01
			uFilter+SVM	0.8386	p<0.01
			U-Test+SVM	0.8207	p<0.01
			uFilter+LDA	0.8621	p<0.01
			U-Test+LDA	0.8725	p=0.2131
			uFilter+NB	0.8152	p<0.01
			U-Test+NB	0.8477	p<0.01
DDSM3	*uFilter*+LDA	0.7819	U-Test+LDA	0.7328	p<0.01
			uFilter+FFBP	0.7806	p=0.9386
			U-Test+FFBP	0.6266	p<0.01
			uFilter+SVM	0.7795	p=0.8441
			U-Test+SVM	0.7393	p<0.01
			uFilter+NB	0.7706	p=2047
			U-Test+NB	0.6467	p<0.01

A head-to-head comparison between the proposed *uFilter* method and the classical Mann Withney U-test (U-Test) is well demonstrated in the experiments reported here. As it is shown in Tables 32, 33 and 34, the *uFilter* method statistically outperformed the U-Test method in a 50% (blue filled box); tied in a 37.5% (green filled box) and lost in a 12.5% (red filled box) of the 24 considered scenarios (see Figure 29).This circumstance could be related with the assigned weights to each feature in the ranking, e.g. in the BCDR1 dataset, the *uFilter* method considered the f_{20} feature (perimeter) as the most relevant feature, meanwhile the U-Test method considered it as irrelevant. A similar situation occurs with the f_{37} feature (Area), which was ranked in the top five features by the *uFilter* and irrelevant by the U-Test method respectively. According to the ACR [7], MC lesions are tiny bright dots in the breast, and masses are very often obscure and greater than MCs. Hence the perimeter and area are important features for discriminating between both lesions. It is clear that the U-Test method underestimated both features on unbalanced datasets.

In addition, for unbalanced datasets this fact could be associated to the Mann-Whitney test criterion [252], which is based on the magnitude of the relationship between both samples (benign and malignant instances). In the BCDR2, DDSM2, BCDR3 and DDSM3 datasets most of the benign instances are greater than most of the malignant instances or vice versa and this would be evidence against random mixing. Therefore, the U-Test method would tend to discredit the null hypothesis of identical distribution [265] and underrate the features weight (like in the balanced datasets). The opposite occur with the *uFilter* method, which computes the separability between both samples, independently of the number of benign and malignant instances.

4.5.2. Performance of *uFilter* versus Classical Feature Selection Methods

This section aims to compare the new developed *uFilter* method against four well known (established) feature selection methods. A total of 720 ranked subsets of image-based features were analyzed and the straightforward statistical comparison based on the mean of AUC performances over 100 runs highlighted interesting results for balanced and unbalanced datasets (see Figure 30).

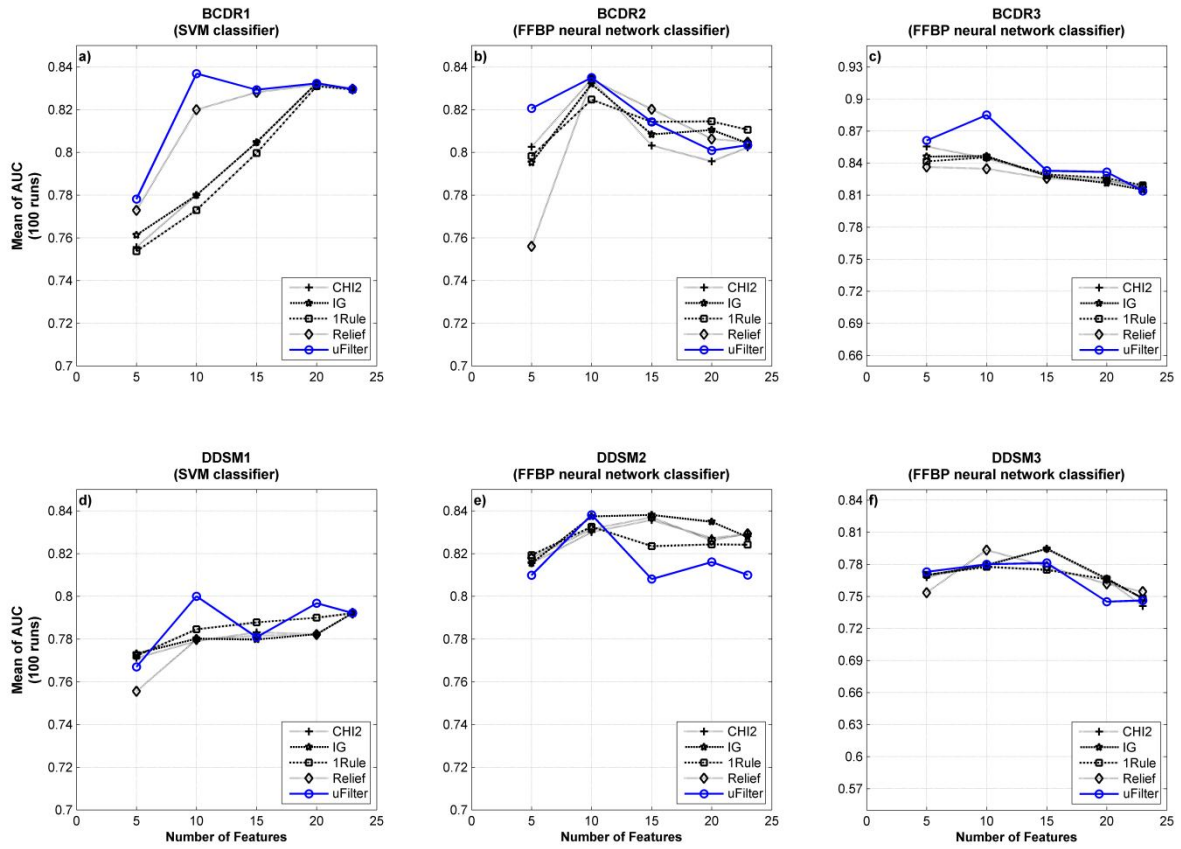

Figure 30 Behavior of the best classification schemes when increasing the number of features on each dataset.

Results on Balanced Datasets

On the BCDR1 dataset, the best classification scheme was obtained when we combine the *uFilter* method and the SVM classifier using 10 features, obtaining an AUC score of 0.8369. The statistical comparison against the other feature selection methods did not provide significant difference in term of AUC scores: CHI2 discretization (AUC=0.8325, p=0.6717), IG (AUC=0.8324, p=0.6725), 1Rule (AUC=0.8310, p=0.6053) and Relief (AUC=0.8316, p=0.6190). However, the *uFilter* method reached this result using the top 10 features, while the other methods required a total of 20 features (see Figure 30 a).

On the DDSM1 dataset, the combination of the *uFilter* method and the SVM classifier using the top 10 features provided the best classification performance obtaining an AUC value of 0.8004. This result was not statistically superior to the obtained result by the CHI2 discretization (AUC=0.7893, p=0.2684), IG (AUC=0.7893, p=0.2840) and 1Rule methods (AUC=0.79, p=0.3450), but it was better than the Relief method (AUC=0.7821, $p<0.05$). Similar to the BCDR1 dataset, the *uFilter* method reached this result using the top 10 features, while the other methods required a total of 20 features (see Figure 30 d).

Results on Unbalanced Datasets

The higher classification performance in the BCDR2 dataset was achieved by the combination of the *uFilter* method and the FFBP neural network classifier with a total of 10 features, obtaining an AUC value of 0.8350. However, this result was not statistically superior to the obtained results by the remaining feature selection methods using the same number of features (see Figure 30 b): CHI2 discretization (AUC=0.8342, p=0.7590), IG (AUC=0.8320, p=0.8022), 1Rule (AUC=0.8259, p=0.8259) and Relief (AUC=0.8344, p=0.8402). Similar to the BCDR2 dataset, the higher classification performance in the DDSM2 dataset was obtained by the combination of the *uFilter* method and the FFBP neural network classifier using a total of 10 features, accomplishment an AUC of 0.8382 (see Figure 30 e). This result did not provide statistical evidences of an AUC improvement respect to the CHI2 discretization (AUC=0.8301, p=0.8079), IG (AUC=0.8374, p=0.9076), 1Rule (AUC=0.8326, p=0.7470) and Relief methods (AUC=0.8315, p=0.3884).

On the other hand, the best classification scheme for the BCDR3 dataset was formed by the combination of the *uFilter* method and the FFBP neural network classifier using a total of 10 features (see Figure 30 c). The AUC value of 0.8850 was statistically superior respect to the obtained result by the CHI2 discretization (AUC=0.8444, $p<0.01$), IG (AUC=0.8465, $p<0.01$), 1Rule (AUC=0.8454, $p<0.01$) and Relief methods (AUC=0.8347, $p<0.01$).

On the DDSM3 dataset, the best classification performance was obtained by the combination of the IG method and the FFBP neural network classifier using 15 features (AUC value of 0.7945). The AUC-based comparison against the other classification schemes using less number of features (10) indicated no significant difference in the classification performance (see Figure 30 f): CHI2 discretization (AUC=0.7798, p=0.0729), 1Rule (AUC=0.7776, p=0.0551), Relief (AUC=0.7933, p=0.9717) and *uFilter* (AUC=0.7806, p=0.0796).

The global comparison demonstrated that *uFilter* method statistically outperformed the CHI2 discretization, IG, 1Rule and Relief methods on BCDR1, DDSM1 and BCDR3 datasets, and it was statistically similar on BCDR2, DDSM2 and DDSM3 datasets while requiring less number of features. This circumstance could be related to the particular nature of employed feature selection methods and datasets respectively. We used datasets without any type of data normalization, and some methods could lead to non-reliable results e.g. the CHI2 discretization (which used the chi-square statistical test as the main evaluation function), IG

(which is an entropy-based feature evaluation), and 1Rule (which is not likely to enhance the performance of classification schemes that require a search space of greater complexity) methods provided the worst results on BCDR1, DDSM1 and BCDR3 datasets (see Figure 30). In contrast, the Relief method computes the feature's weight based on a different semantic independent of data normalization (distance to nearest hit and nearest miss), and this explains the good performance of the Relief method in almost all datasets (see Figure 30). The satisfactory results obtained by the *uFilter* were expected since it is a non-parametric method and thus is tolerant to non-normalized data.

Concerning classifiers performance, results show that the selection of the most appropriate classifier is dependent on the dataset and the feature selection method (see Figure 30). For balanced datasets, the best results were obtained with de SVM classifier; meanwhile for unbalanced datasets were obtained with the FFBP neural network classifier (see Figure 30). These results were expected since the SVM classifier is based on the definition of an optimal hyperplane [244], and for a less complex features space (e. g. balanced datasets), it could easily find the corresponding linear decision boundary. On the other hand, for a more complex features space such as those presented on unbalanced datasets, the FFBP neural network has demonstrated to be capable of generalizing [244].

4.5.3. Performance of *uFilter* versus *RMean* Feature Selection Method

This section aims to present a head-to-head comparison between the contributions of this thesis: the new *uFilter* proposed method, which improves a non-parametric statistical test and the *RMean* method, which is based on the combination of four classical feature selection methods (see Chapter 3 for technical information).

Analogous to the previous section, we analyzed a total of 720 ranked subsets of features containing image-based features and a direct statistical comparison based on the mean of AUC performances over 100 runs was carried out. The Figure 31 shows the behavior (AUC variability when increasing the number of features) of the best classification scheme and the performance of the *uFilter* and *RMean* feature selection methods, for each formed dataset.

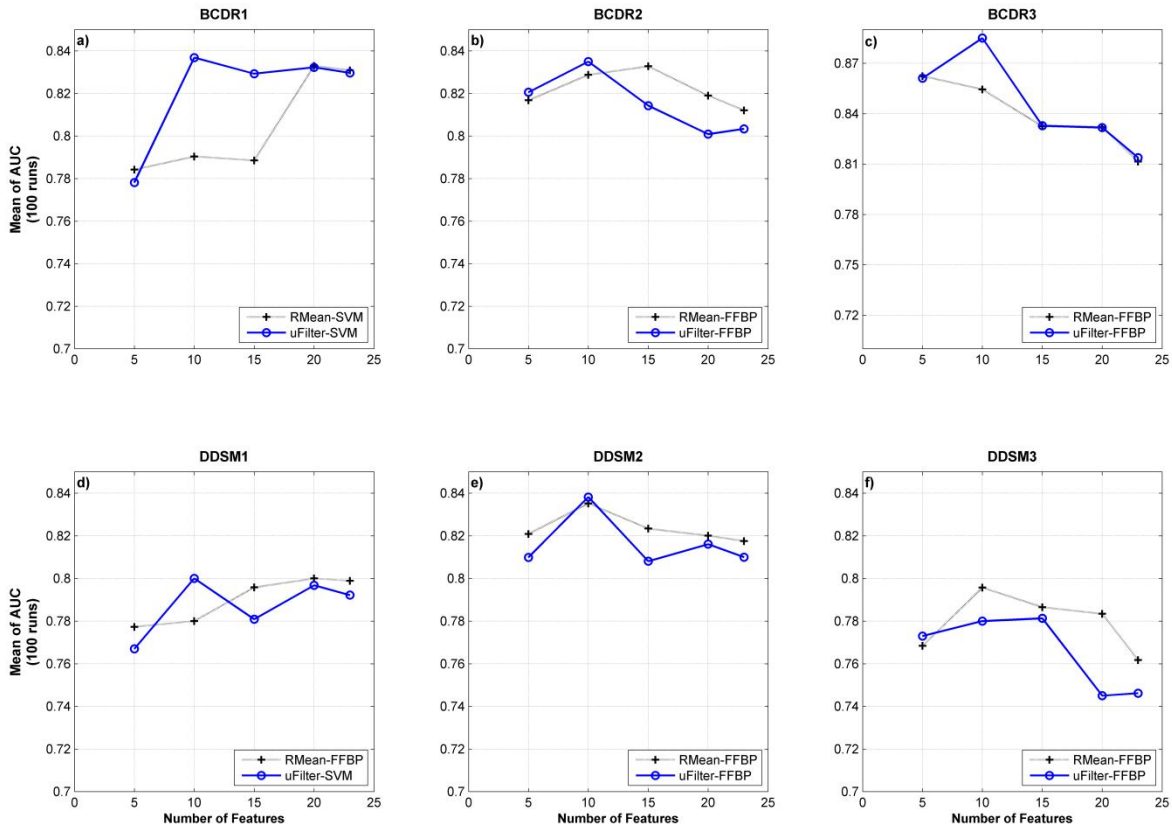

Figure 31 Behavior of the best classification schemes using the *uFilter* and *RMean* methods on each dataset

Results on Balanced Datasets

For the BCDR1 dataset, the best classification scheme was obtained by the combination of the *uFilter* method and the SVM classifier using 10 features, obtaining an AUC score of 0.8369. The statistical comparison against the scheme formed by the *RMean* method and the FFBP neural network classifier did not provide significant difference in term of AUC scores (AUC=0.8330, p=0.698). However, the *uFilter* method reached this result using the top 10 features, while the *RMean* method required a total of 20 features (see Figure 31 a).

On the DDSM1 dataset, the combination of the *uFilter* method and the SVM classifier using the top 10 features provided the best classification performance, obtaining an AUC value of 0.8004. This result was not statistically superior to the obtained result by the *RMean* method and the FFBP neural network classifier with 15 and 20 features: AUC=0.7958, p=0.5873 and AUC=0.80, p=0.7123 respectively (see Figure 31 d).

Results on Unbalanced Datasets

The higher classification performance in the BCDR2 dataset was achieved by the combination of the *uFilter* method and the FFBP neural network classifier with a total of 10 features, obtaining an AUC value of 0.8350. However, this result was not statistically superior to the obtained results by the *RMean* method and the FFBP neural network classifier using the same number of features, which achieved an AUC value of 0.8288, p=0.5922 (see Figure 31 b). Similar to the BCDR2, the higher classification performance in the DDSM2 dataset was obtained by the combination of the *uFilter* method and the FFBP neural network classifier using a total of 10 features, accomplishment an AUC of 0.8382 (see Figure 31 e). This result did not provide statistical evidences of an AUC improvement respect to the *RMean* (AUC=0.8352, p=0.7215).

On the BCDR3, the best classification performance was reached by the combination of the *uFilter* method and the FFBP neural network classifier using a total of 10 features (see Figure 31 c). The AUC value of 0.8850 was statistically superior respect to the obtained result by the *RMean* method and the FFBP neural network classifier (AUC=0.8544, p<0.01).

On the other hand, the higher performance for the DDSM3 dataset was formed by the combination of the *RMean* method and the FFBP neural network classifier using a total of 10 features (see Figure 31 f). The AUC value of 0.7957 was not statistically superior respect to the obtained result by the *uFilter* method (AUC=0.7806, p=0.3112),

The head-to-head comparison demonstrated that *uFilter* method statistically outperformed the *RMean* method on BCDR1, DDSM1 and BCDR3 datasets, and it was statistically similar on BCDR2, DDSM2 and DDSM3 datasets. This result was expected since the *RMean* method is based on the combination of the CHI2 discretization, IG, 1Rule and Relief feature selection methods, which were also statistically outperformed by the *uFilter* method (see previous subsection). It should be pointed out that *RMean* method is an ensemble method and will inherit all the weaknesses presented on each baseline method.

4.5.4. Analysis of the Ranked Features Space

Many methods of variable subset selection are sensitive to small perturbations of the experimental conditions. If the data has redundant variables, different subsets of variables

with identical predictive power may be obtained according to initial conditions of the algorithm, removal or addition of training examples, or the presence of non-normalized data. For some applications, one might want to purposely generate alternative subsets that can be presented to a subsequent stage of processing. Still one might find this variance undesirable because variance is often the symptom of a "bad" model that does not generalize well and results are not reproducible [56].

With the exception of the developed *RMean*, which is an ensemble method, we analyzed the variance of all employed feature selection methods and the new proposed *uFilter* by using two aspects: the average ranking assigned to each feature versus the standard deviation on 100 runs. Furthermore, it was declared the feasibility zone, which consists in the selection of the top 10 features with standard deviation between 0 and 1 (empirical range). With this, it possible to know how each method was consistent in the selection of the most important features and thereby which feature selection method provides generalizable model. The Figures 32, 33 and 34 show the ranked features space by each feature selection method and the respective zone of feasibility for all datasets.

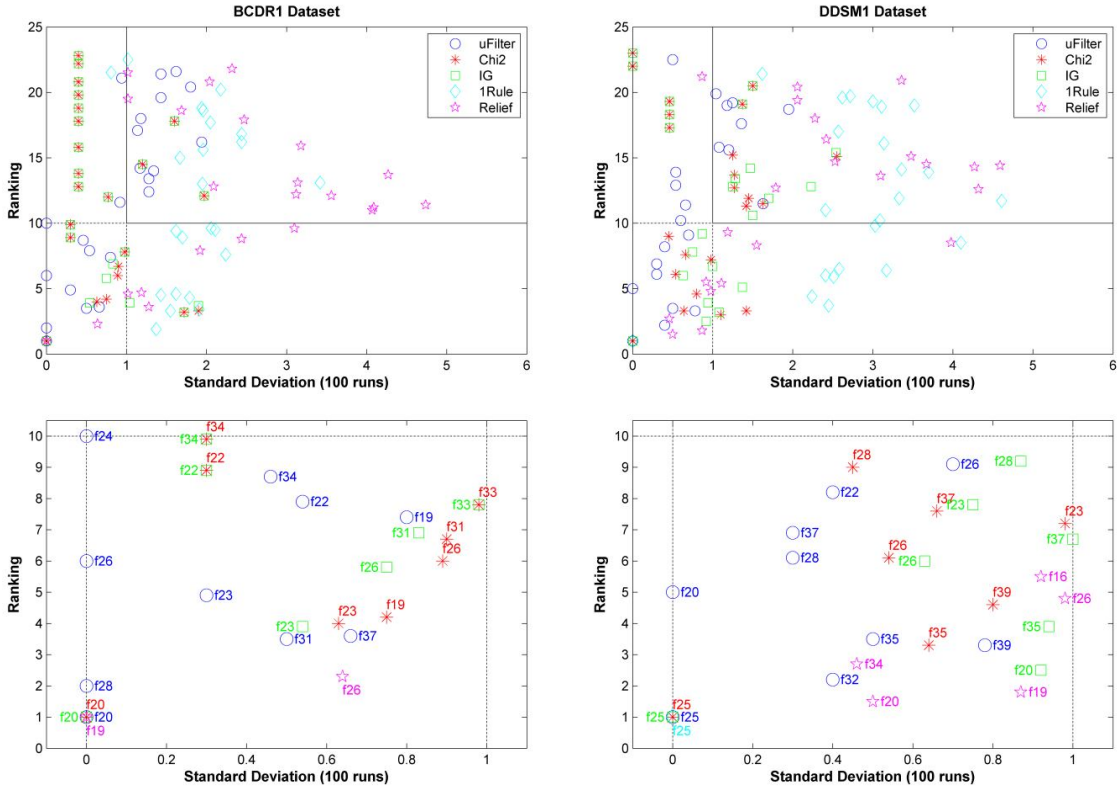

Figure 32 The ranked features space by each feature selection method (first row) and the selected zone of feasibility (second row) for BCDR1 and DDSM1 dataset respectively.

In the BCDR1 dataset, the *uFilter* method considered the top 10 features inside the feasibility zone. Also, the obtained results by the CHI2 discretization and IG methods were close to the *uFilter* method, ranking 8 and 7 features inside this zone respectively. The worst results were presented by the Relief and 1Rule methods, the first one ranked only 2 features inside the feasibility zone and the second ranked the top 10 features out of this zone (see Figure 32 second row).

For the DDSM1 dataset, the best result was obtained by the *uFilter* method, which ranked 9 features inside the feasibility zone. The CHI2 discretization and IG methods considered both 7 features and, the Relief and 1Rule methods provided the worst results, ranking 5 and 1 feature inside the feasibility zone respectively (see Figure 32 second row).

In the BCDR2 dataset, the *uFilter* was slightly superior (selected 9 features) against the CHI2 discretization, IG and Relief methods, which obtained very close results. These methods considered 7, 8 and 7 features inside the feasibility zone respectively. Likewise in the BCDR1 dataset, the 1Rule method resulted in worst without any selection inside the feasibility zone for BCDR2 dataset (see Figure 33 second row).

Besides, for the DDSM2 dataset, the best results were obtained by the *uFilter*, CHI2 discretization and IG methods. All of them ranked 8 features inside the feasibility zone. In contrast, the Relief and 1Rule methods considered only 2 and 3 features within this zone respectively. These latter results were the worst in this dataset (see Figure 33 second row).

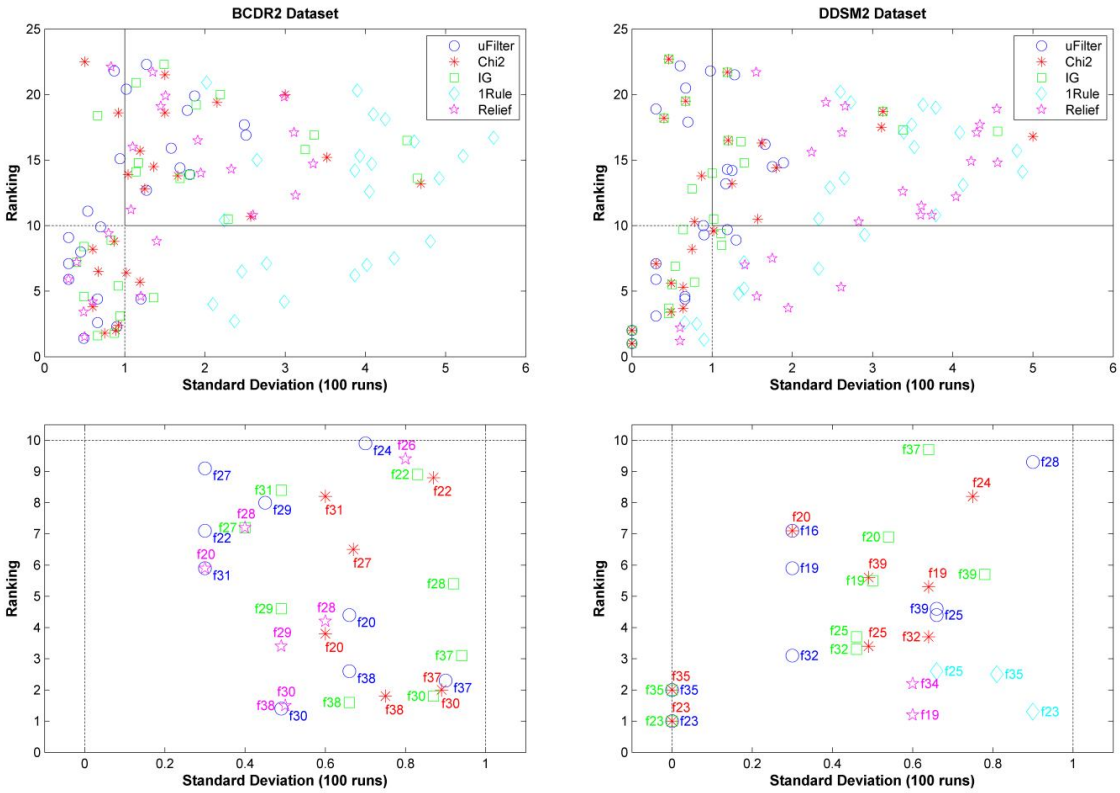

Figure 33 The ranked features space by each feature selection method (first row) and the selected zone of feasibility (second row) for BCDR2 and DDSM2 dataset respectively.

In the BCDR3 dataset, the best result was provided by the *uFilter* method, which ranked 7 features inside the feasibility zone. The CHI2 discretization, IG, 1Rule and Relief methods obtained very close results among them (5, 4, 4 and 6 features respectively), but it were lower respect to the *uFilter* method.

Moreover, for the DDSM3 dataset, the best results were obtained by the *uFilter* and CHI2 discretization methods, both ranked 9 features inside the feasibility zone. The IG method considered 7 features inside this zone and, the worst results were obtained by the 1Rule and Relief methods, which ranked 1 and 5 features respectively (see Figure 34 second row).

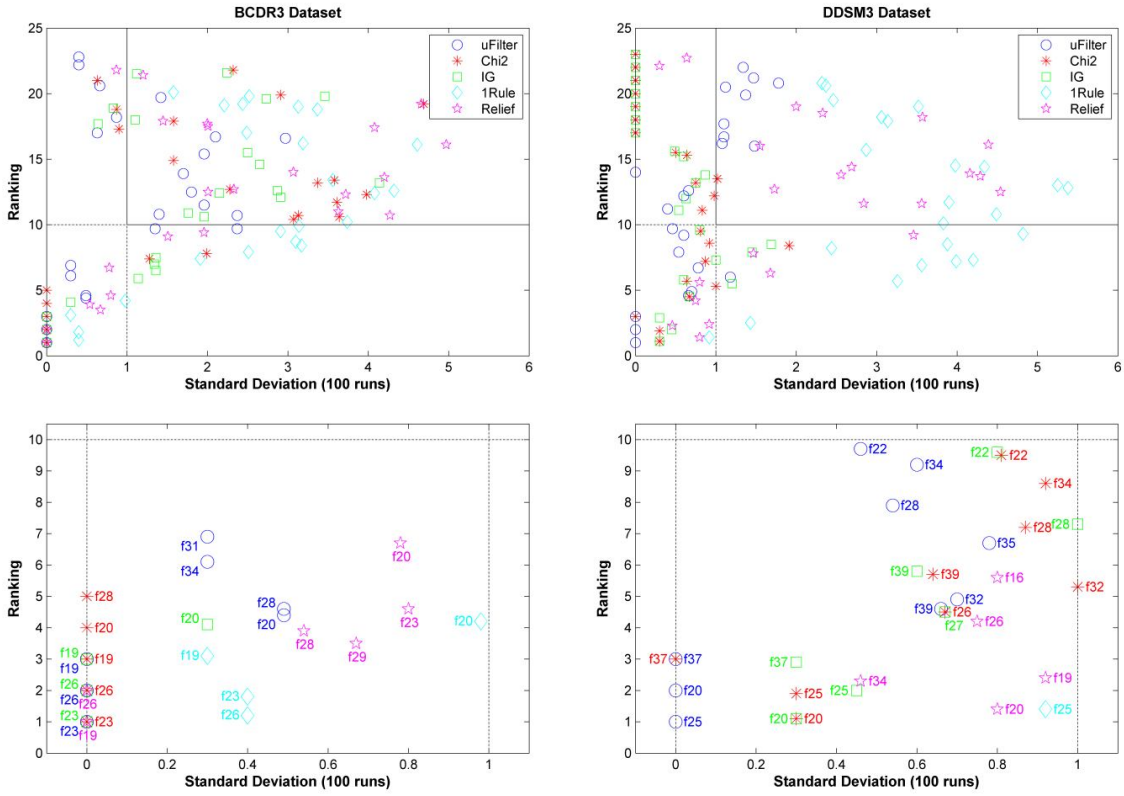

Figure 34 The ranked features space by each feature selection method (first row) and the selected zone of feasibility (second row) for BCDR3 and DDSM3 dataset respectively.

It should be pointed out that the *uFilter* method was the most consistent in ranking features with less variance among all feature selection methods for all datasets, which mean it is capable of provided models that generalize well. In contrast, the 1Rule was the worst method; it ranked the features with high variance in the majority of datasets.

4.5.5. Feature Relevance Analysis

The results showed in previous section clearly provide experimental evidence that the *uFilter* method provided ranked subsets of features with higher discriminant potential. It approximates the set of relevant features by selecting a subset from the top 10 features of each ranking list. According to its linear time complexity in terms of the dimensionality *N* (total of features), the *uFilter* method is efficient for high-dimensional data. However, it is incapable of removing redundant features because it is an individual evaluator of features (i.e. it assigns weights according to their degrees of relevance [56]) and as long as features are considered relevant to the class, they will all be selected even though many of them are highly correlated

to each other (redundant). In this case, a validation of features' subsets through a redundancy analysis is convenient.

Features Subset Validation

To efficiently find an optimal subset of features we introduced an analysis of redundancy to decrease the size of the subset of features and keeping prediction accuracy. We achieved this goal using a two-step procedure involving: (1) selecting the best subset of features for each dataset, and (2) performing the redundancy analysis based on the Pearson correlation [253] to determine and eliminate redundant features from relevant ones, and thus to produce the optimal subset of features.

In order to correctly interpret the results, John and Kohavi in [50] defined two degrees of relevance: strong and weak. Strong relevance implies that the feature is indispensable in the sense that it cannot be removed without loss prediction accuracy. Weak relevance (redundant and non-redundant) implies that the feature can sometimes contribute to prediction accuracy. Thus, features are relevant if they are both strongly or weakly relevant and irrelevant otherwise. Irrelevant features can never contribute to prediction accuracy, by definition.

As it is shown in Figure 30 and described in previous section, the relevance analysis based on the proposed *uFilter* method provided discriminant subsets of features by removing irrelevant ones. Hence, these subsets of features were used as the starting point for the redundancy analysis. Table 35 summarizes the redundancy analysis based on the Pearson correlation [253] for each selected subset of features. It should be pointed out that only higher correlation values were considered in this analysis (more than 0.5 on both positive and negative direction).

Table 35 Summary of the redundancy analysis.

Dataset	Best subset of features	Redundant features	c-Pearson	Weakly relevant	Strongly relevant
BCDR1	f_{20},f_{28},f_{31},f_{37}, f_{23},f_{26},f_{19},f_{22}, f_{34}, f_{24}	f_{37}=f_{20} f_{26}=f_{23},f_{19} f_{19}=f_{23} f_{34}=f_{22}	0.79 0.96, -0.92 -0.84 -0.62	f_{20},$f_{31}^{(+)}$,f_{23}, f_{22}, f_{24}	f_{28}
BCDR2	f_{30},f_{38},f_{37},f_{20}, f_{28},f_{31},f_{22},f_{29}, f_{27},f_{24}	f_{30}=f_{38},f_{29}, f_{27} f_{37}=f_{20} f_{29}=f_{38} f_{24}=f_{22}	0.99, 0.56, 0.56 0.89 0.55 0.75	f_{38},$f_{28}^{(+)}$, $f_{31}^{(+)}$,f_{22},f_{27}	f_{20}
BCDR3	f_{23},f_{26},f_{19},f_{20}, f_{28},f_{34},f_{31},f_{38}, f_{35},f_{29}	f_{26}=f_{23},f_{19}, f_{38} f_{19}=f_{23},f_{38} f_{34}=f_{28} f_{29}=f_{23},f_{26},f_{19},f_{38}	0.97,-0.94,0.56 -0.85,-0.62 -0.75 0.50, 0.57,-0.62, 0.99	f_{23},$f_{20}^{(+)}$,f_{28}, $f_{31}^{(+)}$,f_{38}	f_{35}
DDSM1	f_{25},f_{32},f_{35},f_{39}, f_{20},f_{28},f_{37},f_{22}, f_{26}, f_{31}	f_{39}=f_{25},f_{32},f_{35} f_{37}=f_{20} f_{22}=f_{20}, f_{31} f_{31}=f_{28} f_{32}=f_{35}	0.85, 0.94, 0.94 0.93 0.56,-0.71 -0.79 0.99	$f_{25}^{(+)}$,f_{20},f_{28}, $f_{26}^{(+)}$,f_{35}	-
DDSM2	f_{23},f_{35},f_{32},f_{39}, f_{25},f_{19},f_{16},f_{21}, f_{28},f_{24}	f_{39}=f_{35},f_{32},f_{25},f_{28},f_{24} f_{25}=f_{35},f_{32},f_{24} f_{28}=f_{25}	0.97,0.98,0.89,0.71,0.51 0.92,0.92,0.61 0.68	f_{35},f_{32},$f_{19}^{(+)}$, $f_{16}^{(+)}$,$f_{21}^{(+)}$, f_{24}	f_{23}
DDSM3	f_{25},f_{20},f_{37},f_{39}, f_{32},f_{26}, f_{35},f_{28}, f_{34}, f_{22}	f_{37}=f_{25} f_{39}=f_{25},f_{32},f_{35} f_{32}=f_{25},f_{35} f_{28}=f_{25},f_{20},f_{34},f_{22}	0.84 0.78,0.92,0.91 0.85,0.99 0.60,0.56,0.57,0.76	f_{25},$f_{26}^{(+)}$,f_{35}, f_{34}, f_{22}	f_{20}

$^{(+)}$Weakly relevant features but non-redundant; c-Pearson is the value of correlation of Pearson.

Correlated features are considered redundant (see Table 35). Therefore, only one of them in the correlated pair is selected together with the non-correlated features to form the weakly relevant subset of features. Hence each weakly relevant subset of features was used for selecting the strongly relevant ones.

In the BCDR1 dataset, the Entropy (f_{28}) feature was selected as the strongly relevant feature because its absence in the final subset of features significantly decreased the AUC performance from 0.8315 to 0.791 ($p<0.01$). In the BCDR2 and DDSM3 datasets, the Perimeter (f_{20}) feature constituted the strongly relevant feature. Its participation in the final subset significantly increased the AUC performance from 0.81 to 0.835 ($p<0.01$) and 0.7521 to 0.7806 ($p<0.01$) respectively.

For the BCDR3 dataset, the Mean (f_{35}) feature was considered as the strongly relevant feature because its absence significantly reduced the classification performance from an AUC value of 0.885 to 0.8395 ($p<0.01$). Besides, in the DDSM2 dataset, the strongly relevant feature was the Roughness (f_{23}); this feature contributed to a significantly increment of 0.07 ($p<0.01$) in

the AUC performance when it is included in the final subset (AUC value of 0.8382 versus 0.7727 when is left out). Only in the DDSM1 dataset no feature appears as strongly relevant, which means that all features in this subset contributed with similar effort in the classification model. It should be pointed out that removed features can be inferred from Table 37.

According to the relevant definition of John and Kohavi [270], we put together both weakly and strongly relevant features to form the optimal subset of features. These subsets were evaluated using the same machine learning classifier employed in the evaluation of its precedent subsets of features (for further comparison). Therefore, optimal subset of features for BCDR1 and DDSM1 datasets used the SVM classifier, and for BCDR2, BCDR3, DDSM2 and DDSM3 datasets used the FFBP neural network respectively. Table 36 summarizes the AUC-based statistical comparison (using the Wilcoxon statistical test [249, 250]) between the best subset of features selected by the *uFilter* method, and its corresponding optimal subset of features after the redundancy analysis.

Table 36 AUC-based statistical comparison between the best and optimal subset of features.

Dataset	Best subset of features	AUC	Weakly + Strongly	AUC	Wilcoxon (α=0.05)
BCDR1	$f_{20},f_{28},f_{31},f_{37},f_{23},f_{26},f_{19},f_{22},f_{34},f_{24}$	0.839	$f_{20},f_{31}^{(+)},f_{23},f_{22},f_{24},f_{28}$	0.8315	p=0.811
BCDR2	$f_{30},f_{38},f_{37},f_{20},f_{28},f_{31},f_{22},f_{29},f_{27},f_{24}$	0.835	$f_{38},f_{28}^{(+)},f_{31}^{(+)},f_{22},f_{27},f_{20}$	**0.8413**	p=0.841
BCDR3	$f_{23},f_{26},f_{19},f_{20},f_{28},f_{34},f_{31},f_{38},f_{35},f_{29}$	0.885	$f_{23},f_{20}^{(+)},f_{28},f_{31}^{(+)},f_{38},f_{35}$	0.8821	p=0.918
DDSM1	$f_{25},f_{32},f_{35},f_{39},f_{20},f_{28},f_{37},f_{22},f_{26},f_{31}$	0.8004	$f_{25}^{(+)},f_{20},f_{28},f_{26}^{(+)},f_{35}$	0.8001	p=0.982
DDSM2	$f_{23},f_{35},f_{32},f_{39},f_{25},f_{19},f_{16},f_{21},f_{28},f_{24}$	0.8382	$f_{35},f_{32},f_{19}^{(+)},f_{16}^{(+)},f_{21}^{(+)},f_{24},f_{23}$	**0.8435**	p=0.757
DDSM3	$f_{25},f_{20},f_{37},f_{39},f_{32},f_{26},f_{35},f_{28},f_{34},f_{22}$	0.7806	$f_{25},f_{26}^{(+)},f_{35},f_{34},f_{22},f_{20}$	0.7759	p=0.685

$^{(+)}$Weakly relevant features but non-redundant.

From Table 36, it is possible to conclude that only two optimal subsets of features provided a slight increment in terms of AUC performance, but these results were not significantly superior. Furthermore, the remaining optimal subsets of features did not provide significance difference in the AUC performance.

Concerning redundancy analysis, redundant features were detected on every dataset, which means there are some variables providing similar information to the classifier, and thus it is unnecessarily increasing the complexity of the classification model. With the exception of the DDSM1 dataset, it was possible to find the most relevant feature for all the datasets. In the case of the BCDR2 dataset, the Perimeter (f_{20}) feature was selected as the most appropriated strongly relevant feature, however it has a unique correlation with the Area (f_{37}) feature (c-Pearson value of 0.89). In this case, it is possible to interchange both features (f_{20} or f_{37}) and

select only one of them as the most relevant feature (see Table 36). Likewise, in the DDSM3, the Perimeter (f_{20}) feature was selected as the most relevant feature and is correlated with the Entropy (f_{28}) feature (c-Pearson value of 0.56), but the Entropy (f_{28}) feature is also correlated with others features: Maximum (f_{25}), Correlation (f_{34}) and Standard deviation (f_{22}); under this situation, the selected Perimeter (f_{20}) feature is the only one which can be elected as the most relevant feature. This particular effect on both datasets could be explained by the c-Pearson values; the correlation value between Perimeter (f_{20}) and Area (f_{37}) was high (unique correlation) meanwhile the correlation value between Perimeter (f_{20}) and Entropy (f_{28}) was low (multi-correlation). It means that it is possible interchanging most relevant features only if there is a unique and strong correlation between them.

We considered strongly relevant features as the most important features: Perimeter (f_{20}), Entropy (f_{28}), Mean (f_{35}) and Roughness (f_{23}). They consistently appeared at least 3 times (each one) on the six optimal features subsets (see Table 36). This result was expected due to the binary classification problem (benign-malignant classes) investigated in this work. The perimeter and roughness features are considered significant shape descriptors for masses classification i.e. benign masses possess smooth, round, or oval shapes with possible macrolobulations, as opposed to malignant tumors which typically exhibit rough contours with microlobulations, spiculations, and concavities [7]. On the other hand, the entropy and mean features are more likely to be employed for MC classification i.e the entropy is a feature that represents the texture of the background tissue where the calcifications are embedded in [129, 140]; meanwhile, the mean is an intensity statistics descriptor used with higher frequency [78, 137] because MCs are tiny brighter dots [7].

Regarding classification performances, the proposed *uFilter* method was able to produce subsets of features with higher discriminant potential and the redundancy analysis did not improve the prediction accuracy, but decreased the size of the subset of features without significantly decreasing the performance. This result was expected since the *uFilter* method is an individual evaluator of features (filter paradigm) and it ignores the feature dependencies. This is the main drawback of individual features evaluator methods as is the case of *uFilter*.

CHAPTER 5

Conclusions

This chapter presents an overview of the work that we have developed in the scope of this thesis. Also we summarized the main contributions, limitations and future work.

5.1. Thesis Overview

Breast imaging, which is fundamental to cancer risk assessment, detection, diagnosis and treatment, is undergoing a paradigm shift: the tendency is to move from a primarily qualitative interpretation to a more quantitative-based interpretation model. In term of diagnosis, the mammography and the double reading of mammograms are two useful and suggested techniques for reducing the proportion of missed cancers. But the workload and cost associated are high.

Breast Cancer CADx systems is a more recent technique, which have been improved both the AUC performance of radiologists (see Chapter 1, Table 1) and the classification of cancer in its early stages (see Chapter 2, Table 12). Despite these prominent results, the performance of current and future commercial CADx systems still needs to be improved so that they can meet the requirements of clinics and screening centers [20, 94].

The feature selection constitutes one of the most important steps in the lifecycle of Breast Cancer CADx systems. It presents many potential benefits such as: facilitating data visualization and data understanding, reducing the measurement and storage requirements, reducing training and utilization times and, defining the curse of dimensionality to improve the predictions performance. It is therefore convenient that feature selection methods are fast, scalable, accurate and possibly with low algorithmic complexity.

This thesis was motivated by the need of developing new feature selection methods to provide more accurate and compact subsets of features to feed MLCs supporting breast cancer diagnosis. After some months of research studying previous developed approaches existing at that time, we realized that most of the developed approaches were focused on the wrapper or hybrid paradigm and, in fewer degrees on filter paradigm (see Chapter 2, section “Feature Selection Methods”).

We considered exploring the filter paradigm (univariate and multivariate) over the wrappers or hybrid models; because filter methods provide lower algorithmic complexity, faster performance and are independent of classifiers. It means that filter methods analyze the characteristics of data for ranking the entire space of features, while the wrappers or hybrid methods are extremely dependent of classifiers for selecting a satisfactory subset of features.

The principal limitation of univariate filter methods is that they ignore the dependencies among features and assume a given distribution (Gaussian in most cases) from which the samples (observations) have been collected. In addition, assuming a Gaussian distribution includes the difficulties to validate distributional assumptions because of small sample sizes. On the other hand, multivariate filters methods overcome the problem of ignoring feature dependencies introducing redundancy analysis (models feature dependencies) at some degree, but the improvements are not always significant: domains with large numbers of input variables suffer from the curse of dimensionality and multivariate methods may overfit the data. Also, multivariate methods have shown to be slower and less scalable than univariate methods. These limitations on existing filter methods may lead the Breast Cancer CADx methods to classification performances bellow of its potential.

5.2. Main Contributions and Future Work

While the results achieved in this thesis have been outlined before, into the developed chapters, to follow we summarized the main contributions:

Contribution 1: A new ensemble feature selection method (named *RMean*) supported on the filter paradigm for indexing relevant features extracted from mammographic pathological lesions (image-based and clinical features).

The *RMean* method used four feature selection methods with different evaluation function from the fillter paradigm: the CHI square discretization based on the chi-square statistic function, Information Gain based on the information measure, 1Rule based on rules as principal evaluation functions and Relief based on the distance measure. The application of these methods produces four different ranking of features (one by each applied feature selection method). Then, the mean position of each feature along the four features ranking was computed and, a new ranking was created using the mean position of features as indexing criterion. When applied to the breast cancer datasets under study, the subsets of ranked features produced by using the *RMean* method improved the AUC performance in almost all the explored machine learning classifiers.

Contribution 2: A new feature selection method (named *uFilter*) based on the Mann Whitney U-test for ranking relevant features, which assess the relevance of features by computing the separability between class-data distribution of each feature.

The *uFilter* is an innovative univariate filter method that improves the Mann Whitney U-test for reducing dimensionality and ranking features in binary classification problems. It solves some difficulties remaining on previous developed methods, such as: it is effective in ranking relevant features independently of the samples sizes (tolerant to unbalanced training data); it does not need any type of data normalization; and the most important, it presents a low risk of data overfitting and does not incur the high computational cost of conducting a search through the space of feature subsets as in the wrapper or embedded methods.

Contribution 3: An improvement in the performance of machine learning classifiers supporting Breast Cancer CADx methods.

Both feature selection methods (*RMean* and *uFilter*) were validated on breast cancer datasets for further statistical comparison against other developed existing approaches. According to the Wilcoxon statistic test, the ensemble *RMean* method (contribution 1) was the best on selecting relevant features when compared against the four baseline feature selection methods. It appeared consistently on all succeeds combinations for microcalcifications and masses classification. Also, it improved the performance of mammography-based machine learning classifiers. Despite the good performance of the *RMean* method, it still ignores the features dependence and redundant information could lead to a non-desired classification result.

On the other hand, the *uFilter* method (contribution 2) performed better than the Mann Whitney U-test (its theoretical basis) when applied to reduce and ranking features in binary classification problems. *uFilter* was validated over six different (balanced and unbalanced) datasets representative of two different breast cancer repositories. A head-to-head comparison proved that the *uFilter* method significantly outperformed the U-Test method for almost all of the classification schemes. It was superior in 50%; tied in a 37.5% and lost in a 12.5% of the 24 comparative scenarios. A global comparison against other four well known feature selection methods demonstrated that *uFilter* statistically outperformed the remaining methods on several datasets, and it was statistically similar on three datasets while requiring less number of features. Moreover, a general comparison against the developed *RMean* method also confirmed that the *uFilter* method was statistically superior on three datasets and statistically similar on the remaining datasets. This method revealed competitive and appealing cost-effectiveness results on selecting relevant features, as a support tool for breast cancer CADx methods especially in unbalanced datasets contexts. Finally, the redundancy analysis as a complementary step to the *uFilter* method provided us an effective way for finding optimal subsets of features.

The development of these contributions provided important evidences to support the proposed set of hypothesis in Chapter 1, Section 1.3. This can be reviewed in detail throughout the Chapter 3 and Chapter 4 and, it is summarized here:

Hypothesis 1: *Feature selection methods supported on the filter paradigm can be improved by the creation of new ensemble methods.* Experimental results in Section 3.6.2 statistically demonstrated the satisfactory performance obtained by the developed *RMean* method when compared to four well known (classical) feature selection methods of the filter paradigm.

Hypothesis 2: *Feature selection methods of the filter paradigm can be improved throughout a new filtered function, which provides index of features with better separability between two instance distributions*. The theoretical description of the *uFilter* method (see Section 4.3) and the experimental results reported in Section 4.5 constituted a sustain proof for the corroboration of this hypothesis.

Hypothesis 3: *Breast Cancer CADx systems can be advanced by the inclusion of a new feature selection method that provides features with more discrimination power to yield better AUC-based classifier performance*. The AUC-based classification performance of MLCs was always improved when using both the *RMean* and *uFilter* feature selection methods on breast cancer datasets (see Section 3.6 and 4.5). However, the *uFilter* method demonstrated to be the best, because it improved the main difficulties existing on univariate filter methods, including the *RMean* method (Section 4.5).

In summary, the contributions of this thesis suggest that it possible to improve the feature selection methods of the filter paradigm and the AUC-based classifier performance for breast cancer CADx systems.

Future work will be aimed to three issues: (1) increasing the number of features in benchmarking breast cancer datasets; (2) exploring the performance of *uFilter* method in other knowledge domains and (3) extending the *uFilter* method allowing it to be used on multiclass classification problems.

CHAPTER 6

Bibliographic References

[1] M. D. Althuis, J. M. Dozier, W. F. Anderson, S. S. Devesa, and L. A. Brinton, "Global trends in breast cancer incidence and mortality 1973-1997", *Int. J. Epidemiol.*, 2005, vol. 34, no. 2, pp. 405-412. http://dx.doi.org/10.1093/ije/dyh414.

[2] F. Kamangar, G. M. Dores, and W. F. Anderson, "Patterns of cancer incidence, mortality, and prevalence across five continents: defining priorities to reduce cancer disparities in different geographic regions of the world", *Journal of clinical oncology*, 2006, vol. 24, no. 14, pp. 2137-2150.

[3] V. Veloso, "Cancro da mama mata 5 mulheres por dia em Portugal", in *CiênciaHoje*, ed. Lisboa, Portugal, 2009.

[4] N. Pérez, M. A. Guevara, A. Silva, I. Ramos, and J. Loureiro, "Improving the performance of machine learning classifiers for Breast Cancer diagnosis based on feature selection", in *Proceedings of the 2014 Federated Conference on Computer Science and Information Systems*. M. Ganzha, L. Maciaszek, and M. Paprzycki (Eds.), IEEE, Warsaw, Poland, 2014, pp. 209-217. http://dx.doi.org/10.15439/2014F249.

[5] R. Ramos-Pollan, "Grid computing for breast cancer CAD. A pilot experience in a medical environment", in *4th Iberian Grid Infrastructure Conference*, 2010, pp. 307-318.

[6] "What Is Breast Cancer?".http://www.breastcancer.org/symptoms/understand_bc/what_is_bc (Accessed: Jan 1, 2013).

[7] A. Committee, *American College of Radiology (ACR) ACR BIRADS - Mammography*, 4th ed. Reston, VA, 2003.

[8] H. Zonderland, T. Pope, Jr., and A. Nieborg, "The positive predictive value of the breast imaging reporting and data system (BI-RADS) as a method of quality assessment in breast imaging in a hospital population", *European Radiology*, 2004, vol. 14, no. 10, pp. 1743-1750. http://dx.doi.org/10.1007/s00330-004-2373-6.

[9] S. G. Orel, N. Kay, C. Reynolds, and D. C. Sullivan, "BI-RADS categorization as a predictor of malignancy", *Radiology*, 1999, vol. 211, no. 3, pp. 845-50.

[10] C. G. Ball, M. Butchart, and J. K. MacFarlane, "Effect on biopsy technique of the breast imaging reporting and data system (BI-RADS) for nonpalpable mammographic abnormalities", *Can J Surg*, 2002, vol. 45, no. 4, pp. 259-63.

[11] S. H. Taplin, L. E. Ichikawa, K. Kerlikowske, V. L. Ernster, R. D. Rosenberg, B. C. Yankaskas, *et al.*, "Concordance of Breast Imaging Reporting and Data System Assessments and Management Recommendations in Screening Mammography", *Radiology*, 2002, vol. 222, no. 2, pp. 529-535. http://dx.doi.org/10.1148/radiol.2222010647.

[12] K. Bihrmann, A. Jensen, A. H. Olsen, S. Njor, W. Schwartz, I. Vejborg, *et al.*, "Performance of systematic and non-systematic ('opportunistic') screening mammography: a comparative study from Denmark", *J Med Screen*, 2008, vol. 15, no. 1, pp. 23-6. http://dx.doi.org/10.1258/jms.2008.007055.

[13] M. H. Dilhuydy, "Breast imaging reporting and data system (BI-RADS) or French “classification ACR”: What tool for what use? A point of view", *European Journal of Radiology*, 2007, vol. 61, no. 2, pp. 187-191. http://dx.doi.org/10.1016/j.ejrad.2006.08.032.

[14] "Mammograms and Other Breast Imaging Procedures".http://www.cancer.org/treatment/understandingyourdiagnosis/examsandtestdescriptions/mammogramsandotherbreastimagingprocedures/mammograms-and-other-breast-imaging-procedures-mammo-report (Accessed: Jan 1, 2014).

[15] P. Boyle and B. Levin, *World cancer report 2008*: IARC Press, International Agency for Research on Cancer, 2008.

[16] M. M. Ng KH, "Advances in mammography have improved early detection of breast cancer", *J Hong Kong Coll Radiol*, 2003, vol. 6(3), no. pp. 126-131.

[17] "Digital vs. Film Mammography in the Digital Mammographic Imaging Screening Trial (DMIST): Questions and Answers".http://www.cancer.gov/cancertopics/factsheet/DMISTQandA (Accessed: Feb 2, 2013).

[18] D. Gur, "Digital Mammography: Do We Need to Convert Now?", *Radiology*, 2007, vol. 245, no. 1, pp. 10-11. http://dx.doi.org/10.1148/radiol.2451062078.

[19] E. D. Pisano, R. E. Hendrick, M. Yaffe, E. F. Conant, and C. Gatsonis, "Should Breast Imaging Practices Convert to Digital Mammography? A Response from Members of the DMIST Executive Committee1", *Radiology*, 2007, vol. 245, no. 1, pp. 12-13. http://dx.doi.org/10.1148/radiol.2451070393.

[20] E. D. Pisano, C. Gatsonis, E. Hendrick, M. Yaffe, J. K. Baum, S. Acharyya, *et al.*, "Diagnostic Performance of Digital versus Film Mammography for Breast-Cancer Screening", *N Engl J Med*, 2005, vol. 353, no. 17, pp. 1773-1783. http://dx.doi.org/10.1056/NEJMoa052911.

[21] W. Yang, "Digital mammography update", *Biomed. Imag. Intervention*, 2006, vol. 2, no. 4, pp. 45-12.

[22] M. Reddy and R. Given-Wilson, "Screening for breast cancer", *Women's Health Medicine*, 2006, vol. 3, no. 1, pp. 22-27.

[23] J. Shi, B. Sahiner, H.-P. Chan, J. Ge, L. Hadjiiski, M. A. Helvie, *et al.*, "Characterization of mammographic masses based on level set segmentation with new image features and patient information", *Medical Physics*, 2008, vol. 35, no. 1, pp. 280-290.

[24] D. Guliato, R. M. Rangayyan, J. D. Carvalho, and S. A. Santiago, "Polygonal Modeling of Contours of Breast Tumors With the Preservation of Spicules", *Biomedical Engineering, IEEE Transactions on*, 2008, vol. 55, no. 1, pp. 14-20. http://dx.doi.org/10.1109/TBME.2007.899310.

[25] P. Delogu, M. Evelina Fantacci, P. Kasae, and A. Retico, "Characterization of mammographic masses using a gradient-based segmentation algorithm and a neural classifier", *Computers in Biology and Medicine*, 2007, vol. 37, no. 10, pp. 1479-1491. http://dx.doi.org/10.1016/j.compbiomed.2007.01.009.

[26] A. Karahaliou, S. Skiadopoulos, I. Boniatis, P. Sakellaropoulos, E. Likaki, G. Panayiotakis, *et al.*, "Texture analysis of tissue surrounding microcalcifications on mammograms for breast cancer diagnosis", *British Journal of Radiology*, 2007, vol. 80, no. 956, pp. 648-656. http://dx.doi.org/10.1259/bjr/30415751.

[27] C. Varela, S. Timp, and N. Karssemeijer, "Use of border information in the classification of mammographic masses", *Phys Med Biol*, 2006, vol. 51, no. 2, pp. 425-41. http://dx.doi.org/10.1088/0031-9155/51/2/016.

[28] J. Wei, B. Sahiner, L. M. Hadjiiski, H.-P. Chan, N. Petrick, M. A. Helvie, *et al.*, "Computer-aided detection of breast masses on full field digital mammograms", *Medical physics*, 2005, vol. 32, no. 9, pp. 2827-2838.

[29] E. S. d. Paredes, "Atlas of Mammography, 3rd ed", *Radiology*, 2009, vol. 252, no. 3, p. 663. http://dx.doi.org/10.1148/radiol.2523092526.

[30] "Breast Cancer Digital Repository".http://bcdr.inegi.up.pt/ (Accessed: Jan 1, 2014).

[31] J. S. Suri and R. M. Rangayyan, *Recent advances in breast imaging, mammography, and computer-aided diagnosis of breast cancer* vol. 155: SPIE press, 2006.

[32] C. H. Yip, R. A. Smith, B. O. Anderson, A. B. Miller, D. B. Thomas, E. S. Ang, *et al.*, "Guideline implementation for breast healthcare in low- and middle-income countries: early detection resource allocation", *Cancer*, 2008, vol. 113, no. 8 Suppl, pp. 2244-56. http://dx.doi.org/10.1002/cncr.23842.

[33] J. Brown, S. Bryan, and R. Warren, "Mammography screening: an incremental cost effectiveness analysis of double versus single reading of mammograms", *BMJ (Clinical research ed.)*, 1996, vol. 312, no. 7034, pp. 809-812.

[34] R. Ramos-Pollan, M. A. Guevara-Lopez, C. Suarez-Ortega, G. Diaz-Herrero, J. M. Franco-Valiente, M. Rubio-Del-Solar, *et al.*, "Discovering mammography-based machine learning classifiers for breast cancer diagnosis", *J Med Syst*, 2012, vol. 36, no. 4, pp. 2259-69. http://dx.doi.org/10.1007/s10916-011-9693-2.

[35] R. R. Pollán, "Improving multilayer perceptron classifiers AUC performance: An approach in biomedical image analysis for breast cancer CAD supported by eInfrastructures", Phd, Department of Informatics Engineering, Faculty of Engineering, University of Porto, 2011.

[36] A. Lauria, M. E. Fantacci, U. Bottigli, P. Delogu, F. Fauci, B. Golosio, *et al.*, "Diagnostic performance of radiologists with and without different CAD systems for mammography", in *Medical Imaging 2003*, International Society for Optics and Photonics, 2003, pp. 51-56.

[37] L. H. Eadie, P. Taylor, and A. P. Gibson, "A systematic review of computer-assisted diagnosis in diagnostic cancer imaging", *European Journal of Radiology*, 2012, vol. 81, no. 1, pp. e70-e76. http://dx.doi.org/10.1016/j.ejrad.2011.01.098.

[38] J. J. Fenton, S. H. Taplin, P. A. Carney, L. Abraham, E. A. Sickles, C. D'Orsi, *et al.*, "Influence of Computer-Aided Detection on Performance of Screening Mammography", *New England Journal of Medicine*, 2007, vol. 356, no. 14, pp. 1399-1409. http://dx.doi.org/10.1056/NEJMoa066099.

[39] I. Leichter, S. Fields, R. Nirel, P. Bamberger, B. Novak, R. Lederman, *et al.*, "Improved mammographic interpretation of masses using computer-aided diagnosis", *Eur Radiol*, 2000, vol. 10, no. 2, pp. 377-83.

[40] Z. Huo, M. L. Giger, C. J. Vyborny, and C. E. Metz, "Breast cancer: effectiveness of computer-aided diagnosis observer study with independent database of mammograms", *Radiology*, 2002, vol. 224, no. 2, pp. 560-8.

[41] L. Hadjiiski, H. P. Chan, B. Sahiner, M. A. Helvie, M. A. Roubidoux, C. Blane, *et al.*, "Improvement in radiologists' characterization of malignant and benign breast masses on serial mammograms with computer-aided diagnosis: an ROC study", *Radiology*, 2004, vol. 233, no. 1, pp. 255-65. http://dx.doi.org/10.1148/radiol.2331030432.

[42] L. Hadjiiski, B. Sahiner, M. A. Helvie, H. P. Chan, M. A. Roubidoux, C. Paramagul, *et al.*, "Breast masses: computer-aided diagnosis with serial mammograms", *Radiology*, 2006, vol. 240, no. 2, pp. 343-56. http://dx.doi.org/10.1148/radiol.2401042099.

[43] K. Horsch, M. L. Giger, C. J. Vyborny, L. Lan, E. B. Mendelson, and R. E. Hendrick, "Classification of breast lesions with multimodality computer-aided diagnosis: observer study results on an independent clinical data set", *Radiology*, 2006, vol. 240, no. 2, pp. 357-68. http://dx.doi.org/10.1148/radiol.2401050208.

[44] L. A. Meinel, A. H. Stolpen, K. S. Berbaum, L. L. Fajardo, and J. M. Reinhardt, "Breast MRI lesion classification: Improved performance of human readers with a backpropagation neural network computer-aided diagnosis (CAD) system", *Journal of Magnetic Resonance Imaging*, 2007, vol. 25, no. 1, pp. 89-95. http://dx.doi.org/10.1002/jmri.20794.

[45] M. Dash, K. Choi, P. Scheuermann, and H. Liu, "Feature selection for clustering-a filter solution", in *Data Mining, 2002. ICDM 2003. Proceedings. 2002 IEEE International Conference on*, IEEE, 2002, pp. 115-122.

[46] M. A. Hall, "Correlation-based Feature Selection for Discrete and Numeric Class Machine Learning", presented at the Proceedings of the Seventeenth International Conference on Machine Learning, Morgan Kaufmann Publishers Inc., 2000.

[47] L. Yu and H. Liu, "Feature selection for high-dimensional data: A fast correlation-based filter solution", in *ICML*, 2003, pp. 856-863.

[48] J. G. Dy and C. E. Brodley, "Feature subset selection and order identification for unsupervised learning", in *ICML*, Citeseer, 2000, pp. 247-254.

[49] Y. Kim, W. N. Street, and F. Menczer, "Feature selection in unsupervised learning via evolutionary search", in *Proceedings of the sixth ACM SIGKDD international conference on Knowledge discovery and data mining*, ACM, 2000, pp. 365-369.

[50] R. Kohavi and G. H. John, "Wrappers for feature subset selection", *Artificial intelligence*, 1997, vol. 97, no. 1, pp. 273-324.

[51] E. P. Xing, M. I. Jordan, and R. M. Karp, "Feature selection for high-dimensional genomic microarray data", in *ICML*, 2001, pp. 601-608.

[52] A. Fialho, F. Cismondi, S. Vieira, J. C. Sousa, S. Reti, M. Howell, *et al.*, "Predicting Outcomes of Septic Shock Patients Using Feature Selection Based on Soft Computing Techniques", in *Information Processing and Management of Uncertainty in Knowledge-Based Systems. Applications*. vol. 81, E. Hüllermeier, R. Kruse, and F. Hoffmann (Eds.): Springer Berlin Heidelberg, 2010, pp. 65-74. http://dx.doi.org/10.1007/978-3-642-14058-7_7.

[53] S. M. Vieira, J. M. C. Sousa, and U. Kaymak, "Fuzzy criteria for feature selection", *Fuzzy Sets and Systems*, 2012, vol. 189, no. 1, pp. 1-18. http://dx.doi.org/10.1016/j.fss.2011.09.009.

[54] G. George and V. C. Raj, "Review on feature selection techniques and the impact of SVM for cancer classification using gene expression profile", *arXiv preprint arXiv:1109.1062*, 2011, no.

[55] I.-S. Oh, J.-S. Lee, and B.-R. Moon, "Hybrid genetic algorithms for feature selection", *Pattern Analysis and Machine Intelligence, IEEE Transactions on*, 2004, vol. 26, no. 11, pp. 1424-1437.

[56] I. Guyon and A. Elisseeff, "An introduction to variable and feature selection", *J. Mach. Learn. Res.*, 2003, vol. 3, no. pp. 1157-1182.

[57] I. Guyon and A. Elisseeff, "An Introduction to Feature Extraction", in *Feature Extraction*. vol. 207, I. Guyon, M. Nikravesh, S. Gunn, and L. Zadeh (Eds.): Springer Berlin Heidelberg, 2006, pp. 1-25. http://dx.doi.org/10.1007/978-3-540-35488-8_1.

[58] C. Markopoulos, E. Kouskos, K. Koufopoulos, V. Kyriakou, and J. Gogas, "Use of artificial neural networks (computer analysis) in the diagnosis of microcalcifications on mammography", *European Journal of Radiology*, 2001, vol. 39, no. 1, pp. 60-65. http://dx.doi.org/10.1016/S0720-048X(00)00281-3.

[59] O. Okun, *Feature Selection and Ensemble Methods for Bioinformatics: Algorithmic Classification and Implementations*: Medical Info Science Reference, 2011.

[60] L. Ladha and T. Deepa, "Feature selection methods and algorithms", *International Journal on Computer Science and Engineering*, 2011, vol. 3, no. 5, pp. 1787-1797.

[61] J. Yu, S. Ongarello, R. Fiedler, X. Chen, G. Toffolo, C. Cobelli, *et al.*, "Ovarian cancer identification based on dimensionality reduction for high-throughput mass spectrometry data", *Bioinformatics*, 2005, vol. 21, no. 10, pp. 2200-2209.

[62] R. Varshavsky, A. Gottlieb, M. Linial, and D. Horn, "Novel unsupervised feature filtering of biological data", *Bioinformatics*, 2006, vol. 22, no. 14, pp. e507-e513.

[63] K. Doi, "Computer-aided diagnosis in medical imaging: Historical review, current status and future potential", *Computerized Medical Imaging and Graphics*, 2007, vol. 31, no. 4-5, pp. 198-211.

[64] K. Doi, "Current status and future potential of computer-aided diagnosis in medical imaging", *British Journal of Radiology*, 2005, vol. 78, no. SPEC. ISS., pp. S3-S19.

[65] H. D. Cheng, X. Cai, X. Chen, L. Hu, and X. Lou, "Computer-aided detection and classification of microcalcifications in mammograms: A survey", *Pattern Recognition*, 2003, vol. 36, no. 12, pp. 2967-2991.

[66] Isaac Leichter, Richard Lederman, Shalom Buchbinder, Philippe Bamberger, Boris Novak, and S. Fields4, "Optimizing parameters for computer-aided diagnosis of microcalcifications at mammography ", *Academic Radiology*, 2000, vol. 7, no. 6, pp. 406-412.

[67] Z. Ping, B. Verma, and K. Kuldeep, "A neural-genetic algorithm for feature selection and breast abnormality classification in digital mammography", in *2004 IEEE International Joint Conference on Neural Networks*, 2004, pp. 2303-2308. http://dx.doi.org/10.1109/IJCNN.2004.1380985.

[68] W. Yunfeng, H. Jingjing, M. Yi, and J. I. Arribas, "Neural network fusion strategies for identifying breast masses", in *Neural Networks, 2004. Proceedings. 2004 IEEE International Joint Conference on*, 2004, pp. 2437-2442 vol.3. http://dx.doi.org/10.1109/IJCNN.2004.1381010.

[69] B. Verma and R. Panchal, "Neural Networks for the Classification of Benign and Malignant Patters in Digital Mammograms", in *Intelligent Information Technologies: Concepts, Methodologies, Tools, and Applications*: IGI Global, 2008, pp. 947-967. http://dx.doi.org/10.4018/978-1-59904-941-0.ch056.

[70] E. Malar, A. Kandaswamy, D. Chakravarthy, and A. Giri Dharan, "A novel approach for detection and classification of mammographic microcalcifications using wavelet analysis and extreme learning machine", *Comput Biol Med*, 2012, vol. 42, no. 9, pp. 898-905. http://dx.doi.org/10.1016/j.compbiomed.2012.07.001.

[71] R. Bellotti, F. De Carlo, S. Tangaro, G. Gargano, G. Maggipinto, M. Castellano, *et al.*, "A completely automated CAD system for mass detection in a large mammographic database", *Medical physics*, 2006, vol. 33, no. 8, pp. 3066-3075.

[72] B. Zheng, W. F. Good, D. R. Armfield, C. Cohen, T. Hertzberg, J. H. Sumkin, *et al.*, "Performance Change of Mammographic CAD Schemes Optimized with Most-Recent and Prior Image Databases", *Academic Radiology*, 2003, vol. 10, no. 3, pp. 283-288. http://dx.doi.org/10.1016/S1076-6332(03)80102-2.

[73] L. Zhang, W. Qian, R. Sankar, D. Song, and R. Clark, "A new false positive reduction method for MCCs detection in digital mammography", in *Acoustics, Speech, and Signal Processing, 2001. Proceedings. (ICASSP '01). 2001 IEEE International Conference on*, 2001, pp. 1033-1036 vol.2. http://dx.doi.org/10.1109/ICASSP.2001.941095.

[74] Z. Huo, M. L. Giger, C. J. Vyborny, D. E. Wolverton, R. A. Schmidt, and K. Doi, "Automated computerized classification of malignant and benign masses on digitized mammograms", *Academic Radiology*, 1998, vol. 5, no. 3, pp. 155-168. http://dx.doi.org/10.1016/S1076-6332(98)80278-X.

[75] N. Pérez, M. A. Guevara, and A. Silva, "Improving breast cancer classification with mammography, supported on an appropriate variable selection analysis", in *SPIE Medical Imaging*, International Society for Optics and Photonics, 2013, pp. 867022-14.

[76] M. E. Mavroforakis, H. V. Georgiou, N. Dimitropoulos, D. Cavouras, and S. Theodoridis, "Mammographic masses characterization based on localized texture and dataset fractal analysis using linear, neural and support vector machine classifiers", *Artif Intell Med*, 2006, vol. 37, no. 2, pp. 145-62. http://dx.doi.org/10.1016/j.artmed.2006.03.002.

[77] A. Papadopoulos, D. I. Fotiadis, and A. Likas, "Characterization of clustered microcalcifications in digitized mammograms using neural networks and support vector machines", *Artificial Intelligence in Medicine*, 2005, vol. 34, no. 2, pp. 141-150. http://dx.doi.org/10.1016/j.artmed.2004.10.001.

[78] J. C. Fu, S. K. Lee, S. T. C. Wong, J. Y. Yeh, A. H. Wang, and H. K. Wu, "Image segmentation feature selection and pattern classification for mammographic microcalcifications", *Computerized Medical Imaging and Graphics*, 2005, vol. 29, no. 6, pp. 419-429. http://dx.doi.org/10.1016/j.compmedimag.2005.03.002.

[79] B. Sahiner, N. Petrick, H. P. Chan, L. M. Hadjiiski, C. Paramagul, M. A. Helvie, *et al.*, "Computer-aided characterization of mammographic masses: accuracy of mass segmentation and its effects on characterization", *IEEE Trans Med Imaging*, 2001, vol. 20, no. 12, pp. 1275-84. http://dx.doi.org/10.1109/42.974922.

[80] B. Sahiner, H.-P. Chan, N. Petrick, M. A. Helvie, and L. M. Hadjiiski, "Improvement of mammographic mass characterization using spiculation measures and morphological features", *Medical Physics*, 2001, vol. 28, no. 7, pp. 1455-1465.

[81] D. M. Catarious, Jr., A. H. Baydush, and C. E. Floyd, Jr., "Incorporation of an iterative, linear segmentation routine into a mammographic mass CAD system", *Med Phys*, 2004, vol. 31, no. 6, pp. 1512-20.

[82] J. L. Jesneck, J. Y. Lo, and J. A. Baker, "Breast mass lesions: computer-aided diagnosis models with mammographic and sonographic descriptors", *Radiology*, 2007, vol. 244, no. 2, pp. 390-8. http://dx.doi.org/10.1148/radiol.2442060712.

[83] S. Gupta, P. F. Chyn, and M. K. Markey, "Breast cancer CADx based on BI-RAds descriptors from two mammographic views", *Med Phys*, 2006, vol. 33, no. 6, pp. 1810-7.

[84] A. P. Dhawan, Y. Chitre, and C. Kaiser-Bonasso, "Analysis of mammographic microcalcifications using gray-level image structure features", *Medical Imaging, IEEE Transactions on*, 1996, vol. 15, no. 3, pp. 246-259.

[85] B. Zheng, A. Lu, L. A. Hardesty, J. H. Sumkin, C. M. Hakim, M. A. Ganott, *et al.*, "A method to improve visual similarity of breast masses for an interactive computer-aided diagnosis environment", *Med Phys*, 2006, vol. 33, no. 1, pp. 111-7.

[86] W. J. H. Veldkamp, N. Karssemeijer, J. D. M. Otten, and J. H. C. L. Hendriks, "Automated classification of clustered microcalcifications into malignant and benign types", *Medical Physics*, 2000, vol. 27, no. 11, pp. 2600-2608.

[87] R. Nakayama, R. Watanabe, K. Namba, K. Takeda, K. Yamamoto, S. Katsuragawa, *et al.*, "An improved computer-aided diagnosis scheme using the nearest neighbor criterion for determining histological classification of clustered microcalcifications", *Methods Inf Med*, 2007, vol. 46, no. 6, pp. 716-22.

[88] D. Moura and M. Guevara López, "An evaluation of image descriptors combined with clinical data for breast cancer diagnosis", *International Journal of Computer Assisted Radiology and Surgery*, 2013, vol. 8, no. 4, pp. 561-574. http://dx.doi.org/10.1007/s11548-013-0838-2.

[89] G. I. Salama, M. Abdelhalim, and M. A.-e. Zeid, "Breast Cancer Diagnosis on Three Different Datasets Using Multi-Classifiers", *Breast Cancer (WDBC)*, 2012, vol. 32, no. 569, p. 2.

[90] A. Christobel, "An Empirical Comparison of Data mining Classification Methods", *International Journal of Computer Information Systems*, 2011, vol. 3, no. 2,

[91] L. Zheng, A. K. Chan, G. McCord, S. Wu, and J. S. Liu, "Detection of cancerous masses for screening mammography using discrete wavelet transform-based multiresolution Markov random field", *J Digit Imaging*, 1999, vol. 12, no. 2 Suppl 1, pp. 18-23.

[92] Z. Lei and A. K. Chan, "An artificial intelligent algorithm for tumor detection in screening mammogram", *Medical Imaging, IEEE Transactions on*, 2001, vol. 20, no. 7, pp. 559-567. http://dx.doi.org/10.1109/42.932741.

[93] L. Hadjiiski, B. Sahiner, and H.-P. Chan, "Advances in CAD for diagnosis of breast cancer", *Current opinion in obstetrics & gynecology*, 2006, vol. 18, no. 1, p. 64.

[94] S. Ciatto, N. Houssami, D. Gur, R. M. Nishikawa, R. A. Schmidt, C. E. Metz, *et al.*, "Computer-Aided Screening Mammography", *N Engl J Med*, 2007, vol. 357, no. 1, pp. 83-85. http://dx.doi.org/10.1056/NEJMc071248.

[95] A. Malich, D. R. Fischer, and J. Bottcher, "CAD for mammography: the technique, results, current role and further developments", *Eur Radiol*, 2006, vol. 16, no. 7, pp. 1449-60. http://dx.doi.org/10.1007/s00330-005-0089-x.

[96] H. Liu and R. Setiono, "Chi2: Feature Selection and Discretization of Numeric Attributes", in *2012 IEEE 24th International Conference on Tools with Artificial Intelligence*, 1995, pp. 388-388.

[97] H. Liu, J. Li, and L. Wong, "A comparative study on feature selection and classification methods using gene expression profiles and proteomic patterns", *Genome Inform*, 2002, vol. 13, no. pp. 51-60.

[98] B. P. Flannery, W. H. Press, S. A. Teukolsky, and W. Vetterling, "Numerical recipes in C", *Press Syndicate of the University of Cambridge, New York*, 1992, no.

[99] A. K. Jain and B. Chandrasekaran, "39 Dimensionality and sample size considerations in pattern recognition practice", in *Handbook of Statistics*. vol. Volume 2, P. R. Krishnaiah and L. N. Kanal (Eds.): Elsevier, 1982, pp. 835-855. http://dx.doi.org/http://dx.doi.org/10.1016/S0169-7161(82)02042-2.

[100] M. A. Hall and L. A. Smith, "Feature Selection for Machine Learning: Comparing a Correlation-Based Filter Approach to the Wrapper", in *FLAIRS conference*, 1999, pp. 235-239.

[101] D. Koller and M. Sahami, "Toward optimal feature selection", 1996, no.

[102] L. Yu and H. Liu, "Efficient feature selection via analysis of relevance and redundancy", *Journal of Machine Learning Research*, 2004, vol. 5, no. pp. 1205-1224.

[103] K. Kira and L. A. Rendell, "A practical approach to feature selection", in *Proceedings of the ninth international workshop on Machine learning*, 1992, pp. 249-256.

[104] J. Prados, A. Kalousis, J. C. Sanchez, L. Allard, O. Carrette, and M. Hilario, "Mining mass spectra for diagnosis and biomarker discovery of cerebral accidents", *Proteomics*, 2004, vol. 4, no. 8, pp. 2320-2332.

[105] G. David, "Breast Cancer database provides faster access to patient record. Grid technology is at the heart of this massive database that holds over a million mammography images.", vol. article 174400322, ed: Information Week, 2005.

[106] R. M. Nishikawa, "Mammographic databases", *Breast Dis*, 1998, vol. 10, no. 3-4, pp. 137-50.

[107] R. M. Rangayyan, N. R. Mudigonda, and J. E. L. Desautels, "Boundary modelling and shape analysis methods for classification of mammographic masses", *Medical and Biological Engineering and Computing*, 2000, vol. 38, no. 5, pp. 487-496. http://dx.doi.org/10.1007/BF02345742.

[108] C. J. Garcia-Orellana, R. Gallardo-Caballero, H. M. Gonzalez-Velasco, A. Garcia-Manso, and M. Macias-Macias, "Study of a mammographic CAD performance dependence on the considered mammogram set", *Conf Proc IEEE Eng Med Biol Soc*, 2008, vol. 2008, no. pp. 4776-9. http://dx.doi.org/10.1109/iembs.2008.4650281.

[109] A. Oliver, J. Freixenet, J. Martí, E. Pérez, J. Pont, E. R. E. Denton, *et al.*, "A review of automatic mass detection and segmentation in mammographic images", *Medical Image Analysis*, 2010, vol. 14, no. 2, pp. 87-110. http://dx.doi.org/10.1016/j.media.2009.12.005.

[110] E. Song, S. Xu, X. Xu, J. Zeng, Y. Lan, S. Zhang, *et al.*, "Hybrid segmentation of mass in mammograms using template matching and dynamic programming", *Acad Radiol*, 2010, vol. 17, no. 11, pp. 1414-24. http://dx.doi.org/10.1016/j.acra.2010.07.008.

[111] J. Suckling, J. Parker, D. Dance, S. Astley, I. Hutt, C. Boggis, *et al.*, "The Mammographic Image Analysis Society digital mammogram database", in *2nd International Workshop on Digital Mammography*. A. Gale, S. Astley, D. Dance, and A. Cairns (Eds.), Excerta Medica, Amsterdam, 1994.

[112] Heath M, Bowyer KW, and K. D, "Current status of the digital database for screening mammography", in *Digital Mammography*, Kluwer Academic Publishers, 1998, pp. 457-460.

[113] B. R. Matheus and H. Schiabel, "Online Mammographic Images Database for Development and Comparison of CAD Schemes", *Journal of Digital Imaging*, 2011, vol. 24, no. 3, pp. 500-506. http://dx.doi.org/10.1007/s10278-010-9297-2.

[114] I. C. Moreira, I. Amaral, I. Domingues, A. Cardoso, M. J. Cardoso, and J. S. Cardoso, "INbreast: Toward a Full-field Digital Mammographic Database", *Academic Radiology*, 2012, vol. 19, no. 2, pp. 236-248. http://dx.doi.org/10.1016/j.acra.2011.09.014.

[115] J. E. de Oliveira, A. M. Machado, G. C. Chavez, A. P. Lopes, T. M. Deserno, and A. Araujo Ade, "MammoSys: A content-based image retrieval system using breast density patterns", *Comput Methods Programs Biomed*, 2010, vol. 99, no. 3, pp. 289-97. http://dx.doi.org/10.1016/j.cmpb.2010.01.005.

[116] Júlia E. E. Oliveira, Mark O. Gueld, Arnaldo de A. Araújo, Bastian Ott, and T. M. Deserno., "Towards a Standard Reference Database for Computer-aided Mammography", in *SPIE - Medical Imaging 2008: Computer-Aided Diagnosis*. Maryellen L. Giger and N. Karssemeijer. (Eds.), 69151Y, 2008. http://dx.doi.org/10.1117/12.770325.

[117] A. Oliver, "Automatic mass segmentation in mammographic images ", Phd thesis, Universitat de Girona (Españna) 2007.

[118] R. N. Strickland and H. Hee Il, "Wavelet transforms for detecting microcalcifications in mammograms", *Medical Imaging, IEEE Transactions on*, 1996, vol. 15, no. 2, pp. 218-229.

[119] Z. C. Antoniou, G. P. Giannakopoulou, I. I. Andreadis, K. S. Nikita, P. A. Ligomenides, and G. M. Spyrou, "A web-accessible mammographic image database dedicated to combined training and evaluation of radiologists and machines", in *Information Technology and Applications in Biomedicine, 2009. ITAB 2009. 9th International Conference on*, 2009, pp. 1-4. http://dx.doi.org/10.1109/ITAB.2009.5394465.

[120] Kamaledin Setarehdan S., Singh, and Sameer. (2002). *Advanced Algorithmic Approaches to Medical Image Segmentation*.

[121] M. T. Mandelson, N. Oestreicher, P. L. Porter, D. White, C. A. Finder, S. H. Taplin, *et al.*, "Breast density as a predictor of mammographic detection: comparison of interval- and screen-detected cancers", *J Natl Cancer Inst*, 2000, vol. 92, no. 13, pp. 1081-7.

[122] C. H. van Gils, J. D. Otten, A. L. Verbeek, J. H. Hendriks, and R. Holland, "Effect of mammographic breast density on breast cancer screening performance: a study in Nijmegen, The Netherlands", *J Epidemiol Community Health*, 1998, vol. 52, no. 4, pp. 267-71.

[123] E. S. Burnside, J. E. Ochsner, K. J. Fowler, J. P. Fine, L. R. Salkowski, D. L. Rubin, *et al.*, "Use of microcalcification descriptors in BI-RADS 4th edition to stratify risk of malignancy", *Radiology*, 2007, vol. 242, no. 2, pp. 388-95. http://dx.doi.org/10.1148/radiol.2422052130.

[124] Y. Jiang and C. E. Metz, "BI-RADS data should not be used to estimate ROC curves", *Radiology*, 2010, vol. 256, no. 1, pp. 29-31. http://dx.doi.org/10.1148/radiol.10091394.

[125] M. Elter and A. Horsch, "CADx of mammographic masses and clustered microcalcifications: a review", *Medical physics*, 2009, vol. 36, no. 6, pp. 2052-2068.

[126] M. Kallergi, "Computer-aided diagnosis of mammographic microcalcification clusters", *Medical Physics*, 2004, vol. 31, no. 2, pp. 314-326.

[127] R. Nakayama, Y. Uchiyama, R. Watanabe, S. Katsuragawa, K. Namba, and K. Doi, "Computer-aided diagnosis scheme for histological classification of clustered microcalcifications on magnification mammograms", *Med Phys*, 2004, vol. 31, no. 4, pp. 789-99.

[128] M. De Santo, M. Molinara, F. Tortorella, and M. Vento, "Automatic classification of clustered microcalcifications by a multiple expert system", *Pattern Recognition*, 2003, vol. 36, no. 7, pp. 1467-1477. http://dx.doi.org/10.1016/S0031-3203(03)00004-9.

[129] H. Soltanian-Zadeh, F. Rafiee-Rad, and S. Pourabdollah-Nejad D, "Comparison of multiwavelet, wavelet, Haralick, and shape features for microcalcification classification in mammograms", *Pattern Recognition*, 2004, vol. 37, no. 10, pp. 1973-1986. http://dx.doi.org/10.1016/j.patcog.2003.03.001.

[130] L. Bocchi and J. Nori, "Shape analysis of microcalcifications using Radon transform", *Medical Engineering & Physics*, 2007, vol. 29, no. 6, pp. 691-698. http://dx.doi.org/10.1016/j.medengphy.2006.07.012.

[131] I. Leichter, R. Lederman, S. S. Buchbinder, P. Bamberger, B. Novak, and S. Fields, "Computerized evaluation of mammographic lesions: what diagnostic role does the shape of the individual microcalcifications play compared with the geometry of the cluster?", *AJR Am J Roentgenol*, 2004, vol. 182, no. 3, pp. 705-12. http://dx.doi.org/10.2214/ajr.182.3.1820705.

[132] H.-P. Chan, B. Sahiner, K. L. Lam, N. Petrick, M. A. Helvie, M. M. Goodsitt, *et al.*, "Computerized analysis of mammographic microcalcifications in morphological and texture feature spaces", *Medical Physics*, 1998, vol. 25, no. 10, pp. 2007-2019.

[133] F. Schmidt, E. Sorantin, C. Szepesvari, E. Graif, M. Becker, H. Mayer, *et al.*, "An automatic method for the identification and interpretation of clustered microcalcifications in mammograms", *Phys Med Biol*, 1999, vol. 44, no. 5, pp. 1231-43.

[134] I. Leichter, R. Lederman, P. Bamberger, B. Novak, S. Fields, and S. S. Buchbinder, "The use of an interactive software program for quantitative characterization of microcalcifications on digitized film-screen mammograms", *Invest Radiol*, 1999, vol. 34, no. 6, pp. 394-400.

[135] H. P. Chan, B. Sahiner, N. Petrick, M. A. Helvie, K. L. Lam, D. D. Adler, *et al.*, "Computerized classification of malignant and benign microcalcifications on mammograms: texture analysis using an artificial neural network", *Phys Med Biol*, 1997, vol. 42, no. 3, pp. 549-67.

[136] D. L. Thiele, C. Kimme-Smith, T. D. Johnson, M. McCombs, and L. W. Bassett, "Using tissue texture surrounding calcification clusters to predict benign vs malignant outcomes", *Med Phys*, 1996, vol. 23, no. 4, pp. 549-55.

[137] A. Mohanty, M. Senapati, and S. Lenka, "An improved data mining technique for classification and detection of breast cancer from mammograms", *Neural Computing and Applications*, 2013, vol. 22, no. 1, pp. 303-310. http://dx.doi.org/10.1007/s00521-012-0834-4.

[138] R. M. Haralick, K. Shanmugam, and I. H. Dinstein, "Textural Features for Image Classification", *Systems, Man and Cybernetics, IEEE Transactions on*, 1973, vol. SMC-3, no. 6, pp. 610-621. http://dx.doi.org/10.1109/TSMC.1973.4309314.

[139] S. N. Yu, K. Y. Li, and Y. K. Huang, "Detection of microcalcifications in digital mammograms using wavelet filter and Markov random field model", *Comput Med Imaging Graph*, 2006, vol. 30, no. 3, pp. 163-73. http://dx.doi.org/10.1016/j.compmedimag.2006.03.002.

[140] A. AbuBaker, R. Qahwaji, and S. Ipson, "Texture-Based Feature Extraction for the Microcalcification from Digital Mammogram Images", in *Signal Processing and Communications, 2007. ICSPC 2007. IEEE International Conference on*, 2007, pp. 896-899. http://dx.doi.org/10.1109/ICSPC.2007.4728464.

[141] H. Li, M. L. Giger, O. I. Olopade, and L. Lan, "Fractal Analysis of Mammographic Parenchymal Patterns in Breast Cancer Risk Assessment", *Academic Radiology*, 2007, vol. 14, no. 5, pp. 513-521. http://dx.doi.org/10.1016/j.acra.2007.02.003.

[142] N. Tanki, K. Murase, and M. Nagao, "A new parameter enhancing breast cancer detection in computer-aided diagnosis of X-ray mammograms", *Igaku Butsuri*, 2006, vol. 26, no. 4, pp. 207-15.

[143] T. M. Nguyen and R. M. Rangayyan, "Shape Analysis of Breast Masses in Mammograms via the Fractal Dimension", in *Engineering in Medicine and Biology Society, 2005. IEEE-EMBS 2005. 27th Annual International Conference of the*, 2005, pp. 3210-3213. http://dx.doi.org/10.1109/IEMBS.2005.1617159.

[144] P. Kestener, J. M. Lina, P. Saint-Jean, and A. Arneodo, *Wavelet-based multifractal formalism to assist in diagnosis in digitized mammograms* vol. 20, 2011.

[145] H. Yu-Kun and Y. Sung-Nien, "Recognition of Microcalcifications in Digital Mammograms Based on Markov Random Field and Deterministic Fractal Modeling", in *Engineering in Medicine and Biology Society, 2007. EMBS 2007. 29th Annual International Conference of the IEEE*, 2007, pp. 3922-3925. http://dx.doi.org/10.1109/IEMBS.2007.4353191.

[146] Y. Songyang and G. Ling, "A CAD system for the automatic detection of clustered microcalcifications in digitized mammogram films", *Medical Imaging, IEEE Transactions on*, 2000, vol. 19, no. 2, pp. 115-126. http://dx.doi.org/10.1109/42.836371.

[147] T. Bhangale, U. B. Desai, and U. Sharma, "An unsupervised scheme for detection of microcalcifications on mammograms", in *Image Processing, 2000. Proceedings. 2000 International Conference on*, 2000, pp. 184-187 vol.1. http://dx.doi.org/10.1109/ICIP.2000.900925.

[148] W. Liyang, Y. Yongyi, R. M. Nishikawa, and J. Yulei, "A study on several Machine-learning methods for classification of Malignant and benign clustered microcalcifications", *Medical Imaging, IEEE Transactions on*, 2005, vol. 24, no. 3, pp. 371-380. http://dx.doi.org/10.1109/TMI.2004.842457.

[149] O. Tsujii, M. T. Freedman, and S. K. Mun, "Classification of microcalcifications in digital mammograms using trend-oriented radial basis function neural network", *Pattern Recognition*, 1999, vol. 32, no. 5, pp. 891-903. http://dx.doi.org/10.1016/S0031-3203(98)00099-5.

[150] A. Laine and J. Fan, "Texture classification by wavelet packet signatures", *Pattern Analysis and Machine Intelligence, IEEE Transactions on*, 1993, vol. 15, no. 11, pp. 1186-1191. http://dx.doi.org/10.1109/34.244679.

[151] H. Soltanian-Zadeh, S. Pourabdollah-Nezhad, and F. Rafiee Rad, "Texture feature extraction methods for microcalcification classification in mammograms", 2000, no. pp. 982-989. http://dx.doi.org/10.1117/12.387602.

[152] R. M. Rangayyan, S. Banik, and J. E. Desautels, "Computer-aided detection of architectural distortion in prior mammograms of interval cancer", *J Digit Imaging*, 2010, vol. 23, no. 5, pp. 611-31. http://dx.doi.org/10.1007/s10278-009-9257-x.

[153] F. Soares, M. M. Freire, M. Pereira, F. Janela, and J. Seabra, "Towards the detection of microcalcifications on mammograms through Multifractal Detrended Fluctuation Analysis", in *Communications, Computers and Signal Processing, 2009. PacRim 2009. IEEE Pacific Rim Conference on*, 2009, pp. 677-681. http://dx.doi.org/10.1109/PACRIM.2009.5291288.

[154] T. Stojić, I. Reljin, and B. Reljin, "Adaptation of multifractal analysis to segmentation of microcalcifications in digital mammograms", *Physica A: Statistical Mechanics and its Applications*, 2006, vol. 367, no. 0, pp. 494-508. http://dx.doi.org/10.1016/j.physa.2005.11.030.

[155] Y. Jiang, R. M. Nishikawa, D. E. Wolverton, C. E. Metz, M. L. Giger, R. A. Schmidt, *et al.*, "Malignant and benign clustered microcalcifications: automated feature analysis and classification", *Radiology*, 1996, vol. 198, no. 3, pp. 671-678.

[156] E. S. Burnside, E. A. Sickles, L. W. Bassett, D. L. Rubin, C. H. Lee, D. M. Ikeda, *et al.*, "The ACR BI-RADS® Experience: Learning From History", *Journal of the American College of Radiology*, 2009, vol. 6, no. 12, pp. 851-860. http://dx.doi.org/10.1016/j.jacr.2009.07.023.

[157] T. Mu, A. Nandi, and R. Rangayyan, "Classification of Breast Masses Using Selected Shape, Edge-sharpness, and Texture Features with Linear and Kernel-based Classifiers", *Journal of Digital Imaging*, 2008, vol. 21, no. 2, pp. 153-169. http://dx.doi.org/10.1007/s10278-007-9102-z.

[158] J. Martí, J. Freixenet, X. Muñoz, and A. Oliver, "Active Region Segmentation of Mammographic Masses Based on Texture, Contour and Shape Features", in *Pattern Recognition and Image Analysis*. vol. 2652, F. Perales, A. C. Campilho, N. Blanca, and A. Sanfeliu (Eds.): Springer Berlin Heidelberg, 2003, pp. 478-485. http://dx.doi.org/10.1007/978-3-540-44871-6_56.

[159] J. Wei, H. P. Chan, B. Sahiner, L. M. Hadjiiski, M. A. Helvie, M. A. Roubidoux, *et al.*, "Dual system approach to computer-aided detection of breast masses on mammograms", *Med Phys*, 2006, vol. 33, no. 11, pp. 4157-68.

[160] A. Rojas Domínguez and A. K. Nandi, "Toward breast cancer diagnosis based on automated segmentation of masses in mammograms", *Pattern Recognition*, 2009, vol. 42, no. 6, pp. 1138-1148. http://dx.doi.org/10.1016/j.patcog.2008.08.006.

[161] X. Liu, X. Xu, J. Liu, and J. Tang, "Mass Classification with Level Set Segmentation and Shape Analysis for Breast Cancer Diagnosis Using Mammography", in *Advanced Intelligent Computing Theories and Applications. With Aspects of Artificial Intelligence*. vol. 6839, D.-S. Huang, Y. Gan, P. Gupta, and M. M. Gromiha (Eds.): Springer Berlin Heidelberg, 2012, pp. 630-637. http://dx.doi.org/10.1007/978-3-642-25944-9_82.

[162] N. R. Mudigonda, R. Rangayyan, and J. E. L. Desautels, "Gradient and texture analysis for the classification of mammographic masses", *Medical Imaging, IEEE Transactions on*, 2000, vol. 19, no. 10, pp. 1032-1043.

[163] Z. Huo, M. L. Giger, C. J. Vyborny, D. E. Wolverton, and C. E. Metz, "Computerized classification of benign and malignant masses on digitized mammograms: a study of robustness", *Acad Radiol*, 2000, vol. 7, no. 12, pp. 1077-84.

[164] W. K. Lim and M. J. Er, "Classification of mammographic masses using generalized dynamic fuzzy neural networks", *Med Phys*, 2004, vol. 31, no. 5, pp. 1288-95.

[165] S. Gupta and M. K. Markey, "Correspondence in texture features between two mammographic views", *Med Phys*, 2005, vol. 32, no. 6, pp. 1598-606.

[166] H. Alto, R. M. Rangayyan, and J. E. L. Desautels, "Content-based retrieval and analysis of mammographic masses", *Journal of Electronic Imaging*, 2005, vol. 14, no. 2, pp. 023016-023016-17. http://dx.doi.org/10.1117/1.1902996.

[167] F. Ayres and R. Rangayyan, "Reduction of false positives in the detection of architectural distortion in mammograms by using a geometrically constrained phase portrait model", *International Journal of Computer Assisted Radiology and Surgery*, 2007, vol. 1, no. 6, pp. 361-369.

[168] R. Rangayyan and F. Ayres, "Gabor filters and phase portraits for the detection of architectural distortion in mammograms", *Medical and Biological Engineering and Computing*, 2006, vol. 44, no. 10, pp. 883-894.

[169] F. J. Ayres and R. M. Rangayvan, "Characterization of architectural distortion in mammograms", *Engineering in Medicine and Biology Magazine, IEEE*, 2005, vol. 24, no. 1, pp. 59-67.

[170] Z. Huo, M. L. Giger, and C. J. Vyborny, "Computerized analysis of multiple-mammographic views: potential usefulness of special view mammograms in computer-aided diagnosis", *IEEE Trans Med Imaging*, 2001, vol. 20, no. 12, pp. 1285-92. http://dx.doi.org/10.1109/42.974923.

[171] P. Miller and S. Astley, "Automated detection of breast asymmetry using anatomical features", *International Journal of Pattern Recognition and Artificial Intelligence (IJPRAI)*, 1993, vol. 7, no. 6, pp. 1461-1476.

[172] D. Mladenić, "Feature Selection for Dimensionality Reduction", in *Subspace, Latent Structure and Feature Selection*. vol. 3940, C. Saunders, M. Grobelnik, S. Gunn, and J. Shawe-Taylor (Eds.): Springer Berlin Heidelberg, 2006, pp. 84-102. http://dx.doi.org/10.1007/11752790_5.

[173] S. Das, "Filters, wrappers and a boosting-based hybrid for feature selection", in *ICML*, Citeseer, 2001, pp. 74-81.

[174] K. Kira and L. A. Rendell, "The feature selection problem: Traditional methods and a new algorithm", in *AAAI*, 1992, pp. 129-134.

[175] M. Robnik-Šikonja and I. Kononenko, "Theoretical and empirical analysis of ReliefF and RReliefF", *Machine learning*, 2003, vol. 53, no. 1-2, pp. 23-69.

[176] H. Almuallim and T. G. Dietterich, "Learning with Many Irrelevant Features", in *AAAI*, 1991, pp. 547-552.

[177] D. Aijuan and W. Baoying, "Feature selection and analysis on mammogram classification", in *Communications, Computers and Signal Processing, 2009. PacRim 2009. IEEE Pacific Rim Conference on*, 2009, pp. 731-735. http://dx.doi.org/10.1109/PACRIM.2009.5291281.

[178] M. F. Akay, "Support vector machines combined with feature selection for breast cancer diagnosis", *Expert Systems with Applications*, 2009, vol. 36, no. 2, Part 2, pp. 3240-3247. http://dx.doi.org/10.1016/j.eswa.2008.01.009.

[179] D. W. Aha and R. L. Bankert, "Feature selection for case-based classification of cloud types: An empirical comparison", in *Proceedings of the 1994 AAAI workshop on case-based reasoning*, 1994, pp. 106-112.

[180] G. Chandrashekar and F. Sahin, "A survey on feature selection methods", *Computers & Electrical Engineering*, 2014, vol. 40, no. 1, pp. 16-28. http://dx.doi.org/10.1016/j.compeleceng.2013.11.024.

[181] V. Sindhwani, S. Rakshit, D. Deodhare, D. Erdogmus, J. C. Principe, and P. Niyogi, "Feature selection in MLPs and SVMs based on maximum output information", *Neural Networks, IEEE Transactions on*, 2004, vol. 15, no. 4, pp. 937-948.

[182] J. M. Cadenas, M. C. Garrido, and R. Martínez, "Feature subset selection Filter–Wrapper based on low quality data", *Expert Systems with Applications*, 2013, vol. 40, no. 16, pp. 6241-6252. http://dx.doi.org/10.1016/j.eswa.2013.05.051.

[183] R. K. Sivagaminathan and S. Ramakrishnan, "A hybrid approach for feature subset selection using neural networks and ant colony optimization", *Expert Systems with Applications*, 2007, vol. 33, no. 1, pp. 49-60. http://dx.doi.org/10.1016/j.eswa.2006.04.010.

[184] J. Huang, Y. Cai, and X. Xu, "A hybrid genetic algorithm for feature selection wrapper based on mutual information", *Pattern Recognition Letters*, 2007, vol. 28, no. 13, pp. 1825-1844. http://dx.doi.org/10.1016/j.patrec.2007.05.011.

[185] D. Chakraborty and N. R. Pal, "A neuro-fuzzy scheme for simultaneous feature selection and fuzzy rule-based classification", *Neural Networks, IEEE Transactions on*, 2004, vol. 15, no. 1, pp. 110-123. http://dx.doi.org/10.1109/TNN.2003.820557.

[186] D. P. Muni, N. R. Pal, and J. Das, "Genetic programming for simultaneous feature selection and classifier design", *Systems, Man, and Cybernetics, Part B: Cybernetics, IEEE Transactions on*, 2006, vol. 36, no. 1, pp. 106-117.

[187] A. Rakotomamonjy, "Variable selection using svm based criteria", *The Journal of Machine Learning Research*, 2003, vol. 3, no. pp. 1357-1370.

[188] M. Richeldi and P. L. Lanzi, "ADHOC: a tool for performing effective feature selection", in *Tools with Artificial Intelligence, 1996., Proceedings Eighth IEEE International Conference on*, 1996, pp. 102-105. http://dx.doi.org/10.1109/TAI.1996.560434.

[189] S. Salcedo-Sanz, G. Camps-Valls, F. Perez-Cruz, J. Sepulveda-Sanchis, and C. Bousono-Calzon, "Enhancing genetic feature selection through restricted search and Walsh analysis", *Systems, Man, and Cybernetics, Part C: Applications and Reviews, IEEE Transactions on*, 2004, vol. 34, no. 4, pp. 398-406. http://dx.doi.org/10.1109/TSMCC.2004.833301.

[190] Y. Peng, Z. Wu, and J. Jiang, "A novel feature selection approach for biomedical data classification", *Journal of Biomedical Informatics*, 2010, vol. 43, no. 1, pp. 15-23. http://dx.doi.org/10.1016/j.jbi.2009.07.008.

[191] B. Wu, T. Abbott, D. Fishman, W. McMurray, G. Mor, K. Stone, *et al.*, "Comparison of statistical methods for classification of ovarian cancer using mass spectrometry data", *Bioinformatics*, 2003, vol. 19, no. 13, pp. 1636-1643.

[192] A. Arauzo-Azofra, J. M. Benitez, and J. L. Castro, "A feature set measure based on relief", in *Proceedings of the fifth international conference on Recent Advances in Soft Computing*, Citeseer, 2004, pp. 104-109.

[193] G. Bhanot, G. Alexe, B. Venkataraghavan, and A. J. Levine, "A robust meta-classification strategy for cancer detection from MS data", *Proteomics*, 2006, vol. 6, no. 2, pp. 592-604.

[194] M. Ben-Bassat, "Pattern recognition and reduction of dimensionality", *Handbook of Statistics*, 1982, vol. 2, no. pp. 773-910.

[195] J. Yu and X.-W. Chen, "Bayesian neural network approaches to ovarian cancer identification from high-resolution mass spectrometry data", *Bioinformatics*, 2005, vol. 21, no. suppl 1, pp. i487-i494.

[196] Z. Xiao, E. Dellandrea, W. Dou, and L. Chen, "ESFS: A new embedded feature selection method based on SFS", *Rapports de recherché*, 2008, no.

[197] J. Kittler, "Feature set search algorithms", *Pattern recognition and signal processing*, 1978, no. pp. 41-60.

[198] W. Siedlecki and J. Sklansky, "On automatic feature selection", *International Journal of Pattern Recognition and Artificial Intelligence*, 1988, vol. 2, no. 02, pp. 197-220.

[199] D. B. Skalak, "Prototype and Feature Selection by Sampling and Random Mutation Hill Climbing Algorithms", in *ICML*, Citeseer, 1994, pp. 293-301.

[200] I. Inza, P. Larrañaga, R. Etxeberria, and B. Sierra, "Feature Subset Selection by Bayesian network-based optimization", *Artificial Intelligence*, 2000, vol. 123, no. 1–2, pp. 157-184. http://dx.doi.org/10.1016/S0004-3702(00)00052-7.

[201] C. M. Bishop and N. M. Nasrabadi, *Pattern recognition and machine learning* vol. 1: springer New York, 2006.

[202] P. Ferreira, N. A. Fonseca, I. Dutra, R. Woods, and E. Burnside, "Predicting malignancy from mammography findings and image–guided core biopsies", *International Journal of Data Mining and Bioinformatics*, 2015, vol. 11, no. 3, pp. 257-276.

[203] P. Ferreira, I. de Castro Dutra, N. A. Fonseca, R. W. Woods, and E. S. Burnside, "Studying the Relevance of Breast Imaging Features", in *HEALTHINF*, 2011, pp. 337-342.

[204] R. Woods, L. Oliphant, K. Shinki, D. Page, J. Shavlik, and E. Burnside, "Validation of Results from Knowledge Discovery: Mass Density as a Predictor of Breast Cancer", *Journal of Digital Imaging*, 2010, vol. 23, no. 5, pp. 554-561. http://dx.doi.org/10.1007/s10278-009-9235-3.

[205] M. Kim and J. Ryu, "Optimized Fuzzy Classification Using Genetic Algorithm", in *Fuzzy Systems and Knowledge Discovery*. vol. 3613, L. Wang and Y. Jin (Eds.): Springer Berlin Heidelberg, 2005, pp. 392-401. http://dx.doi.org/10.1007/11539506_51.

[206] H. Song, S. Lee, D. Kim, and G. Park, "New Methodology of Computer Aided Diagnostic System on Breast Cancer", in *Advances in Neural Networks – ISNN 2005*. vol. 3498, J. Wang, X.-F. Liao, and Z. Yi (Eds.): Springer Berlin Heidelberg, 2005, pp. 780-789. http://dx.doi.org/10.1007/11427469_124.

[207] W. Xu, S. Xia, and H. Xie, "Application of CMAC-Based Networks on Medical Image Classification", in *Advances in Neural Networks – ISNN 2004*. vol. 3173, F.-L. Yin, J. Wang, and C. Guo (Eds.): Springer Berlin Heidelberg, 2004, pp. 953-958. http://dx.doi.org/10.1007/978-3-540-28647-9_157.

[208] J. Abonyi and F. Szeifert, "Supervised fuzzy clustering for the identification of fuzzy classifiers", *Pattern Recognition Letters*, 2003, vol. 24, no. 14, pp. 2195-2207. http://dx.doi.org/10.1016/S0167-8655(03)00047-3.

[209] S. N. Ghazavi and T. W. Liao, "Medical data mining by fuzzy modeling with selected features", *Artif Intell Med*, 2008, vol. 43, no. 3, pp. 195-206. http://dx.doi.org/10.1016/j.artmed.2008.04.004.

[210] M. A. Alolfe, A. M. Youssef, Y. M. Kadah, and A. S. Mohamed, "Computer-Aided Diagnostic System based on Wavelet Analysis for Microcalcification Detection in Digital Mammograms", in *Biomedical Engineering Conference, 2008. CIBEC 2008. Cairo International*, 2008, pp. 1-5. http://dx.doi.org/10.1109/CIBEC.2008.4786080.

[211] K. Hechenbichler and K. Schliep, "Weighted k-nearest-neighbor techniques and ordinal classification", 2004.

[212] C. C. Burges, "A Tutorial on Support Vector Machines for Pattern Recognition", *Data Mining and Knowledge Discovery*, 1998, vol. 2, no. 2, pp. 121-167. http://dx.doi.org/10.1023/A:1009715923555.

[213] R. O. Duda, P. E. Hart, and D. G. Stork, *Pattern Classification (2nd Edition)*: Wiley-Interscience, 2000.

[214] P. A. Lachenbruch, *Discriminant Analysis*: Hafner Press, New York, NY, 1975.

[215] S. A. Medjahed, T. A. Saadi, and A. Benyettou, "Breast Cancer Diagnosis by using k-Nearest Neighbor with Different Distances and Classification Rules", *International Journal of Computer Applications*, 2013, vol. 62, no. 1, pp. 1-5.

[216] D. Kramer and F. Aghdasi, "Classification of microcalcifications in digitised mammograms using multiscale statistical texture analysis", in *Communications and Signal Processing, 1998. COMSIG '98. Proceedings of the 1998 South African Symposium on*, 1998, pp. 121-126. http://dx.doi.org/10.1109/COMSIG.1998.736934.

[217] D. Kramer and F. Aghdasi, "Texture analysis techniques for the classification of microcalcifications in digitised mammograms", in *AFRICON, 1999 IEEE*, 1999, pp. 395-400 vol.1.

[218] H. Soltanian-Zadeh, S. Pourabdollah-Nezhad, and F. Rafiee Rad, "Shape-based and texture-based feature extraction for classification of microcalcifications in mammograms", 2001, pp. 301-310.

[219] Y. Wu, C. Wang, S. C. Ng, A. Madabhushi, and Y. Zhong, "Breast cancer diagnosis using neural-based linear fusion strategies", presented at the Proceedings of the 13th international conference on Neural information processing - Volume Part III, Springer-Verlag, Hong Kong, China, 2006.

[220] B. Verma, "Impact of multiple clusters on neural classification of ROIs in digital mammograms", in *Neural Networks, 2009. IJCNN 2009. International Joint Conference on*, 2009, pp. 3220-3223. http://dx.doi.org/10.1109/IJCNN.2009.5178942.

[221] Y. López, Novoa, Andra., Guevara, Miguel., Silva, Augusto, "Breast Cancer Diagnosis Based on a Suitable Combination of Deformable Models and Artificial Neural Networks Techniques", in *Progress in Pattern Recognition, Image Analysis and Applications*. vol. Volume 4756/2008: Springer Berlin / Heidelberg, 2008, pp. 803-811.

[222] Y. López, Novoa, Andra., Guevara, Miguel., Quintana, Nicolás., Silva, Augusto, "Computer Aided Diagnosis System to Detect Breast Cancer Pathological Lesions", in *Progress in Pattern Recognition, Image Analysis and Applications*. vol. Volume 5197/2008: Springer Berlin / Heidelberg, 2008, pp. 453-460.

[223] I. El-Naqa, Y. Yongyi, M. N. Wernick, N. P. Galatsanos, and R. M. Nishikawa, "A support vector machine approach for detection of microcalcifications", *Medical Imaging, IEEE Transactions on*, 2002, vol. 21, no. 12, pp. 1552-1563. http://dx.doi.org/10.1109/TMI.2002.806569.

[224] R. Ramos-Pollan, J. M. Franco, J. Sevilla, M. A. Guevara-Lopez, N. G. de Posada, J. Loureiro, *et al.*, "Grid infrastructures for developing mammography CAD systems", *Conf Proc IEEE Eng Med Biol Soc*, 2010, vol. 2010, no. pp. 3467-70. http://dx.doi.org/10.1109/iembs.2010.5627832.

[225] E. D. Pisano, C. A. Gatsonis, M. J. Yaffe, R. E. Hendrick, A. N. A. Tosteson, D. G. Fryback, *et al.*, "American College of Radiology Imaging Network Digital Mammographic Imaging Screening Trial: Objectives and Methodology", *Radiology*, 2005, vol. 236, no. 2, pp. 404-412. http://dx.doi.org/10.1148/radiol.2362050440.

[226] M. A. Helvie, L. Hadjiiski, E. Makariou, H. P. Chan, N. Petrick, B. Sahiner, *et al.*, "Sensitivity of noncommercial computer-aided detection system for mammographic breast cancer detection: pilot clinical trial", *Radiology*, 2004, vol. 231, no. 1, pp. 208-14. http://dx.doi.org/10.1148/radiol.2311030429.

[227] R. L. Birdwell, P. Bandodkar, and D. M. Ikeda, "Computer-aided detection with screening mammography in a university hospital setting", *Radiology*, 2005, vol. 236, no. 2, pp. 451-7. http://dx.doi.org/10.1148/radiol.2362040864.

[228] S. V. Destounis, P. DiNitto, W. Logan-Young, E. Bonaccio, M. L. Zuley, and K. M. Willison, "Can computer-aided detection with double reading of screening mammograms help decrease the false-negative rate? Initial experience", *Radiology*, 2004, vol. 232, no. 2, pp. 578-84. http://dx.doi.org/10.1148/radiol.2322030034.

[229] S. A. Butler, R. J. Gabbay, D. A. Kass, D. E. Siedler, F. O'Shaughnessy K, and R. A. Castellino, "Computer-aided detection in diagnostic mammography: detection of clinically unsuspected cancers", *AJR Am J Roentgenol*, 2004, vol. 183, no. 5, pp. 1511-5. http://dx.doi.org/10.2214/ajr.183.5.1831511.

[230] C. Marx, A. Malich, M. Facius, U. Grebenstein, D. Sauner, S. O. Pfleiderer, *et al.*, "Are unnecessary follow-up procedures induced by computer-aided diagnosis (CAD) in mammography? Comparison of mammographic diagnosis with and without use of CAD", *Eur J Radiol*, 2004, vol. 51, no. 1, pp. 66-72. http://dx.doi.org/10.1016/s0720-048x(03)00144-x.

[231] J. A. Baker, J. Y. Lo, D. M. Delong, and C. E. Floyd, "Computer-aided detection in screening mammography: variability in cues", *Radiology*, 2004, vol. 233, no. 2, pp. 411-7. http://dx.doi.org/10.1148/radiol.2332031200.

[232] D. Gur, J. S. Stalder, L. A. Hardesty, B. Zheng, J. H. Sumkin, D. M. Chough, *et al.*, "Computer-aided detection performance in mammographic examination of masses: assessment", *Radiology*, 2004, vol. 233, no. 2, pp. 418-23. http://dx.doi.org/10.1148/radiol.2332040277.

[233] K. J. McLoughlin, P. J. Bones, and N. Karssemeijer, "Noise equalization for detection of microcalcification clusters in direct digital mammogram images", *Medical Imaging, IEEE Transactions on*, 2004, vol. 23, no. 3, pp. 313-320.

[234] K. Drukker, K. Horsch, and M. L. Giger, "Multimodality computerized diagnosis of breast lesions using mammography and sonography", *Acad Radiol*, 2005, vol. 12, no. 8, pp. 970-9. http://dx.doi.org/10.1016/j.acra.2005.04.014.

[235] M. Velikova, M. Samulski, P. J. Lucas, and N. Karssemeijer, "Improved mammographic CAD performance using multi-view information: a Bayesian network framework", *Phys Med Biol*, 2009, vol. 54, no. 5, pp. 1131-47. http://dx.doi.org/10.1088/0031-9155/54/5/003.

[236] M. F. Salfity, R. M. Nishikawa, Y. Jiang, and J. Papaioannou, "The use of a priori information in the detection of mammographic microcalcifications to improve their classification", *Med Phys*, 2003, vol. 30, no. 5, pp. 823-31.

[237] S. Timp and N. Karssemeijer, "A new 2D segmentation method based on dynamic programming applied to computer aided detection in mammography", *Med Phys*, 2004, vol. 31, no. 5, pp. 958-71.

[238] C. J. D'Orsi, L. W. Bassett, W. A. Berg, and et.al, *Breast Imaging Reporting and Data System: ACR BI-RADS-Mammography*, 4th Edition ed.: American College of Radiology, 2003.

[239] L. Talavera, "An Evaluation of Filter and Wrapper Methods for Feature Selection in Categorical Clustering", in *Advances in Intelligent Data Analysis VI*. vol. 3646, A. F. Famili, J. Kok, J. Peña, A. Siebes, and A. Feelders (Eds.): Springer Berlin Heidelberg, 2005, pp. 440-451. http://dx.doi.org/10.1007/11552253_40.

[240] M. Dash and H. Liu, "Feature Selection for Classification", *Intelligent Data Analysis*, 1997, vol. 1, no. 3, pp. 131-156. http://dx.doi.org/10.3233/IDA-1997-1302.

[241] R. Holte, "Very Simple Classification Rules Perform Well on Most Commonly Used Datasets", *Machine Learning*, 1993, vol. 11, no. 1, pp. 63-90. http://dx.doi.org/10.1023/A:1022631118932.

[242] M. Hall, E. Frank, G. Holmes, B. Pfahringer, P. Reutemann, and I. H. Witten, "The WEKA data mining software: an update", *ACM SIGKDD explorations newsletter*, 2009, vol. 11, no. 1, pp. 10-18.

[243] F. García López, M. García Torres, B. Melián Batista, J. A. Moreno Pérez, and J. M. Moreno-Vega, "Solving feature subset selection problem by a parallel scatter search", *European Journal of Operational Research*, 2006, vol. 169, no. 2, pp. 477-489.

[244] Y. H. Hu and J.-N. Hwang, "Introduction to Neural Networks for Signal Processing", in *Handbook of neural network signal processing*: CRC press, 2001.

[245] S. Wang and R. M. Summers, "Machine learning and radiology", *Medical Image Analysis*, 2012, vol. 16, no. 5, pp. 933-951. http://dx.doi.org/10.1016/j.media.2012.02.005.

[246] N. Pérez, A. Silva, I. Ramos, and M. Guevara, "Ensemble features selection method as tool for Breast Cancer classification", in *Advanced Computing Services for Biomedical Image Analysis*, M. Guevara and N. Dey (Eds.): International Journal of Image Mining, 2015.

[247] N. Pérez, M. A. Guevara, and A. Silva, "Evalualtion of features selection methods for Breast Cancer classification", in *15th International Conference on Experimental Mechanics*, 2012, p. 10.

[248] T. Hastie, R. Tibshirani, J. Friedman, and J. Franklin, "The elements of statistical learning: data mining, inference and prediction", *The Mathematical Intelligencer*, 2005, vol. 27, no. 2, pp. 83-85.

[249] J. Demšar, "Statistical comparisons of classifiers over multiple data sets", *The Journal of Machine Learning Research*, 2006, vol. 7, no. pp. 1-30.

[250] M. Hollander and D. A. Wolfe, *Nonparametric statistical methods*, 2nd Edition ed.: Wiley-Interscience, 1999.

[251] H. B. Mann and D. R. Whitney, "On a Test of Whether One of Two Random Variables is Stochastically Larger Than the Other", *Annals of Mathematical Statistics*, 1947, vol. 18, no. pp. 50-60. http://dx.doi.org/MR0022058.

[252] R. E. Kirk, *Statistics: An Introduction*: Thomson/Wadsworth, 2007.

[253] J. Gibbons and S. Chakraborti, "Nonparametric Statistical Inference", in *International Encyclopedia of Statistical Science*, M. Lovric (Ed.): Springer Berlin Heidelberg, 2011, pp. 977-979. http://dx.doi.org/10.1007/978-3-642-04898-2_420.

[254] P. A. Devijver and J. Kittler, *Pattern recognition: a statistical approach*. London, UK: Prentice/Hall International, 1982.

[255] F. E. Koehn and G. T. Carter, "The evolving role of natural products in drug discovery", *Nat Rev Drug Discov*, 2005, vol. 4, no. 3, pp. 206-20. http://dx.doi.org/10.1038/nrd1657.

[256] M. Blanco, J. Coello, H. Iturriaga, S. Maspoch, and C. de la Pezuela, "Near-infrared spectroscopy in the pharmaceutical industry", *The Analyst*, 1998, vol. 123, no. 8, pp. 135R-150R. http://dx.doi.org/10.1039/a802531b.

[257] H. Hashemi, D. M. J. Tax, R. P. W. Duin, A. Javaherian, and P. de Groot, "Gas chimney detection based on improving the performance of combined multilayer perceptron and support vector classifier", *Nonlinear Processes in Geophysics*, 2008, vol. 15, no. 6, pp. 863-871. http://dx.doi.org/10.5194/npg-15-863-2008.

[258] Y. Kaifeng, L. Wenkai, D. Wenlong, Z. Shanwen, X. Huanqin, and L. Yanda, "Hydrocarbon Prediction Method Based on Svm Feature Selection", *Natural Gas Industry*, 2004, vol. 24, no. 7, pp. 36-38.

[259] K. Chanwoo and R. M. Stern, "Feature extraction for robust speech recognition based on maximizing the sharpness of the power distribution and on power flooring", in *Acoustics Speech and Signal Processing (ICASSP), 2010 IEEE International Conference on*, Dallas, TX, 2010, pp. 4574-4577. http://dx.doi.org/10.1109/ICASSP.2010.5495570.

[260] Y. Pei, I. Essa, T. Starner, and J. M. Rehg, "Discriminative feature selection for hidden Markov models using Segmental Boosting", in *IEEE International Conference on Acoustics, Speech and Signal Processing. ICASSP 2008.* , IEEE, Las Vegas, NV, USA, 2008, pp. 2001-2004. http://dx.doi.org/10.1109/ICASSP.2008.4518031.

[261] R. Dutta, E. L. Hines, J. W. Gardner, and P. Boilot, "Bacteria classification using Cyranose 320 electronic nose", *BioMedical Engineering OnLine*, 2002, vol. 1, no. 1, p. 4. http://dx.doi.org/10.1186/1475-925x-1-4.

[262] M. Holmberg, F. Gustafsson, E. G. Hornsten, F. Winquist, L. E. Nilsson, L. Ljung, *et al.*, "Bacteria classification based on feature extraction from sensor data", *Biotechnology Techniques*, 1998, vol. 12, no. 4, pp. 319-324. http://dx.doi.org/10.1023/A:1008862617082.

[263] S.-K. Lee, P.-c. Chung, C.-I. Chang, C.-S. Lo, T. Lee, G.-C. Hsu, *et al.*, "Classification of clustered microcalcifications using a Shape Cognitron neural network", *Neural Networks*, 2003, vol. 16, no. 1, pp. 121-132. http://dx.doi.org/10.1016/S0893-6080(02)00164-8.

[264] Y. Saeys, I. Inza, and P. Larranaga, "A review of feature selection techniques in bioinformatics", *Bioinformatics*, 2007, vol. 23, no. 19, pp. 2507-17. http://dx.doi.org/10.1093/bioinformatics/btm344.

[265] J. Marques de Sá, "Estimating Data Parameters Applied Statistics Using SPSS, STATISTICA, MATLAB and R", J. P. Marques de Sá (Ed.): Springer Berlin Heidelberg, 2007, pp. 81-109. http://dx.doi.org/10.1007/978-3-540-71972-4_3.

[266] F. Wilcoxon, "Some rapid approximate statistical procedures", *Annals of the New York Academy of Sciences*, 1950, vol. 52, no. 6, pp. 808-814.

[267] W. J. Conover and W. Conover, "Practical nonparametric statistics", 1980, no.

[268] S. E. Maxwell and H. D. Delaney, *Designing experiments and analyzing data: A model comparison perspective* vol. 1: Psychology Press, 2004.

[269] N. P. Pérez, M. A. Guevara López, A. Silva, and I. Ramos, "Improving the Mann–Whitney statistical test for feature selection: An approach in breast cancer diagnosis on mammography", *Artificial Intelligence in Medicine*, 2015, vol. 63, no. 1, pp. 19-31. http://dx.doi.org/10.1016/j.artmed.2014.12.004.

[270] G. H. John, R. Kohavi, and K. Pfleger, "Irrelevant Features and the Subset Selection Problem", in *Machine Learning, Proceedings of the Eleventh International Conference*. W. W. Cohen and H. Hirsh (Eds.), Morgan Kaufmann, Rutgers University, New Brunswick, NJ, USA, 1994, pp. 121-129.